THE EFFECT OF THE LOAD LEVEL ON THE FIRE RESISTANCE OF PARTIALLY ENCASED COLUMNS

Mehdi Mellef

Final Dissertation Report presented to

School of Technology and Management

Polytechnic Institute of Bragança

For the fulfilment of the Master's degree in

Construction Engineering

November 2020

THE EFFECT OF THE LOAD LEVEL ON THE FIRE RESISTANCE OF PARTIALLY ENCASED COLUMNS

Mehdi Mellef

Final Dissertation Report presented to

School of Technology and Management

Polytechnic Institute of Bragança

For the fullfilment of the Master's degree in

Construction Engineering

Supervisor:

Prof. Dr. Paulo Alexandre Gonçalves Piloto (IPB)

November 2020

ACKNOWLEDGEMENTS

At the end of this work carried out within the Polytechnic Institute of Bragança I would like, first, to thank God who always gave me sustain throughout this work.

I also want to express my gratitude and thankfulness from the bottom of heart to my mother and my late father and my largest family who supported me since my first day in school until this level.

Subsequently, my most sincere thanks go to my supervisor professor Dr. Paulo Piloto, for supervising this work so kindly and who has continued to closely follow all the stages of my work. May he find here the expression of my great gratitude and my deep respect.

My thanks also go to all the staff of Applied Mechanics Departement of Technology and Management School and to all the workers of Institut Polytechinic of Bragança and my teachers who allowed me to acquire a complete and well-enriched training allowing me to develop this work.

I also wish to express my gratitude to those who contributed directly or indirectly to the development of this graduation project.

Finally, my gratitude and thanks to the members of the jury who took the trouble to evaluate this work, showing care and patience.

ABSTRACT

Partially encased composite columns (PEC) present better structural performance under fire situation than simple steel columns. Thus, it is not possible to calculate the fire resistance of its components, taking just into account the temperature of the steel, because the concrete increases considerably the fire resistance of the column.

However, the annex G of EN 1994-1-2 presents the balanced summation model to determine the fire resistance of the partially encased columns, by calculating the buckling resistance around the weak axis when exposed to the standard fire curve ISO834 for different fire ratings.

Thereafter a new proposal was presented to improve this simple method, taking into consideration the average temperature of all components of the cross section, the residual height of the web based on 400ºC isothermal and the residual concrete area based on the 500ºC isothermal.

Later the finite element method is used to calculate the buckling resistance of partially encased columns using an incremental and iterative procedure, investigating the behavior of thirty different PEC cross sections, being ten of each specified steel profile series (HEA, HEB and HD) for two different columns height (3 and 4 meter).

The results of the numerical solution are compared with the balanced summation method of annex G from EN 1994-1-2 as well the new proposed solution model.

Key words:

Partially encased columns, composite columns, fire resistance, balanced summation model, ANSYS, buckling resistance

RESUMO (PT)

Os pilares mistos parcialmente revestidos (PEC) apresentam um melhor desempenho estrutural em situação de incêndio do que os pilares de aço simples. Assim, não é possível calcular a resistência ao fogo de seus componentes levando em consideração apenas a temperatura do aço, pois o concreto aumenta consideravelmente a resistência ao fogo do pilar.

No entanto, o anexo G da norma europeia EN1994-1.2 apresenta um método de soma equilibrada para determinar a resistência ao fogo das colunas parcialmente revestidas, calculando a resistência à encurvadura em torno do eixo fraco quando exposto à curva de fogo padrão ISO834 para diferentes tempos de resistência ao fogo.

Em seguida, uma nova proposta foi apresentada para melhorar este método simples, levando em consideração a temperatura média de todos os componentes da seção transversal, a altura residual da alma baseada na isotérmica de 400ºC e a área residual de betão baseada na isotérmica 500ºC.

Posteriormente, o método dos elementos finitos é usado para calcular a resistência à encurvadura de colunas parcialmente revestidas usando um procedimento incremental e iterativo, investigando trinta seções transversais PEC diferentes, sendo dez de cada série de perfil de aço (HEA, HEB e HD) para duas alturas de coluna diferentes (3 e 4) metros.

Os resultados da solução numérica são comparados com o método da soma balanceada do anexo G da EN1994-1-2, bem como com o novo modelo de solução proposto.

Palavras chave:

Colunas parcialmente revestidas, colunas mistas, resistência ao fogo, método de soma balanceada, ANSYS, resistência à encurvadura

INDEX

LIST OF FIGURES

LIST OF TABLES

NOTATIONS

Latin upper-case letters

A_c	Cross-sectional area of the concrete.
A_m/V	Section factor in $[m^{-1}]$.
A_s	Cross-sectional area of the reinforcement bars.
C_a	Specific heat of steel.
C_p	Specific heat of dry concrete.
E_a	Modulus of elasticity of structural steel at 20 ºC.
$E_{a,f}$	Modulus of elasticity of profile steel flange at 20 ºC.
$E_{a,f,\theta}$	Modulus of elasticity of profile steel flange at elevated temperatures.
$E_{a,w}$	Modulus of elasticity of profile steel web at 20 ºC.
$E_{a,w,\theta}$	Modulus of elasticity of profile steel web at elevated temperatures.
$E_{a,\theta}$	Modulus of elasticity of structural steel at elevated temperatures.
$E_{c,sec}$	Secant modulus of elasticity of concrete at 20 ºC.
$E_{c,sec,\theta}$	Characteristic value for the secant modulus of concrete.
E_{cm}	Secant modulus of elasticity of concrete at elevated temperatures.
$(EI)_{c,z}$	Flexural stiffness of concrete (around the Z axis) at 20 ºC.
$(EI)_{eff}$	Effective flexural stiffness at 20 ºC.
$(EI)_{f,z}$	Flexural stiffness of the two flanges (around the Z axis) at 20 ºC.
$(EI)_{fi,c,z}$	Flexural stiffness of concrete (around the Z axis) under fire situation.
$(EI)_{fi,eff}$	Effective flexural stiffness under fire situation.
$(EI)_{fi,c,z}$	Flexural stiffness of concrete (around the Z axis) under fire situation.
$(EI)_{fi,f,z}$	Flexural stiffness of the two flanges (around the Z axis) under fire.
$(EI)_{fi,s,z}$	Flexural stiffness of reinforcing bars (around the Z axis) under fire.
$(EI)_{fi,eff,z}$	Effective flexural stiffness for bending (around the Z axis) under fire.
$(EI)_{fi,w,z}$	Flexural stiffness of the web of profile (around the Z axis) under fire.
E_s	Modulus of elasticity of reinforcing bars at 20 ºC.
$E_{s,\theta}$	Modulus of elasticity of reinforcing bars at elevated temperatures.
$(EI)_{s,z}$	Flexural stiffness of reinforcing bars (around the Z axis) at 20 ºC.

$(EI)_{w,z}$	Flexural stiffness of the web of profile (around the Z axis) at 20 ºC.
H_t	Empirical coefficient for reducing the height of the web of profile.
$I_{s,z}$	Second order moment of the reinforcement bars around the Z axis.
I_y	Moment of inertia relative to the axis y-y.
I_z	Moment of inertia relative to the axis z-z.
L	Length of the column.
L_θ	Buckling length of the column.
$N_{fi,cr,z}$	Elastic critical load around Z axis in the fire situation.
$N_{fi,pl,Rd}$	Plastic resistance to axial compression of the column under fire.
$N_{fi,pl,Rd,c}$	Plastic resistance to axial compression of the concrete under fire.
$N_{fi,pl,Rd,f}$	Plastic resistance to axial compression of the profile flange under fire.
$N_{fi,pl,Rd,s}$	Plastic resistance to axial compression of the rebars under fire.
$N_{fi,pl,Rd,w}$	Plastic resistance to axial compression of the profile web under fire.
$N_{fi,Rd}$	Axial buckling load of the column under fire.
$N_{fi,Rd,z}$	Plastic resistance to axial compression of the profile under fire.
$N_{pl,Rd}$	Plastic resistance to axial compression of the column at 20 ºC.
$N_{pl,Rd,c}$	Plastic resistance to axial compression of the concrete at 20 ºC.
$N_{pl,Rd,f}$	Plastic resistance to axial compression of the profile flange at 20 ºC.
$N_{pl,Rd,s}$	Plastic resistance to axial compression of the reinforcing bars at 20 ºC.
$N_{pl,Rd,w}$	Plastic resistance to axial compression of the profile web at 20 ºC.
W_{pl}	Plastic modulus of the section.

Latin lower-case letters

b	Width of the cross section.
$b_{0,ch}$	Parameter for calculating the horizontal reduction of concrete.
$b_{0,cv}$	Parameter for calculating the vertical reduction of concrete.
$b_{c,fi}$	Neglected external layer of concrete.
$b_{c,fi,h}$	Neglected external layer of concrete in horizontal directions.
$b_{c,fi,v}$	Neglected external layer of concrete in vertical directions.

e_f	Thickness of the flange of the steel profile.
e_w	Thickness of the web of the steel profile.
$f_{ap,\theta}$	Proportional stress of structural steel at elevated temperatures.
f_{au}	Maximum tensile stress of structural steel at 20 ºC.
f_{ay}	Flow stress of structural steel at 20 ° C.
$f_{ay,f}$	Flow stress of the flange of the steel profile at 20 ° C.
$f_{ay,f,t}$	Flow stress of the flange of the steel profile at elevated temperatures.
$f_{ay,w}$	Flow stress of the web of the steel profile at 20 ° C.
$f_{ay,w,t}$	Flow stress of the web of the steel profile at elevated temperatures.
$f_{ay,\theta}$	Flow stress of structural steel of the steel profile at elevated Tº.
f_c	Compressive strength of concrete at 20 ° C.
$f_{c,\theta}$	Compressive strength of concrete at elevated temperature.
f_{ck}	Characteristic value of the compressive strength of the concrete at 20ºC
$f_{ck,cube}$	Characteristic cubic value of the compressive strength of the concrete.
$f_{ck,\theta}$	Characteristic value of the compressive strength of the concrete.
f_{cm}	The average design value of the yield strength of the steel at 20 ° C.
f_{ctm}	The Average design value of tensile strength of concrete at 20 ° C.
f_{su}	Maximum tensile strength of reinforcing bars at 20 ° C.
f_{sy}	Flow stress of the reinforcing bars at 20 ° C.
$f_{sy,\theta}$	Flow stress of the reinforcing bars at elevated temperatures.
h	Height of a cross section.
$\dot{h}_{net}$	Total heat flow.
$\dot{h}_{net,c}$	Heat flow by convection.
$\dot{h}_{net,r}$	Heat flow by radiation.
$\vec{n}$	Director vector.
$h_{w,fi}$	Geometric reduction of the web.
K	Ratio between yield strength and maximum reinforcement steel.
k_{ct}	Reduction of the tensile strength of concrete at elevated temperatures.
$k_{c,\theta}$	Reduction of compressive strength of concrete at elevated Tº.
$k_{E,t}$	Reduction in the modulus of elasticity of rebares at elevated Tº.
$k_{E,\theta}$	Reduction in the modulus of elasticity of structural steel at elevated Tº.

$k_{f,cv}$	Empirical Coefficient for the vertical reduction of the flange.
$k_{f,f}$	Empirical Coefficient for the average temperature of the flange.
$k_{sE,\theta}$	Reduction in the modulus of elasticity of rebars at elevated Tº.
$k_{sy,\theta}$	Reduction in the yield strength of reinforcing bars at elevated Tº.
k_t	Empirical Coefficient for the average temperature of the flange.
$k_{t,c}$	Empirical Coefficient for the average temperature of the concrete.
$k_{t,ch}$	Empirical Coefficient for the horizontal reduction of concrete.
$k_{t,cv}$	Empirical Coefficient for the vertical reduction of concrete.
$k_{t,f}$	Empirical Coefficient for the vertical reduction of the flange.
$k_{t,s}$	Empirical Coefficient for the average temperature of the rebars.
$k_{t,w}$	Empirical Coefficient for the average temperature of the web.
$k_{w,c}$	Empirical Coefficient for the average temperature of the concrete.
$k_{w,ch}$	Empirical Coefficient for the horizontal reduction of concrete.
$k_{w,w}$	Empirical Coefficient for the average temperature of the web.
$k_{y,t}$	Reduction in the yield strength of reinforcing steel elevated Tº.
$k_{y,\theta}$	Reduction in the yield strength of structural steel elevated Tº.
t	Time.
u	The geometrical average of the axis distances u_1 and u_2 .
u_1	The axis distance from the outer rebars to the inner flange edge.
u_2	The axis distance from the outer reinforcing bar to the concrete surface.
v	Poisson coefficient.

Greek capital letters

∇	Gradient vector.
Θ_g	Temperature of gas.
Θ_m	Temperature of material
Θ_r	Radiated temperature.
Φ	View factor.
Ω	Domain interior.

Greek lowercase letters

$\gamma_{M\ fi,a}$	Partial factor for the strength of structural steel in the fire situation.
$\gamma_{M\ fi,c}$	Partial factor for the strength of concrete in the fire situation.
$\gamma_{M\ fi,s}$	Partial factor for the strength of reinforcing bars in the fire situation.
$\bar{\lambda}_{\theta}$	Non-dimensional slenderness.
α_c	Convection coefficient.
ε	Strain.
$\varepsilon_{ap,\theta}$	Steel strain at tension proportional at elevated temperature.
$\varepsilon_{au,\theta}$	Steel strain at tension maximal at elevated temperature.
$\varepsilon_{ay,\theta}$	Steel strain at yield strength at elevated temperature.
ε_{ce}	Maximum concrete deformation under compression.
$\varepsilon_{ce,\theta}$	Maximum concrete deformation under compression at elevated Tº.
ε_{cu}	Concrete deformation at maximum compression.
$\varepsilon_{cu,\theta}$	Concrete deformation at maximum compression at elevated Tº.
ε_f	Emissivity of fire.
ε_m	Emissivity of material.
θ	Temperature in [º C].
$\theta_{0,c}$	Improved Parameter for calculating the average concrete temperature.
$\theta_{0,f}$	Improved Parameter for calculating the average flange temperature.
$\theta_{0,s}$	Improved Parameter for calculating the average rebars temperatures.
$\theta_{0,w}$	Improved Parameter for calculating the average web temperature.
$\theta_{c,t}$	Average concrete temperature.
$\theta_{f,t}$	Average flange temperature.
$\theta_{s,t}$	Average reinforcing bars temperature.
$\theta_{w,t}$	Average web temperature.
$\lambda_{(T)}$	Thermal conductivity of the material as a function of temperature.
λ_a	Thermal conductivity of steel.
λ_c	Thermal conductivity of concrete.
$\rho_{(T)}$	Specific mass of the material as a function of temperature
ρ_a	Specific mass of the steel.
ρ_c	Specific mass of the concrete.

σ	Stephan-Boltzmann coefficient.
Φ	Diameter of reinforcing bars.
χ_z	Reduction factor of the Buckling resistance.
$\varphi_{f,\theta}$	Weighting reduction coefficient of flexural stiffness for flange.
$\varphi_{w,\theta}$	Weighting reduction coefficient of effective flexural stiffness for web.
$\varphi_{c,\theta}$	Weighting coefficient of effective flexural stiffness for concrete.
$\varphi_{s,\theta}$	Weighting coefficient of effective flexural stiffness for rebars.

1- INTRODUCTION

1-1 Fire safety engineering

Fire is a process in which substances combine chemically with oxygen from the air and typically give out heat and flames, which can be a very destructive accidental phenomenon.

The fire risk will always exist because most houses have a fireplace and because it is impossible to use only incombustible stuffs in building.

Fire safety engineering consists in preventing fire and minimizing losses in the event of fire, avoiding significant damage to the element of a structure. This can be achieved through active and passive measures, using the design of fire-resistant materials in construction and eventually protect the structural elements.

Among the most common means of prevention suggested by engineers of this field for construction, one possible solution is the use of PEC (Partially Encased Columns)**.**

1-2 Composite columns

Composite columns as shown in the figure 1 below, are a column, made by a structural steel profile and a reinforced concrete applied between flanges. These types of columns combine the mechanical properties of steel with that of concrete, resulting in better structural performance than traditional columns, made of steel sections, because the concrete portion is known to increase fire resistance, mainly due to his small thermal conductivity.

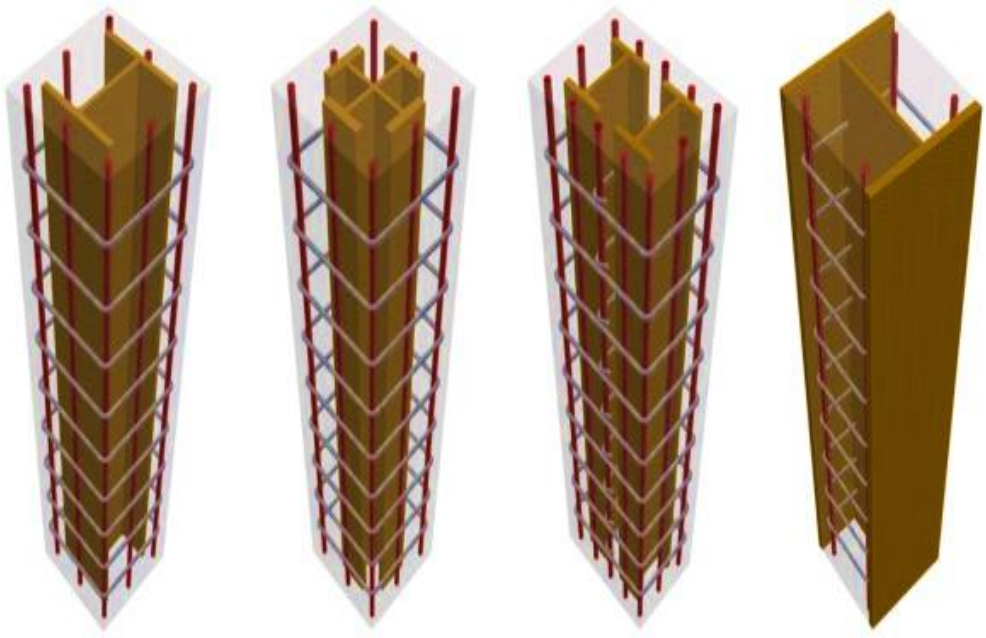

a) *Embeded I-shape* *b) Embeded Cruciform* *c) Embeded Twin-section* *d) Partially encased*

Figure 1: Types of mixed columns

1-3 Objectives of study

The mechanical properties of the materials used for partially encased columns show a decrease in the values when subjected to high temperatures under fire situations. The fire resistance is difficult to determine on PEC due to the non uniform temperature field obtained in the cross section. To overcome this difficulty, the effect of the temperature may be determined on the 4 componentes of PEC, for a specified fire rating (R30, R60, R90 and R120). The strength and the stiffness of each component of the PEC will be evaluated to determinate after the plastic resistance to axial compression and the effective flexural stiffness of the column under fire situation. This process is used to determine the buckling resistance of PEC exposed to fire, which is the main objective of our study.

1-4 Motivation of study

The behavior of columns and beams under fire situation has been studied by several authors in recent years, but specifically for the partially encased columns subjected to fire there are few studies. In view of the work done previously, this work will present a new contribution on the study of the load level on the fire resistance of partially encased columns with the objective of improving existing knowledge in this field.

1-5 Methodology of the study

To study the behavior of partially encased columns and to determine the buckling resistance under fire situation, three different series of profiles (HEA, HEB and HD) have been used with 10 different cross section of each profile. Two different column lengths have been selected, (3-4) meter, submitting them to a fire resistance rating of (30, 60, 90 and 120 minutes). The choice of profiles was made according to the scope of application of Annex G from the EN1994-1-2 [1].

In this context, three different methods will be used to determinate the buckling resistance and after a comparison between them is presented. Starting by the balanced summation model, which is a simple calculation method presented in the annex G from EN1994-1.2, using a weighted sum of the strength and stiffness of the four components existing in the cross section of the columns (flanges, web, concrete and reinforcing bars) subjected to the fire curve standard ISO834 [2]. After a numerical simumaltion, new formulas will be presented for this simplified method. These new equations and parameters should correct unsafe results and oversized results given by the current version of EN1994-1.2. This new proposal is based on the results obtained by numerical simulations based on the finite element method, using models developed by ANSYS (Mechanical APDL) version 18 release 1 [3]. The non-linear transient thermal simulations allow to obtain the temperature distribution in the profile for 4 levels of fire resistance classes (R30, R60, R90 and R120) with more accurate results then other simplified methods.

1-6 Organization of the thesis

This thesis is organized in seven chapters which are described in the outline in the following paragraph:

Chapter 1 presnets an introduction to the field studied and the framework of the project. Defines the main objectives of the study, describes the methodology used to carry out the research and presents the state of the art.

Chapter 2 defines the mechanical and thermal properties of the partially enacsed columns, and its four components at elevated temperature. The action of the fire is also explained.

Chapter 3 presents the simplified calculation method according to the Annex G from EN 1994-1-2[1].

Chapter 4 shows the improvement proposed for the balanced summation method, presenting for each component new equations and parameters developed.

Chapter 5 presents the advanced calculation method using the ANSYS [3] program and the results obtained on this numerical simulation.

Chapter 6 presents a comparison between the current model and the improvement made and the numerical model.

Chapter 7 presents a conclusion and future proposition.

1-6 State of the art

The lack of information on the effect of the load level on the fire resistance of partially encased columns is noted but some research by authors carried out on topics are relevant to this study and contributed to the advance of knowledge in this field.

In 1964, R. F. Stevens and H. L. Malhotra [4] carried out a study showing the effect of fire resistance of totally encased columns, considering the recommendations of the British standard BS 449. The authors concluded, among other things, that the fire resistance of the encased columns is approximately inversely proportional to the applied load and that the concrete with light weight concrete (LWC) subjected to high temperature suffers less physical damage when compared to normal weight concrete (NWC).

In 1984, J.C Dotreppe, J.M Franssen and J.B Schleich [5] presented a study on fire resistance, for steel and mixed structures using finite element methods, using beam elements with subdivision of the cross section in a mesh of quadrilaterals, subjected to ISO834 curve and analyzed by increment, with the Newton-Raphson method. The comparison of theoretical and experimental results was carried out for a mixed beam, obtaining good results, in situations of low and medium temperatures, requiring an improvement in the model for high temperatures.

In 1987, J. B. Schleich [6] was the project leader of an important experimental and numerical campaign developed to test and analyse the behaviour of Partially Encased Columns (PEC) and Beams (PEB) with different connection to the slab. This project demonstrated the possibilities of the computer code CEFICOSS- which means "Computer Engineering of the Fire resistance for Composite and Steel Structures", able to cover most structural fire applications. This program CEFICOSS must be considered as a general thermo-

mechanical numerical Computer code allowing to predict the behaviour under fire conditions of structural building parts such as columns, beams, or frames. These structural elements could be composed either of bare steel profiles or of steel sections protected by any insulation, either of any composite cross-section type.

In 1989, K. Kordina [7] presented tables to be used as guides for design of composite columns subjected to fire, based on full-scale experiments. These results were verified in the partially encased columns and beams, for a certain degree of utilization (load level), support conditions and materials at different times of fire resistance.

In 1990, T. T. Lie and M. Chabot [8] presented an article that described a mathematical model for steel columns filled with concrete, developed for calculating temperature, deformation and fire resistance. The results obtained through the mathematical model were compared with experimental results. For the mathematical model, the standard fire curve present in ASTM-E119 and thirty column models were used, being compared with five experimental tests. As a result, they managed to obtain a mathematical model that suited the experimental results, being able to predict the fire resistance of circular steel columns filled with concrete. Resistance of the columns were compared with those of the plain and bar-reinforced concrete.

In 2002, S. Winter and J. Lange [9] presented a study where tests were carried out on mixed columns partially coated using a high-strength steel profile, subjected to high temperatures. The results were compared to the design formulas of the German standards, but with the existing data they have failed to prove the reliability of the standards. The authors came to the conclusion that high temperatures cause an extreme weakening in resistance, greatly reducing the efficiency of columns made with high-strength steel

In 2010, António Correia and João Paulo Rodrigues [10] presented the results of a series of fire resistance tests on composite partially encased columns with restricted thermal elongation. An experimental setup was designed at the University of Coimbra in Portugal, so that the axial restraint system and column rotation are similar to the conditions in a real building. The parameters studied were the load level, the axial and rotation retention indexes and slenderness. The main conclusion of this work was that, for low load levels, the stiffness of the surrounding structure has a great influence on the behavior of columns subject to fire.The increased rigidity of the surrounding structure tends to reduce the critical time. The critical time was defined exactly as the moment when the axial loading reaches the load initially applied. The same behavior was not observed for the higher load levels.

In 2013, S. Huang, B. Davison and I. W. Burgess [11] presented a study on connections between metal beams and columns with H profile, both encased and partially encased with concrete, subjected to high temperatures. The tests aimed to investigate the behavior of connections between beams and columns, subject to connection and torsional forces in fire situations, providing data for validation and development of simplified connection models, based on the components.

It has been found that reverse-channel connections provide not only high strength, but also the high ductility which is required to reduce the possibility of connection fracture and to improve the robustness of buildings in fire.

Still in 2013, P. A.G. Piloto et al. [12] carried out an experimental investigation on the fire resistance of composite beams partially encased with concrete, using twelve experimental

tests, according to the European Standard EN1363-1 exposure to fire ISO834 standard, preceded by three tests at room temperature to assess the resistance the load of partially coated beams. As the author expected, fire resistance decreased as the load level increased. The results obtained provided essential data for the validation and calibration of new simplified models, tabulated data and advanced numerical methods.

In 2014, S. Arezki and I. Said [13], showed a study on the resistance design of a partially coated column using the simplified method of annex G of the European Standard EN 1994-1-2, using a practical method based on Campus-Massonet criterion, adapted for calculating buckling resistance of columns with eccentric load. It was found that the fire resistance of a partially coated column, subjected to an eccentric load, gradually decreases with the increase in the load level, the slenderness ratio or the amount of eccentricity.

In 2015, P. A. G. Piloto et al. [14], presented a study on partially encased columns under fire situations, where new equations were proposed to improve the simplified calculation method presented in Annex G of EN 1994-1-2, in order to calculate the plastic resistance to axial compression and the effective flexural stiffness of the composite column. Using a series of IPE and HEB profiles, numerical thermal simulations were performed as a comparison method demonstrating that there are unsafe values in the current version of EN1994-1.2.

On the same year of 2015, M. Milanović, M. Cvetkovska and P. Knežević [15], presented an article on the resistance of three different configurations of composite columns (Totally encased, Partially encased with concrete) subjected to fire, comparing them to a reinforced concrete column of reference. Analyzing the heat absorption, it was found that partially encased columns have the highest absorption of heat, due to the metal being in direct contact with the fire which reduces its load bearing capacity, decreasing its resistance to fire. At room temperature and for the same cross-sectional dimensions, it is the configuration with the greatest resistance due to the large percentage of the steel profile in the cross section.

In 2016, Piquer and Hernandez-Figueirido [16] conducted a study of columns of metallic profile I, with and without fire protection and mixed columns partially coated, focusing on the performance and monetary cost of these columns. The considerations regarding the geometry and the materials described used European standards and commercial materials. The results obtained by checking the resistance and stability of columns exposed to fire demonstrated that the worst performances were those of steel without passive coating, whereas coated columns and partially coated columns performed well at high temperatures. The results also demonstrated that a column with a partially coated mixed profile has the best cost-benefit ratio, since it saves about 50% when compared to the other two types when exposed to the fire with times over 30 minutes for HE profiles and 120 minutes for HP profiles. This conclusion stems from the fact that the best protective materials are expensive at the final cost.

On the same year on 2016, Králik et al [17] published a work on the design of steel and mixed steel and concrete columns in a fire situation considering the geometric non-linearity of the material. The work presented a structural analysis using the ANSYS software resolving the finite element method, using the elements “SOLID65”, “SHELL181” and “LINK180” the columns were modeled according to the ISO834 curve. As a result, the authors analyzed the fire resistance of the two types of pillars. The fire resistance was

calculated by fixing a requesting load and looking for the ultimate resistance of the section, where it was evident that the mixed pillar obtained a better fire performance

Still in 2016, A. Fellouh et al. [18] presented a study on partially encased columns under fire situations, where new equations were proposed to improve the simplified calculation method presented in Annex G of EN 1994-1-2[1]. The study presents numerical simulations with 3D models, solved in two stages, first finding thermal results of temperature distribution in the element of two different series of IPE and HEB profiles, and second finding the resistance to buckling under fire conditions. With the results obtained, new equations and parameters have been proposed to correct some unsafe points present on the EN1994.1-2 and concluded that the buckling curve "c", proposed in the EN1993.1-1, is not adequate.

In 2017 P.A.G Piloto et al [19] published an article on experimental tests on partially coated beams subjected to high temperatures, the lateral flexion performance of twenty-seven beams at different temperature levels was presented, using the four point bending configuration. From this study, it was verified that it is necessary to include the lateral torsional curving failure mode in partially coated beams in Eurocode 4 for mixed steel and concrete structures exposed to fire.

On the same year on 2017, L. Calió, P. Piloto and R. Rigobello [20], with the intention to improve Fellouh's study in 2016, studied the effects of strength and stiffness of PEC of a series of HEB and IPE profiles, based on the simplified calculation method presented in Annex G of EN 1994-1-2[1]. New formulas and parameters were proposed for the balanced summation method. It was concluded that the EN1994-1.2 presents some unsafe results, and with the new formulations proposed, safer values are obtained, compared to the results of advanced calculation models.

In 2018, B. Afredo, P.A.G. Piloto and D. Rossetto [21], presented a new study with the intention to improve Calio's work in 2017. They studied the behavior of 3 different series of (HEB, HD and UD) profiles of partially encased columns under fire situation. They proposed new formulas and parameters for the balanced summation method from Annex G of EN 1994-1-2[1]. It was concluded, in agreement with the Calio's previous study, that except for the fire resistance class of 30 minute, the EN 1994-1.2 presents some unsafe points for the profiles with a higher section factor, and large dimensions.

2- PARTIALLY ENCASED COLUMNS UNDER FIRE

Partially encased columns (PEC) as shown in the figure 2 below, are made generally by a hot-rolled metal profile of type I or H, with a concrete infilled between the flanges and reinforced by bars. Both components combine together giving great flexural stiffness and axial resistance without increasing the dimension of the cross section. In addition to the structural mechanical advantages, the added concrete increases the fire resistance of these structures.

Furthermore, partially encased columns have higher load capacity than simple structural steel columns and in generally the composite elements of steel and concrete are the most used in construction of modern buildings in the last century.

Figure 2: Example of partially encased columns[22]

2-1 Field of application

Within the framework of this thesis, 30 different cross sections of 3 Steel profiles (HEA – HEB – UD) were selected, with 2 different height (3 - 4) meter of the column for each series, in order to analyze the effect of the fire on the PEC, as presented in the table 1 below.

The model's scope of application restricts the choice of profiles according to European standard EN 1994-1-2[1] with the following conditions:

		Buckling length l_θ	≤	13.5 b
230 mm	≤	Height of cross section h	≤	110 mm
230 mm	≤	Width of cross section b	≤	500 mm
1 %	≤	Percentage of reinforcing steel	≤	6 %
		As / As+Ac **[%]**		
		Standard fire resistance	≤	120 min

With *As : Area of the reinforcing bars*
Ac : Area of the concrete

Profiles	h [m]	b [m]	e_f [m]	e_w [m]	*Bars* ϕ [m]	*As / As+Ac* [%]
HEA 240	0.23	0.24	0.012	0.0075	0.02	2.64%
HEA 280	0.27	0.28	0.013	0.008	0.025	2.98%
HEA 300	0.29	0.3	0.014	0.0085	0.025	2.59%
HEA 360	0.35	0.3	0.0175	0.01	0.025	2.16%
HEA 400	0.39	0.3	0.019	0.011	0.025	1.94%
HEA 450	0.44	0.3	0.021	0.0115	0.032	2.82%
HEA 500	0.49	0.3	0.023	0.012	0.032	2.53%
HEA 600	0.59	0.3	0.025	0.013	0.032	2.08%
HEA 700	0.69	0.3	0.027	0.0145	0.04	2.78%
HEA 800	0.79	0.3	0.028	0.015	0.04	2.41%
HEB 240	0.24	0.24	0.017	0.01	0.02	2.67%
HEB 280	0.28	0.28	0.018	0.01	0.025	2.95%
HEB 300	0.3	0.3	0.019	0.011	0.025	2.61%
HEB 360	0.36	0.3	0.0225	0.0125	0.025	2.18%
HEB 400	0.4	0.3	0.024	0.0135	0.025	1.96%
HEB 450	0.45	0.3	0.026	0.014	0.032	2.84%
HEB 500	0.5	0.3	0.028	0.0145	0.032	2.55%
HEB 600	0.6	0.3	0.03	0.0155	0.032	2.10%
HEB 700	0.7	0.3	0.032	0.017	0.04	2.80%
HEB 800	0.8	0.3	0.033	0.0175	0.04	2.43%
HD 260x54.1	0.244	0.26	0.0095	0.0065	0.02	2.22%
HD 260x142	0.278	0.265	0.0265	0.0155	0.02	2.26%
HD 320x127	0.32	0.3	0.0205	0.0115	0.025	2.46%
HD 320x198	0.343	0.306	0.032	0.018	0.025	2.46%
HD 320x300	0.375	0.313	0.048	0.027	0.025	2.48%
HD 400x237	0.38	0.395	0.032	0.0189	0.032	2.68%
HD 400x382	0.416	0.406	0.048	0.0298	0.032	2.68%
HD 400x551	0.455	0.418	0.0676	0.042	0.032	2.68%
HD 400x818	0.514	0.437	0.097	0.0605	0.032	2.67%
HD 400x1299	0.6	0.476	0.14	0.1	0.032	2.68%

Table 1: Parameters of profiles studied.

50 mm was selected as the value for the geometrical average parameter ($\boldsymbol{u} = \sqrt{u_1.u_2}$) of the axial distances u_1 and u_2 of the bars, with respect to the outer borders of the concrete as presented in the figure 3.

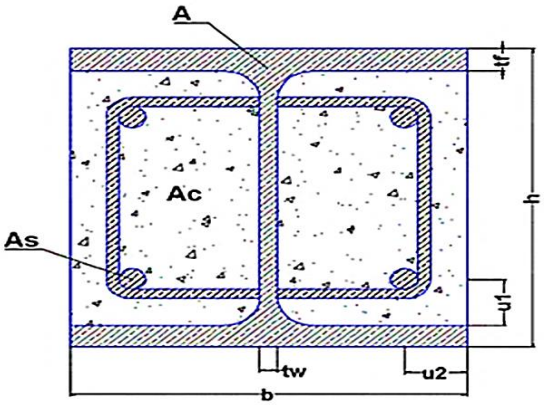

Figure 3: Cross section of PEC

2-2 Materials properties

Steel grade S275 is commonly used for hot rolled and has been selected to steel profile, while the steel grade B500 has been used for the reinforcing bars, while C20/25 concrete grade has been considered to normal weight concrete (NC). The properties of these materials are presented in the next sections.

Structural Steel profile S275

According to EN1993-1-1[23], Under normal temperature conditions, the S275 steel hot rolled with thickness less than 40mm, presents the following nominal values of the mechancical properties in table 2:

	E_a [MPa]	f_y [MPa]	f_u [MPa]	G_a [GPa]	v
S275	210	275	0.012	81	0.3

Table 2: Material properties of Steel 275

Normal Weight Concrete C20/25

According to EN1992-1-1[24], at room temperature, the normal weight concrete C20/25 presents the following nominal values of the mechanical properties in table 3:

	f_{ck} [MPa]	$f_{ck,cube}$ [MPa]	f_{cm} [MPa]	f_{ctm} [MPa]	E_{cm} [MPa]	ε_{c1} [%]	ε_{cu1} [%]
C20/25	20	25	28	2.2	30	2.0	3.5

Table 3: Material properties of Concrete C20/25

Reinforcing bars B500

According to European standards Eurocode EN1993-1-1[23], Under normal condition the reinforcing steel for the reinforcing bars S500 NR class B, presents the nominal values of material properties in table 4:

	f_y [MPa]	f_u [MPa]	E_s [m]	k
B500	500	540	210	1.08

Table 4: Materials properties of the reinforced steel

2-2-1 Mechanical properties

The mechanical properties used to determine the material behavior, according to the material which ensures stiffness and resistance and it is necessary to take into account the evolution of the temperature because it implies directly a reduction in the mechanical properties of the materials.

Structural Steel profile S275

According to EN 1993-1-2[25], to consider the effect of high temperatures on the mechanical properties of the steel, the reduction factors for the effective yield strength $\boldsymbol{k_{y,\theta}}$ and to the slope of the linear elastic range $\boldsymbol{k_{E,\theta}}$ are presented in Figure 4 below obtained from table 5.

Steel T $\boldsymbol{\theta_{a/s}}$ [°C]	$\boldsymbol{K_{y,\theta}} = f_{ay,\theta}/f_{ay}$	$\boldsymbol{K_{E,\theta}} = E_{a,\theta}/E_a$
20	1.0000	1.0000
100	1.0000	1.0000
200	1.0000	0.9000
300	1.0000	0.8000
400	1.0000	0.7000
500	0.7800	0.6000
600	0.4700	0.3100
700	0.2300	0.1300
800	0.1100	0.0900
900	0.0600	0.0675
1000	0.0400	0.0450
1100	0.0200	0.0225
1200	0.0000	0.0000

Table 5: Reduction factors $\boldsymbol{K_\theta}$ for stress-strain

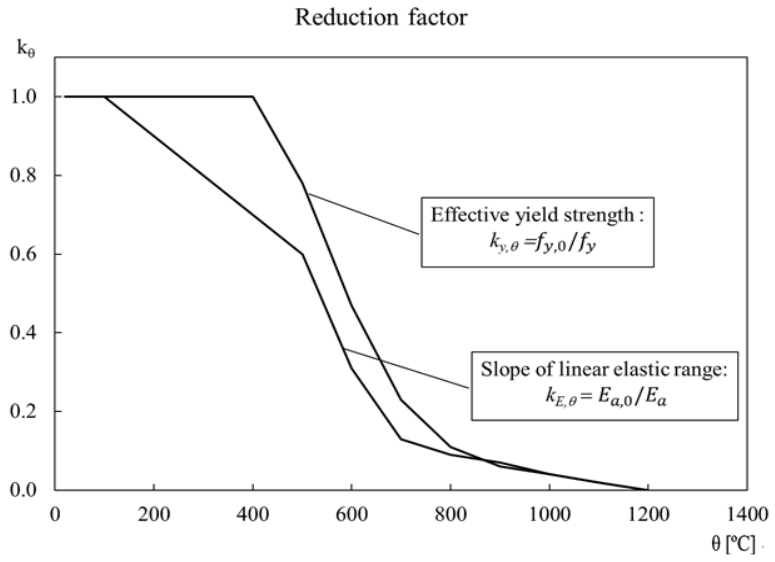

Figure 4: Reduction factor for the mechanical properties

According to European standard 1993-1-2[25], the variation of the stress-strain relationship for the carbon steel at different temperature levels, from T =20 ºC (room temperature) to T = 1200 ºC is presented on the figure 5 where the formulas are presented on the table 6 below.

Stain range	***Stress σ***	***Tangent modulus***
$\boldsymbol{\varepsilon \leq \varepsilon_{p,\theta}}$	$\varepsilon\, E_{a,\theta}$	$E_{a,\theta}$
$\boldsymbol{\varepsilon_{p,\theta} < \varepsilon \leq \varepsilon_{y,\theta}}$	$f_{p,\theta} - c + (b/a)\left[a^2 - (\varepsilon_{y,\theta} - \varepsilon)^2\right]^{0.5}$	$\dfrac{b\,(\varepsilon_{y,\theta} - \varepsilon)}{a\left[a^2 - (\varepsilon_{y,\theta} - \varepsilon)^2\right]^{0.5}}$
$\boldsymbol{\varepsilon_{y,\theta} < \varepsilon \leq \varepsilon_{t,\theta}}$	$f_{y,\theta}$	0
$\boldsymbol{\varepsilon_{t,\theta} < \varepsilon \leq \varepsilon_{u,\theta}}$	$f_{y,\theta}\left[1 - (\varepsilon - \varepsilon_{t,\theta})/(\varepsilon_{u,\theta} - \varepsilon_{t,\theta})\right]$	-
$\boldsymbol{\varepsilon = \varepsilon_{u,\theta}}$	0.00	-
Parameters	$\varepsilon_{p,\theta} = f_{p,\theta}/E_{a,\theta}$ $\quad \varepsilon_{y,\theta} = 0.02$ $\quad \varepsilon_{t,\theta} = 0.15$ $\quad \varepsilon_{u,\theta} = 0.20$	
Functions	$a^2 = (\varepsilon_{y,\theta} - \varepsilon_{p,\theta})(\varepsilon_{y,\theta} - \varepsilon_{p,\theta} + c/E_{a,\theta})$ $b^2 = c\,(\varepsilon_{y,\theta} - \varepsilon_{p,\theta})E_{a,\theta} + c^2$ $c = \dfrac{(f_{y,\theta} - f_{p,\theta})^2}{(\varepsilon_{y,\theta} - \varepsilon_{p,\theta})E_{a,\theta} - 2(f_{y,\theta} - f_{p,\theta})}$	

Table 6: Stress-strain formulas for carbon steel at elevated temperature.

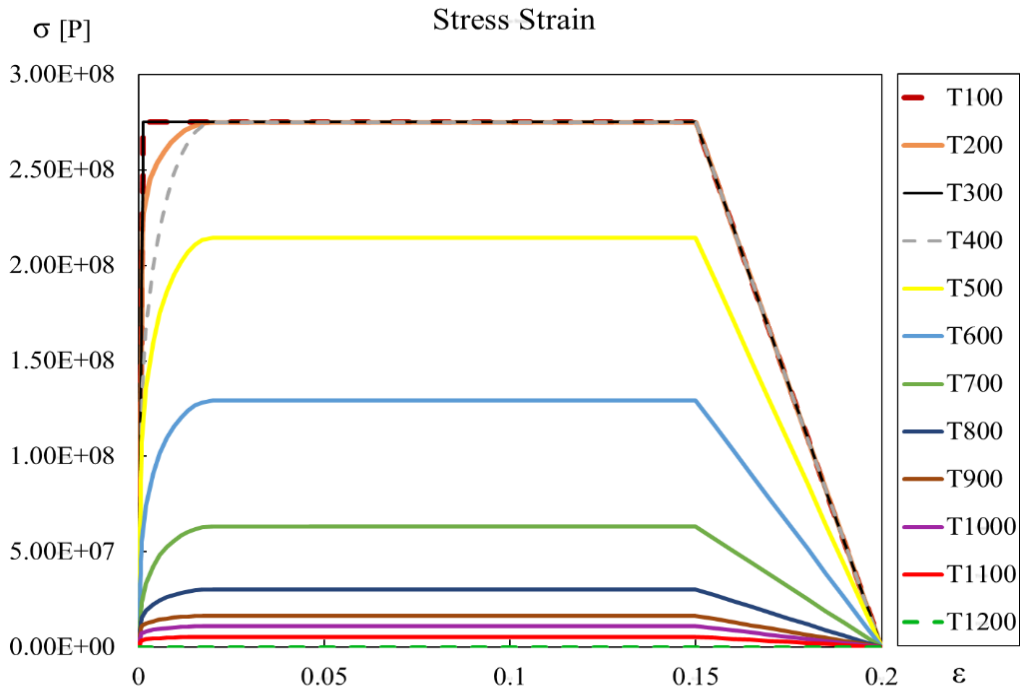

Figure 5: Stress-strain relationship for carbon steel at elevated temperature.

Normal Weight Concrete C20/25

According to EN 1994-1-2[1], the values for the yield strength reduction factor $\boldsymbol{k_{c,\theta}}$ of the stress-strain relationships of normal weight concrete (NC) at elevated temperatures, which affect directly the mechanical properties, are represented graphically on the figure 6 and taken from table7.

Concrete Temperature $\boldsymbol{\theta_c}$ [°C]	$\boldsymbol{K_{c,\theta} = f_{c,\theta}/f_c}$	$\boldsymbol{\varepsilon_{cu,\theta}}$
20	1.00	0.0025
100	1.00	0.0040
200	0.95	0.0055
300	0.85	0.0070
400	0.75	0.0100
500	0.60	0.0150
600	0.45	0.0250
700	0.30	0.0250
800	0.15	0.0250
900	0.08	0.0250
1000	0.04	0.0250
1100	0.01	0.0250
1200	0.00	-

Table 7: Reduction factors for stress-strain of concrete

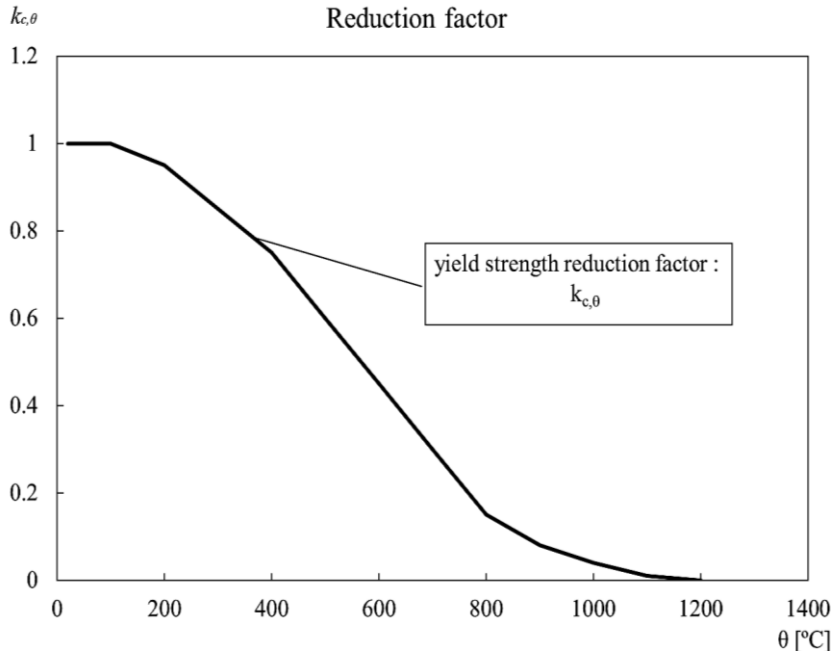

Figure 6: Reduction factor for mechanical properties for the concrete

According to European standard 1994-1-2[1], the variation of the stress-strain relationship for the concrete C20/25 for different temperature levels from T = 20 ºC (room temperature) to T = 1200 ºC under compression is presented on the figure 7 where the formulas are presented on the table 8:

Range	***Stress σ(θ)***
$\boldsymbol{\varepsilon \leq \varepsilon_{c1,\theta}}$	$\dfrac{3\,\boldsymbol{\varepsilon}\, \boldsymbol{f_{c,\theta}}}{\boldsymbol{\varepsilon_{c1,\theta}}\left(\mathbf{2}+\left(\dfrac{\boldsymbol{\varepsilon}}{\boldsymbol{\varepsilon_{c1,\theta}}}\right)^{\mathbf{3}}\right)}$
$\boldsymbol{\varepsilon_{c1,\theta} < \varepsilon \leq \varepsilon_{cu1,\theta}}$	For numerical purposes a descending branch should be adopted. Linear or non-linear models are permitted.

Table 8: Stress-strain relationships of concrete elevated temperature

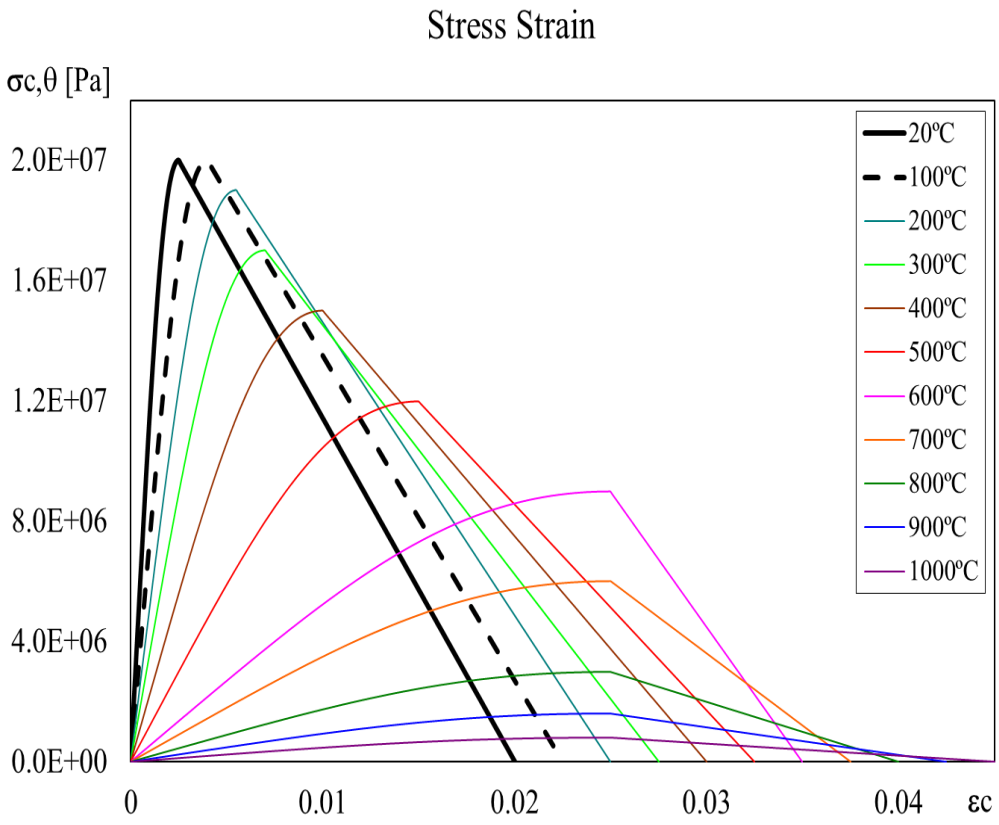

Figure 7: Stress-strain relationships of concrete elevated temperature

Reinforcing bars B500

According to EN 1994-1-2[1], to consider the effect of high temperatures on the mechanical properties of the rebars, the reduction factors for the effective yield strength $\boldsymbol{k_{sy,\theta}}$ and to the slope of the linear elastic range $\boldsymbol{k_{SE,\theta}}$ are illustrated in Figure 8 below and obtained from table 9.

Steel Temperature $\boldsymbol{\theta_{a/s}}$ **[°C]**	$\boldsymbol{K_{sy,\theta}} = f_{sy,\theta}/f_{sy}$	$\boldsymbol{K_{sE,\theta}} = E_{s,\theta}/E_s$
20	1.00	1.00
100	1.00	1.00
200	1.00	0.87
300	1.00	0.72
400	0.94	0.56
500	0.67	0.40
600	0.40	0.24
700	0.12	0.08
800	0.11	0.06
900	0.08	0.05
1000	0.05	0.03
1100	0.03	0.02
1200	0.00	0.00

Table 9: Reduction factors $\boldsymbol{K_\theta}$ for stress-strain

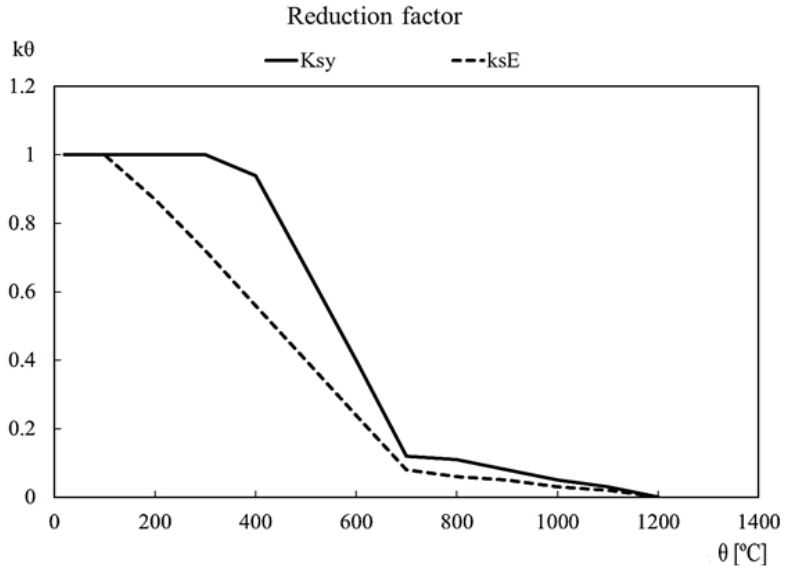

Figure 8: Reduction factor for the mechanical properties

According to the EN 1994-1-2[1], the values for relationship stress strain for the reinforcing steel can be applied in the same way than structural steel and its obtained from the formulas presented on the table 6 for carbon steel, and its presented graphically on the Figure 9.

2-2-2 Thermal properties

The thermal properties show the interaction between the material and the heat flow under fire situation. European standards present the thermal properties of the materials and their variations with the temperature.

Structural and reinforcing Steel profile

According to European standard 1993-1-2[26], the specific heat of structural steel, $\boldsymbol{C_a}$ **[J/kg.k]** is also valid for reinforcing steel. This property is defined by the amount of energy that is necessary to raise the unit mass of steel temperature by 1 degree °C. It is also the measure of the materials ability to absorb heat and its obtained following the equations:

$20[°C] \leq \theta \leq 600[°C]$

$$\boldsymbol{C_a} = 425 + 7{,}73.10^{-1}\theta_a - 1{,}69.10^{-3}\theta_a^2 + 2{,}22.10^{-6}\theta_a^3 \quad (1)$$

$600[°C] \leq \theta \leq 735[°C]$

$$\boldsymbol{C_a} = 666 + \frac{13002}{(738-\theta_a)} \quad (2)$$

$735[°C] \leq \theta \leq 900[°C]$

$$\boldsymbol{C_a} = 545 + \frac{17820}{(\theta_a-731)} \quad (3)$$

$900[°C] \leq \theta \leq 1200[°C]$

$$\boldsymbol{C_a} = 650 \quad (4)$$

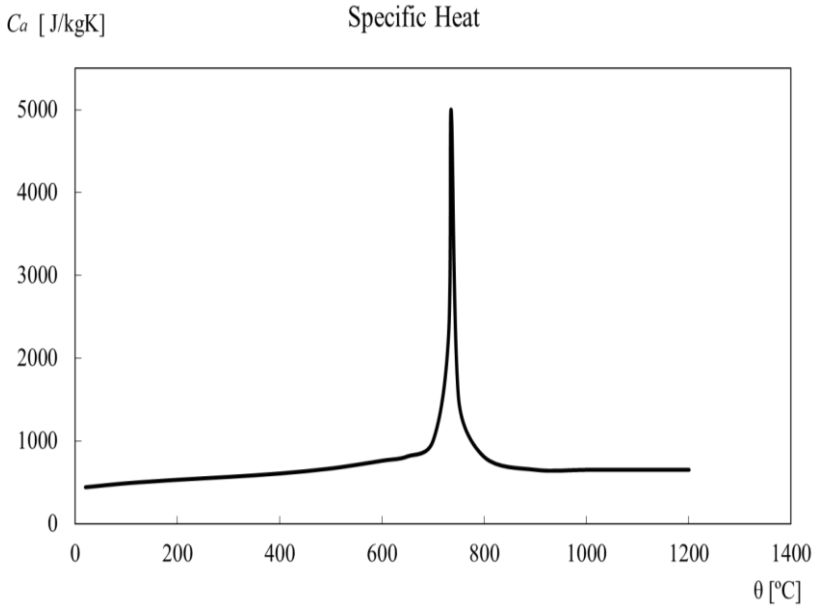

Figure 9: Specific Heat of steel at elevated temperature

According to EN 1993-1-2[26], the thermal conductivity of the steel λ_a [W/mk] is obtained from the following equations and its variation depends on the temperature level, being represented graphically in Figure 11.

$20[°C] \leq \theta \leq 600[°C]$

$$\boldsymbol{\lambda_a} = 54 - 3.33.10^{-2}\theta_a \quad (5)$$

$600[°C] \leq \theta \leq 735[°C]$

$$\boldsymbol{\lambda_a} = 54 - 3.33.10^{-2}\theta_a \quad (6)$$

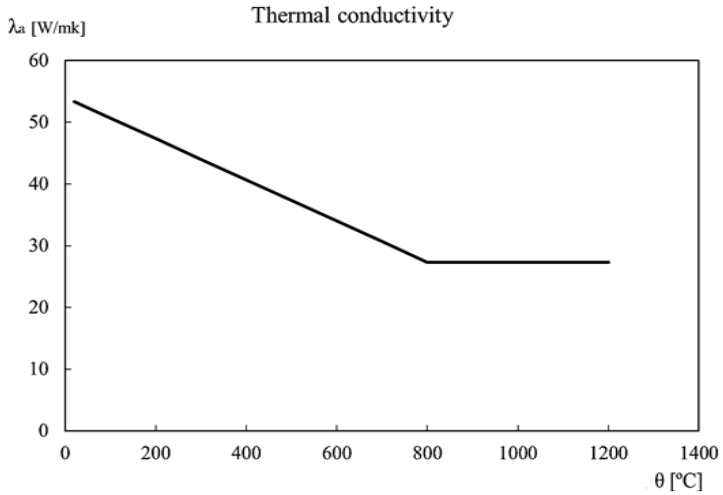

Figure 10: Thermal conductivity of steel at elevated temperatures

According to EN1993 part 1-2[26], the specific mass of steel is constant ρ=7850 kg/m^3 and doesn't vary with temperature, its represented in Figure 12:

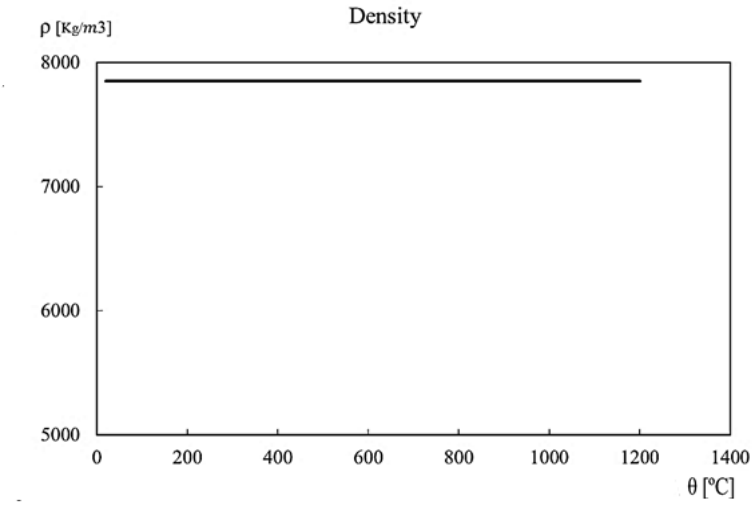

Figure 11: Specific mass of steel at elevated temperature

Concrete Siliceous aggregates C20/25

According to EN1992 part 1-2[27], the specific heat *(C_p)* [J/kg.K] of conventional dry Concrete with siliceous aggregates (u = 0%), can be determined through the following equations in which θ_c represents the temperature of the concrete in [ºC] :

$$20[ºC] \leq \theta_c \leq 100[ºC]$$

$$\boldsymbol{C_p} = 900 \tag{7}$$

$$100[ºC] < \theta_c \leq 200[ºC]$$

$$\boldsymbol{C_p} = 900 + (\theta_c - 100) \tag{8}$$

$$200[ºC] < \theta_c \leq 400[ºC]$$

$$\boldsymbol{C_p} = 1000 + (\theta_c - 200)/2 \tag{9}$$

$$400[ºC] < \theta_c \leq 1200[ºC]$$

$$\boldsymbol{C_p} = 1100 \tag{10}$$

While the moisture content is not considered explicitly in the calculation method, the function given for the specific heat of concrete with siliceous aggregates may be modelled by a constant value, ($C_{p,peak}$) situated between 100°C and 115°C with linear decrease between 115°C and 200°C.

In the present work, a moisture content of 3% was considered for the concrete, *where*:

$$C_{p,peak}(u = 3\%) = 2020 \text{ [J/kg.K]}$$

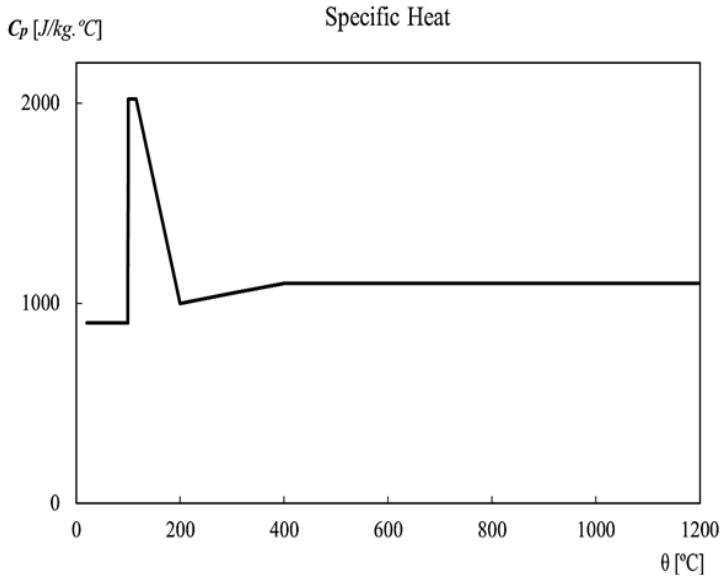

Figure 12: Specific Heat of concrete at elevated temperature

According to the standard EN 1994-1-2[1], the thermal conductivity of concrete λ_c [w/mk] must be determined between its lower and upper limits depending on the temperature rise from the following equations in chich θ_c is the temperature of the concrete in [°C]:

For : 20[°C] $\leq \theta_c \leq$ 1200[°C]

The upper limite

$$\boldsymbol{\lambda_c} = 2 - 0.2451(\theta_c/100) + 0.0107(\theta_c/100)^2 \quad (11)$$

The lower limite

$$\boldsymbol{\lambda_c} = 1.36 - 0.136(\theta_c/100) + 0.0057(\theta_c/100)^2 \quad (12)$$

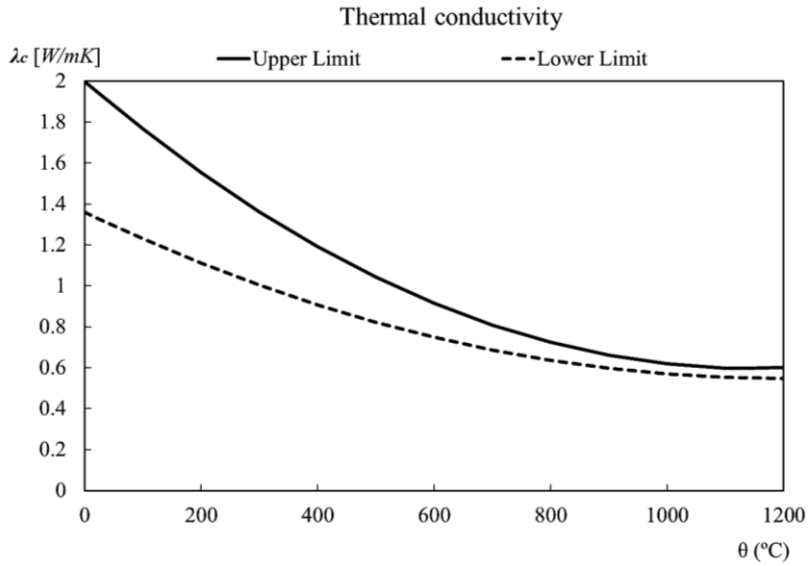

Figure 13: Thermal conductivity of concrete at elevated temperature

2-3 Fire Actions

This study is focused on the behavior of partially encased columns under fire actions. In this sense, it is important to know the actions of fire, as well as their means of heat transfer and how they affect the resistance of elements of the structure.

2-3-1 Heat transfer

According to EN 1991-1-2[28], the total heat flux which is the net heat flux per unite surface $\dot{\boldsymbol{h}}_{\boldsymbol{net,d}}$ [w/m2] is obtained from the following equation, where all surfaces exposed to fire must assume the heat transfer by convection and radiation:

$$\dot{h}_{net,d} = \dot{h}_{net,c} + \dot{h}_{net,r} \quad (13)$$

$\dot{h}_{net,c}$ [w/m^2] is the convective heat transfer, defined by the transfer of heat from one place to another by the fluid's movement, given by Newton's law of cooling in Equation (14)

$$\dot{h}_{net,c} = \alpha_c \, (\theta_g - \theta_m) \tag{14}$$

With: α_c equal to 25 [w/m^2] (surfaces exposed to the ISO834 fire curve),
θ_g is the gas temperature in [ºC].
θ_m is the surface temperature of the component in [ºC].

$\dot{h}_{net,r}$ [w/m^2] is transfer of heat by electromagnetic waves which depends on the differences of the individual body surface temperatures to the fourth power, given by Equation (15):

$$\dot{h}_{net,r} = \phi . \varepsilon_m . \varepsilon_f . \sigma \, [(\theta_r + 273)^2 - (\theta_m + 273)^4] \tag{15}$$

With: ϕ = 1 (all sides of the column are directly exposed to fire), ε_m = 0.7 (the emissivity of the material for steel and concrete) ε_f = 1.0 (the emissivity of the flames) θ_r is the temperature's surface of element that receives the radiation[ºC] and θ_m is the temperature of fire environment [ºC]

2-4-2 Fire Curves

According to Valdir Silva [29], the main characteristic of a fire, when will analyze its influence on structures, it is the temperature curve as a function of time.

Natural fire curve

Unlike the nominal fire curve, a natural fire model considers how the environment, density of combustible materials and ventilation will affect the development of the fire, with a heating and cooling phase According to European standard EN1991-1-2[28] :

The temperature-time curves in the heating phase are given by eq. (16):

$$\theta_g = 20 + 1325 \, (1 - 0.324 \, e^{-0.2t^*} - 0.204 \, e^{-1.7t^*} - 0.472 \, e^{-19t^*}) \tag{16}$$

where θ_g = is the gas temperature in the fire compartment.
$t^* = t \, . \, \Gamma$

with : $\Gamma = \left[A_v \sqrt{h_{eq}/A_t} / \sqrt{\rho c \lambda}\right]^2 / (0.04/1160)^2$

A_v is total area of vertical openings on walls
h_{eq} is weighted average of window heights on all walls
A_t is total area of enclosure

The temperature-time curve in the cooling phase are presented following the equations below:

$$\begin{array}{rl} t^*_{max} \leq 0.5 & \theta_g = \theta_{max} - 625(t^* - t^*_{max} - x) \\ 0.5 < t^*_{max} < 2 & \theta_g = \theta_{max} - 250(3 - t^*_{max})(t^* - t^*_{max} - x) \\ t^*_{max} \geq 0.5 & \theta_g = \theta_{max} - 250\,(t^* - t^*_{max} - x) \end{array}$$

Where: $t^*_{max} = (0.2\ 10^{-3}.q_{t,d}/O).\Gamma$ *With:* $q_{t,d} = q_{f,d}\,.A_f/A_t$

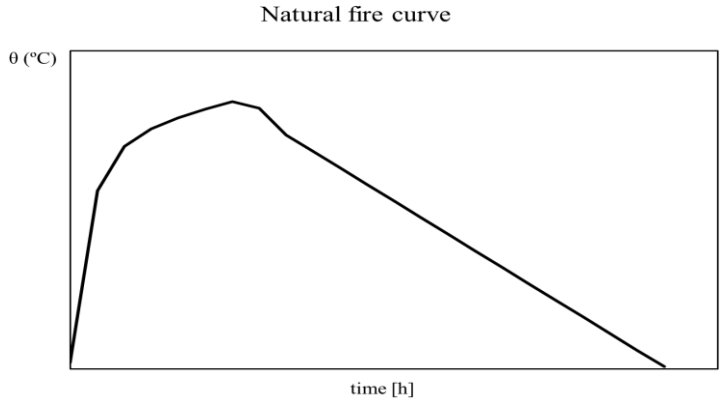

Figure 14: Natural fire curve

Nominal fire curve

According to the EN 1991-1-2[28], and in accordance with ISO834-1[2] the standard time-temperature curve which is the simplest way to represent a fire event. Is recommended for determining fire resistance for structural elements and the gas temperature inside the furnace should follow the equation (17):

$$\theta_g = 20 + 345\ log_{10}(8t + 1) \qquad (17)$$

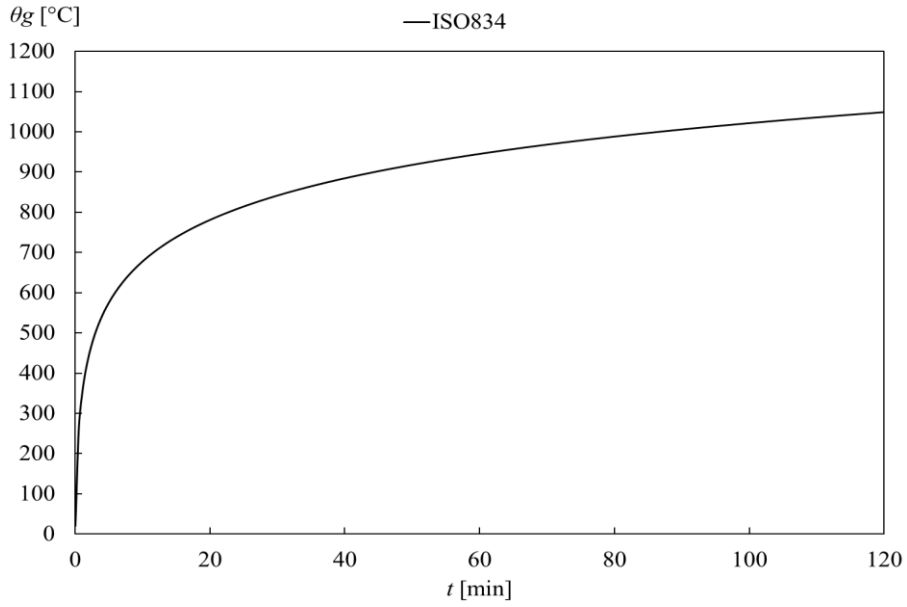

Figure 15: Nominal fire curve

3- SIMPLIFIED CALCULATION METHOD USING EUROCODE 4_ANNEX G

The EN1994-1-2[1] presents different ways for calculating the buckling resistance for various types of composite columns under standard fire ISO834 [2]. The Annex G presents the balanced summation model, which was originally developed by O. Jungbluth [30] in 1982, with the objective to determine the load bearing capacity of partially encased columns (PEC) in a fire event.
The current approach of this simplified method is defined in Annex G on EN 1994-1.2 [1] and is based on simple formulas and empirical coefficients that seem to be unsafe.

3-1 Balanced summation model

The principle of the simplified calculation method is to divide the cross section into four components which are: The flanges of the steel profile, represented by (f); the web of the steel profile (w); the concrete confined by the profile (c) and the reinforcing bars (s). The cross section is assumed to be exposed to the standard fire, and the load bearing capacity may be determined for R30, R60, R90 and R120 fire effect, assuming the fire by four sides of the profile.

Each component has a specific calculation method to determine the plastic resistance to axial compression and to determine the effective flexural stiffness. This method is based on the evolution of the temperature, so that all can be added in a balanced summation in order to determine the buckling resistance in a standar fire condition, according to the equations (18) and (19).

$$N_{fi,pl,Rd} = N_{fi,pl,Rd,f} + N_{fi,pl,Rd,w} + N_{fi,pl,Rd,c} + N_{fi,pl,Rd,s} \quad (18)$$

$$(EI)_{fi,eff,z} = \varphi_{f,\theta}(EI)_{fi,f,z} + \varphi_{w,\theta}(EI)_{fi,w,z} + \varphi_{c,\theta}(EI)_{fi,c,z} + \varphi_{s,\theta}(EI)_{fi,s,z} \quad (19)$$

where $\boldsymbol{\varphi_{i,\theta}}$ is a reduction coefficient depending on the effect of thermal stresses. The values of $\varphi_{i,\theta}$ for each component are given in Table 10.

Standard fire resistance class	$\varphi_{f,\theta}$	$\varphi_{w,\theta}$	$\varphi_{c,\theta}$	$\varphi_{s,\theta}$
R30	1.0	1.0	0.8	1.0
R60	0.9	1.0	0.8	0.9
R90	0.8	1.0	0.8	0.8
R120	1.0	1.0	0.8	1.0

Table 10: Reduction coefficients for bending stiffness

After determining the plastic resistance to axial compression and the effective flexural stiffness for each component, it is necessary to calculate the critical axial compression resistance or Euler buckling load ($N_{fi,cr,z}$) using equation (20).

$$N_{fi,cr,z} = \pi^2 (EI)_{fi,eff,z} / L_\theta^2 \quad (20)$$

Where: L_θ the buckling length which depends on the boundary conditions from figure 16.

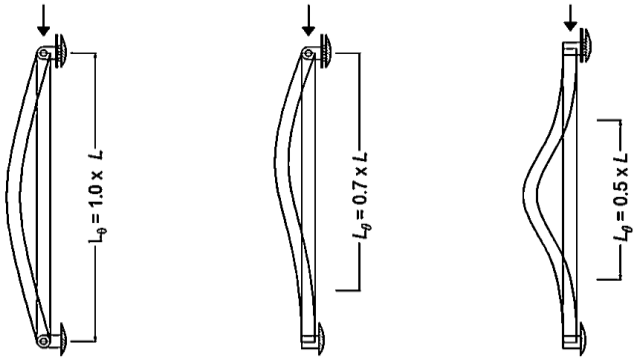

Figure 16: The boundary conditions

Thus, Euler's buckling load calculated around the Z axis and plastic resistance to axial compression under fire, the non-dimensional slenderness ratio is obtained from the equation (21):

$$\bar{\lambda}_\theta = \sqrt{N_{fi,pl,R} / N_{fi,cr,z}} \tag{21}$$

Where $N_{fi,Rd,z} = N_{fi,pl,Rd}$

The partial safety factors $\gamma_{M\,fi,a}$, $\gamma_{M\,fi,c}$, $\gamma_{M\,fi,s}$ are taken as 1.0

Using $\bar{\lambda}_\theta$ and the buckling **curve c** of EN 1993-1-1[13], one can find the reduction coefficient χ_z , used for the axial buckling design load in the fire event (22):

$$N_{fi,Rd,z} = \chi_z \, N_{fi,pl,Rd} \tag{22}$$

Where: $\chi_z = \frac{1}{\varphi + \sqrt{\varphi^2 - \bar{\lambda}_\theta^2}}$

The intermediate coefficient is: $\varphi = 0.5 \times [1 + \alpha \times (\bar{\lambda}_\theta - 0.2) + \bar{\lambda}_\theta^2]$.

The imperfection factor α should be equal to 0.49 depending to the buckling curve **c.**

To summarizes the balanced summation model, one should start by calculating the design value of the plastic resistance to axial compression and the effective flexural stiffness of the cross-section for each component. The next step hould be the Euler buckling load and the non-dimensional slenderness and using curve c to obtain the reduction factor therefore the design axial buckling load of the partially encased columns in the fire situations.

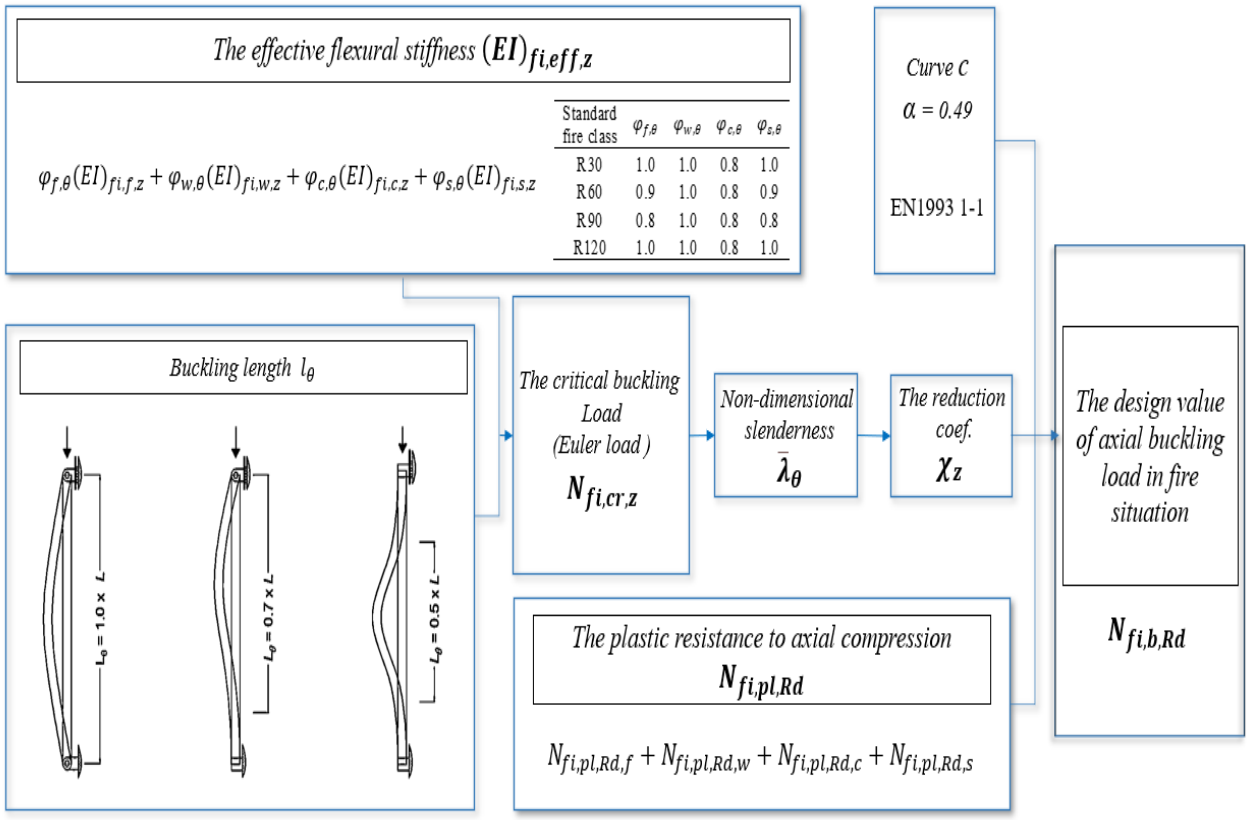

Figure 17: The balanced summation model

3-2 Application

These columns were tested under standard fire ISO834 [2], using three buckling lengths as explained before for 2 different length 3 m and 4 m.
The work will be divided into 4 stages, as the number of components of the steel profile.

3-2-1 Flanges of the steel profile

According to EN 1994-1-2[1] from annex G, the average temperature of the flanges ($\boldsymbol{\theta_{f,t}}$), as a function of the fire resistance time may be determined following the equation(23):

$$\theta_{f,t} = \theta_{0,t} + k_t(A_m / V) \qquad (23)$$

Where: t is the duration in minutes of the fire exposure
A_m/V is the section factor in m^{-1} , with $A_m = 2(h+b)$ [m] *and* $V = h.b$ [m^2]
$\theta_{0,t}$ is temperature in ºC given in table 11.
k_t is an empirical coefficient given in table 11.

Standard fire resistance class	$\theta_{0,t}$ [ºC]	k_t [mºC]
R30	550	9.65
R60	680	9.55
R90	805	6.15
R120	900	4.65

Table 11: Parameters for the flange temperature

For the average temperature $\theta = \theta_{f,t}$, the corresponding maximum stress level (yield stress) and the modulus of elasticity of the steel's flange should be updated, based on the reduction factors. According to the temperature effect on the mechanical properties, these properties should be determined from equation (24) et (25), which will be affecting the design value of the plastic resistance and the flexural stiffness.

$$f_{ay,f,t} = f_{ay,f}\, K_{y,\theta} \tag{24}$$

$$E_{a,f,t} = E_{ay,f}\, K_{E,\theta} \tag{25}$$

Where: $K_{y,\theta}$ and $K_{E,\theta}$ are the reduction factors for stress-strain relationships of structural steel at elevated temperature following the table 5 from section 2-2.1. Linear interpolation may be assumed for the exact temperature of the component $\theta = \theta_{f,t}$.

Finally, in the last step, the flange contribution to the design value of the plastic resistance to axial compression and the effective flexural stiffness of the cross section may be determined, according to the two equations (26) and (27)

$$N_{fi,pl,Rd,f} = 2\left(b\, e_f\, f_{ay,f,t}\right) / \gamma_{M,fi,a} \tag{26}$$

$$(EI)_{fi,f,z} = E_{a,f,t}\left(e_f\, b^3\right) / 6 \tag{27}$$

3-2-2 Web of the steel profile

In order to calculate the strength and the stiffness of the web of the steel profile, one must take into consideration that a part of the web may be neglected, corresponding to the height $\boldsymbol{h_{w,fi}}$ which starting at the inner edge of the flange,. This part $\boldsymbol{h_{w,fi}}$ is determined from the equation (28):

$$\boldsymbol{h_{w,fi}} = 0{,}5(h - 2e_f)\left(1 - \sqrt{1 - 0{,}16(H_t/h)}\,\right) \tag{28}$$

Where: $\boldsymbol{H_t}$ the height reduction of the web is given from the table 12 below:

Standard fire resistance class	H_t [mm]
R30	350
R60	770
R90	1100
R120	1250

Table 12: the height reduction of the web

In this case there is no temperature calculation, therefore the maximum stress level depends only of $\boldsymbol{H_t}$ and its obtained from the equation (29). This expression looks like a reduction factor to be used for the yield stress.

$$f_{ay,w,t} = f_{ay,,w}\sqrt{1 - 0{,}16(H_t/h)}\,) \tag{29}$$

Finally, the design value of the plastic resistance to axial compression and the flexural stiffness of the web component of the steel profile, in the fire situation, are determined from equations (30) and (31).The residual areal is also assumed.

$$N_{fi,pl,Rd,w} = \left[e_w\left(h - 2\,e_f - 2h_{w,fi}\right)f_{ay,w,t}\,\right]/\gamma_{M,fi,a} \tag{30}$$

$$(EI)_{fi,f,z} = \left[\,E_{a,w}\left(h - 2\,e_f - 2h_{w,fi}\right)e_w^3\,\right]/\,12 \tag{31}$$

3-2-3 Concrete

From the approach presented in the Annex G EN 1994-1.2 [1], an exterior layer of concrete with a thickness $\boldsymbol{b_{c,fi,h}}$ may be neglected in the calculation, as shown on the figure 18 (residual area for concrete). The thickness reduction of the area $\boldsymbol{b_{c,fi}}$ and the average temperature $\theta_{c,t}$ for the concrete, are given in table 13 and table 14, respectively, depending on the fire rating and on the section factor $\boldsymbol{A_m/V}$ $[m^{-1}]$ of the entire composite cross-section..There is no distinction between the horizontal and vertical layer of concrete, that is assumed to be neglected.

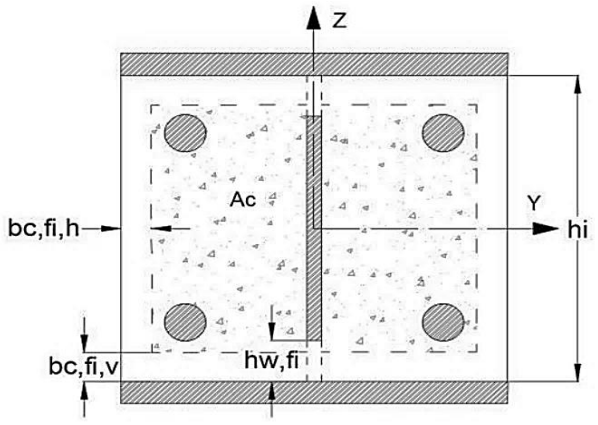

Figure 18: Cross section of PEC [31]

Standard fire resistance class	$b_{c,fi}$ [mm]
R30	4,0
R60	15,0
R90	0,5 (A_m/V) + 22,5
R120	2,0 (A_m/V) + 24,0

Table 13: Thickness reduction of the concrete area

R30		**R60**		**R90**		**R120**	
A_m/V $[m^{-1}]$	$\theta_{c,t}$ [ºC]	A_m/V $[m^{-1}]$	$\theta_{c,t}$ [ºC]	A_m/V $[m^{-1}]$	$\theta_{c,t}$ [ºC]	A_m/V $[m^{-1}]$	$\theta_{c,t}$ [ºC]
4	136	4	214	4	256	4	265
23	300	9	300	6	300	5	300
46	400	21	400	13	400	9	400
-	-	50	600	33	600	23	600
-	-	-	-	54	800	38	800
-	-	-	-	-	-	41	900
-	-	-	-	-	-	43	1000

Table 14: Average concrete temperature

For the temperature $\theta = \theta_{c,t}$, the corresponding secant modulus (modulus of elasticity) of concrete according to the increase of his temperature is obtained from equation (32):

$$E_{c,sec,\theta} = f_{c,\theta} / \varepsilon_{cu,\theta} \tag{32}$$

Where $f_{c,\theta} = f_c \, k_{c,\theta}$, with $k_{c,\theta}$ and $\varepsilon_{cu,\theta}$, being the the two reduction factors of the stress-strain relationships of normal weight concrete (NC) at elevated temperatures, given from the table 7.

In conclusion, after calculating the elastic modulus of the concrete, one can obtain the design value of the plastic resistance to axial compression and the effective flexural stiffness of the concrete part, assuming the standard fire event from the equations (33) and (34):

$$N_{fi,pl,Rd,c} = 0{,}86\left\{\left((h - 2\,e_f - 2h_{c,fi})(b - 2\,e_w - 2h_{c,fi}) - A_s\right)\right\} f_{c,\theta} / \gamma_{M,fi,c} \tag{33}$$

$$(EI)_{fi,f,z} = E_{c,sec,\theta}\left[\left\{(h - 2\,e_f - 2h_{c,fi})\left((b - 2b_{c,fi})^3 - e_w^3\right)/12\right\} - I_{s,z}\right] \tag{34}$$

Where: A_s is the cross-section and $I_{s,z}$ is the second moment of area of the reinforcing bars related to the central axis Z of the composite cross section

3-2-4 Reinforcing bars

For the reinforcing bars, one must start with the calculation of the geometrical average factor **u** , representing the axis distances u_1 (vertical) and the axial distance u_2 (horizontal) of the bars to the outer borders of the concrete, as presented on the previous chapter in the figure 3. The equation (35), should be used to determinate of the geometric factor **u**:

$$u = \sqrt{u_1 . u_2} \tag{35}$$

While taking into account the conditions imposed to **u** :

- if $(u_1 - u_2) > 10$ mm, Then ➔ $u = \sqrt{u_2(u_2 + 10)}$
- or $(u_2 - u_1) > 10$ mm, Then ➔ $u = \sqrt{u_1(u_1 + 10)}$

After calculating u, one can determine the reduction factor $K_{y,t}$ for the yield stress f_{sy} , and the reduction factor $K_{E,t}$ for the modulus of elasticity E_s for the reinforcing bars, given on the table 15 and 16 .

	$K_{y,t}$				
Standard fire resistance | u $[mm]$	40	45	50	55	60
R30	1	1	1	1	1
R60	0.789	0.883	0.976	1	1
R90	0.314	0.434	0.572	0.696	0.822
R120	0.170	0.223	0.288	0.367	0.436

Table 15: Reduction factor for the yield point

	$K_{E,t}$				
Standard fire resistance | u $[mm]$	40	45	50	55	60
R30	0.830	0.865	0.888	0.914	0.935
R60	0.604	0.647	0.689	0.729	0.763
R90	0.193	0.283	0.406	0.522	0.619
R120	0.110	0.128	0.173	0.233	0.285

Table 16: Reduction factor for modulus of elasticity

This calculation method does not provide the average temperature of the reinforcing bars.

As in every final step for each component, the design value of the plastic resistance to axial compression and the effective flexural stiffness in the fire situation, for the reinforcing bar are obtained from equations (36) and (37):

$$N_{fi,pl,Rd,f} = A_s \, K_{y,t} \, f_{sy} / \, \gamma_{M,fi,s} \tag{36}$$

$$(EI)_{fi,f,z} = \, K_{E,t} \, E_s \, I_{s,z} \tag{37}$$

3-3 Results

All the results and calculation steps are presented in the Annex A of this work and will be compared after with the two other solution methods.

4- NEW PROPOSAL FORMULAS FOR THE BALANCED SUMMATION MODEL

A new formula is proposed by B. Alfredo and P. Piloto [12] to improve the simplified calculation method from Eurocode 1994-1.2 annex-G [1] for determining the buckling resistance of the partially encased columns under fire situation.

4-1 Method

The principle of this improvement for the model consists of calculating the average temperature with new non-linear equations for the four different components of the PEC cross section , along with their different parameters for each profile series, considering the variation in the geometry of the profile series.

These new equations are presented only for the calculation of the plastic resistance and flexural stiffness of the four components, keeping the rest of the formulation in accordance with the European standard.

Due to this methodology, the squencial steps of the simplified method will not be repeated.

	EN1994-1-2_ANNEX G	*New improvement proposed_by_B.Alfredo & P.Piloto*
Flange	✓ Not reduced area ✓ Linear temperature ✓ E_{ay} Elastic modulus affected at elevated T° ✓ f_{ay} Yield strength affected at elevated T°	✓ Not reduced area ➢ Multilinear temperature ✓ E_{ay} Elastic modulus affected at elevated T° ✓ f_{ay} Yield strength affected at elevated T°
Web	✓ Reduced area : empirical equation ✓ Temperature not considered ✓ E_{ay} Elastic modulus affected at ambient T° ✓ f_{ay} Yield strength affected at elevated T°	➢ Not reduced area ➢ Multilinear temperature ➢ E_{ay} Elastic modulus affected at elevated T° ✓ f_{ay} Yield strength affected at elevated T°
Concrete	✓ Reduced area : reduction for vertical direction ✓ Temperature tabulated ✓ E_c Elastic modulus affected at elevated T° ✓ f_c Yield strength affected at elevated T°	➢ Reduced area : reduction for vertical and horizontal direction (based on 500 °C isotherm criterion) ➢ Temperature not uniformed less than 500 °C ✓ E_c Elastic modulus affected at elevated T° ✓ f_c Yield strength affected at elevated T°
Rebars	✓ Not reduced area ✓ Temperature inferred ✓ E_s Elastic modulus affected at elevated T° ✓ f_y Yield strength affected at elevated T°	✓ Not reduced area ➢ Linear temperature in function of section factor ✓ E_s Elastic modulus affected at elevated T° ✓ f_y Yield strength affected at elevated T°

Table 17: Comparaison between annex G and the new improvement proposed

4-2 Application

For all column configurations and for all the fire resistance classes, the current proposal presents temperatures slightly higher than those obtained with the ANSYS program [3], in order to keep safer results for the temperature.

As on the simplified calculation method presented, the balanced summation model will take over the 4 components of the PEC.

4-2.1 Flanges of the steel profile

Compared to the annex G of the EN1994-1.2 [1], the improvement here presentd for the calculation of the temperature on the cross section of the flanges of each steel profile should be calculated.

The new temperature will be multilinear and no longer linear, by adding a new factor, which takes into consideration the thickness of the flange with parameter, determined for each time of fire resistance as shown on the equation (38):

$$\theta_{f,t} = \theta_{0,f} + k_{f,f}\,(e_f) + k_{t,f}(A_m / V) \tag{38}$$

Where: $\theta_{0,f}$ is average temperature in ºC given in table 18

$k_{f,f}$ is an empirical coefficient affected by the thickness given in table 18

$k_{t,f}$ is an empirical coefficient affected by the section factor from table 18

A_m/V is the section factor in m^{-1} , with A_m= *2 (h+b)* [m] *and V = h.b* [m^2]

	HEA / HEB			HD		
Standard fire class	$\boldsymbol{\theta_{0,f}}$ $[ºC]$	$\boldsymbol{k_{f,f}}$ $[mm^{-1}ºC]$	$\boldsymbol{k_{t,f}}$ $[mºC]$	$\boldsymbol{\theta_{0,f}}$ $[ºC]$	$\boldsymbol{k_{f,f}}$ $[mm^{-1}ºC]$	$\boldsymbol{k_{t,f}}$ $[mºC]$
R30	687.00	-4.50	3.43	463.00	-2.00	16.91
R60	909.00	-3.76	2.06	785.00	-1.90	8.73
R90	971.00	-1.38	1.42	965.00	-1.80	3.29
R120	1018.00	-0.89	1.37	1063.00	-1.55	0.53

Table 18: Improved parameters for average flange temperature

For the temperature $\theta = \theta_{f,t}$, the corresponding maximum stress level (yield stress) and the modulus of elasticity of the steel's flange, depends on the increase of their temperature, being determined from equations (39) and (40) taking into account the values of the reduction factors :

$$f_{ay,f,t} = f_{ay,f}\, K_{y,\theta} \tag{39}$$

$$E_{a,f,t} = E_{ay,f}\, K_{E,\theta} \tag{40}$$

Where: $\boldsymbol{K_{y,\theta}}$ and $\boldsymbol{K_{E,\theta}}$ the reduction factors following the table 5 corresponding to $\theta = \theta_{f,t}$

Finally, in the last step for the flange component, and similar to the current version of the balanced summation model presents in the EN 1994-1.2-Annex G, the design value of the plastic resistance to axial compression and the flexural stiffness should be determined by the two equations (41) and (42) :

$$N_{fi,pl,Rd,f} = 2\left(b\, e_f\, f_{ay,f,t}\right) /\ \gamma_{M,fi,a} \tag{41}$$

$$(EI)_{fi,f,z} = E_{a,f,t}\left(e_f\, b^3\right) / 6 \tag{42}$$

4-2.2 Web of the steel profile

Compared to the balanced summation model from Annex G of EN1994-1.2 [1], on this improved model, the area of the web of the steel profile will not be reduce and will consider that the whole area as resistant. Therefore $\boldsymbol{H_t}$ the height reduction of the web will be neglected and note that the web will have its mechanical properties affected by the evolution of temperature, usingthe same reduction coefficients, as used for the flange.

From this hypothesis, it is necessary to determine the average temperature of the web, according to the equation (43) which is similar to that used in the flange, while taking into consideration the effect of the web thickness, which best characterizes the temperature evolution in the profiles.

$$\theta_{w,t} = \theta_{0,w} + k_{w,w}\,(1/e_w) + k_{t,w}(A_m/V) \tag{43}$$

Where: $\theta_{0,w}$ is average temperature in ºC given in table 19

$k_{w,w}$ is an empirical coefficient affected by the thickness given in table 19

$k_{t,w}$ is an empirical coefficient affected by the section factor from table 19

A_m/V is the section factor in m^{-1} , with A_m= *2(h+b)* [m] *and V = h.b* [m^2]

	HEA / HEB			**HD**		
Standard fire resistance class	$\boldsymbol{\theta_{0,w}}$ $[ºC]$	$\boldsymbol{k_{w,w}}$ $[mm^{-1}ºC]$	$\boldsymbol{k_{t,w}}$ $[mºC]$	$\boldsymbol{\theta_{0,w}}$ $[ºC]$	$\boldsymbol{k_{w,w}}$ $[mm^{-1}ºC]$	$\boldsymbol{k_{t,w}}$ $[mºC]$
R30	-159	2500	14	-83	-480	30
R60	-233	4170	23	15	-810	40
R90	-221	4900	29	126	-1120	44
R120	-186	550	31	233	-1100	45

Table 19: Improved parameters for average web temperature

Since the temperature is calculated, for $\theta = \theta_{f,t}$, the corresponding maximum stress level (yield stress) and the modulus of elasticity of the steel's flange, should be updated,according to the increase of their temperature, being determined from equations (44) and (45), taking into account the values of the reduction factors :

$$f_{ay,w,t} = f_{ay,w}\,K_{y,\theta} \tag{44}$$

$$E_{a,w,t} = E_{a,w}\,K_{E,\theta} \tag{45}$$

Where: $K_{y,\theta}$ and $K_{E,\theta}$ the reduction factors following the table 5 corresponding to $\theta = \theta_{w,t}$

Obviously the equations for calculating the design value of the plastic resistance to axial compression and the effective flexural stiffness in the fire situation have also been changed, as there is no longer a reduction in the resistant area of the web and the mechanical properties are affected by temperature as shown in the new proposed equations (46) and (47):

$$N_{fi,pl,Rd,w} = \left[e_w\left(h - 2\,e_f\right)f_{ay,w,t}\,\right]/\gamma_{M,fi,a} \tag{46}$$

$$(EI)_{fi,f,z} = \left[\,E_{a,w}\left(h - 2\,e_f - 2h_{w,fi}\right)e_w^3\,\right]/\,12 \tag{47}$$

4-2.3 Concrete

In comparison with the model presented in the annex G in EN 1994-1.2 [1], there is still a reduction on the concrete component of its area according to the fire resistance class, but actually the external layer of concrete to be neglected may be calculated in both directions (horizonal and vertical). This new approach considers a specific vertical reduction and specific reduction in the horizontal directionThis layer have been determined, using the isothermal criterion of 500°C to determine the reductions while keeping the same properties of the concrete at elevated temperature.

Concerning the temperature, it will no longer be tabulated, the entire resistant section of the concrete must have a temperature below 500 ºC, because this material should be inside the isothermal. The temperature of the concrete inside this region can be obtained from the new proposed equation (48).

$$\theta_{c,t} = \theta_{0,c} + k_{w,c}\,(1/e_w) + k_{t,c}(A_m/\,V\,) \tag{48}$$

Where: $\theta_{0,c}$ is average temperature in ºC given in table 20

$k_{w,c}$ is an empirical coefficient affected by the thickness given in table 20

$k_{t,c}$ is an empirical coefficient affected by the section factor from table 20

A_m/V is the section factor in m^{-1} , with A_m= *2(h+b)* [m] *and V = h.b* [m^2]

	HEA / HEB			**HD**		
Standard fire resistance class	$\boldsymbol{\theta_{0,c}}$ $[ºC]$	$\boldsymbol{k_{w,c}}$ $[mmºC]$	$\boldsymbol{k_{t,c}}$ $[mºC]$	$\boldsymbol{\theta_{0,c}}$ $[ºC]$	$\boldsymbol{k_{w,c}}$ $[mmºC]$	$\boldsymbol{k_{t,c}}$ $[mºC]$
R30	29	-230	14.8	4	-255	16.8
R60	-6	-950	30.5	20	-600	27.5
R90	-3	1355	22.2	60	-822	32.8
R120	35	2140	19.4	129	-867	31.9

Table 20: Improved parameters for average concrete temperature

For this improvement, as mentioned before, it was necessary to determine an equation for each concrete layer reduction, vertical and horizontal, similar to that of temperature.The proposal sonsiders the quadratic variation of the section factor.

For the vertical reduction with the influence of the thickness of the flange is obtained from equation (49) below:

$$b_{c,fi,v} = b_{0,cv} + k_{f,cv}\,(e_f) + k_{t,cv}\,(A_m/V)^2 \tag{49}$$

Where: $b_{0,cv}$ is average vertical reduction in [mm] given in table 21
$k_{f,cv}$ is an empirical coefficient affected by the thickness given in table 21
$k_{t,cv}$ is an empirical coefficient affected by the section factor from table 21
A_m/V is the section factor in m^{-1} , with A_m= *2(h+b)* [m] and *V = h.b* [m^2]

	HEA / HEB			HD		
Standard fire resistance class	$\boldsymbol{b_{0,cv}}$ $[mm]$	$\boldsymbol{k_{f,cv}}$	$\boldsymbol{k_{t,cv}}$ $[m^2mm]$	$\boldsymbol{b_{0,cv}}$ $[mm]$	$\boldsymbol{k_{f,cv}}$	$\boldsymbol{k_{t,cv}}$ $[m^2mm]$
R30	-0.960	0.08	0.025	-1.450	0.01	0.045
R60	12.46	0.06	0.062	14.11	-0.10	0.068
R90	-75.80	2.39	0.435	19.00	-0.10	0.200
R120	-208.0	5.40	1.120	-11.00	0.04	0.650

Table 21: Improved parameters for vertical reduction of concrete

For the horizontal reduction with the influence of the thickness of the web, is obtained from the equation (50):

$$b_{c,fi,h} = b_{0,ch} + k_{w,ch}\,(1/e_w) + k_{t,ch}\,(A_m/V) \tag{50}$$

Where: $b_{0,ch}$ is average horizontal reduction in [mm] given in table 22
$k_{w,ch}$ is an empirical coefficient affected by the thickness given in table 22
$k_{t,ch}$ is an empirical coefficient affected by the section factor from table 22
A_m/V is the section factor in m^{-1} , with A_m= *2(h+b) [m] and V = h.b* [m^2]

	HEA / HEB			HD		
Standard fire resistance class	$\boldsymbol{b_{0,ch}}$ $[mm]$	$\boldsymbol{k_{w,ch}}$ $[mm^2]$	$\boldsymbol{k_{t,ch}}$ $[m.mm]$	$\boldsymbol{b_{0,cv}}$ $[mm]$	$\boldsymbol{k_{w,ch}}$ $[mm^2]$	$\boldsymbol{k_{t,ch}}$ $[m.mm]$
R30	11.68	0	0.000	11.68	0	0.000
R60	25.40	-102	0.050	22.00	-10	0.026
R90	43.10	-636	0.300	26.60	-85	0.135
R120	39.60	-1000	0.690	26.60	-189	0.300

Table 22: Improved parameters for horizontal reduction of concrete

For the temperature $\theta = \theta_{c,t}$, the corresponding secant modulus (modulus of elasticity) of concrete according to the increase of his temperature is obtained from equation (51):

$$E_{c,sec,\theta} = f_{c,\theta} / \varepsilon_{cu,\theta} \quad (51)$$

Where: $f_{c,\theta} = f_c \, k_{c,\theta}$, With: $\boldsymbol{k_{c,\theta}}$ and $\boldsymbol{\varepsilon_{cu,\theta}}$ the two reduction factors of the stress-strain relationships of normal weight concrete (NC) at elevated temperatures from Table 7

Finally, as preented before for the simplified method according to the Annex-G of the EN1994-1.2[1], after calculating the elasticity modulus we can obtain the design value of the plastic resistance to axial compression and the effective flexural stiffness of the concrete in the fire situation from the following equations (52) and (53) :

$$N_{fi,pl,Rd,c} = 0{,}86\left\{\left(\left(h - 2\,e_f - 2h_{c,fi,v}\right)\left(b - 2\,e_w - 2h_{c,fi,h}\right) - A_s\right)\right\} f_{c,\theta} / \gamma_{M,fi,c} \quad (52)$$

$$(EI)_{fi,f,z} = E_{c,sec,\theta}\left[\left\{\left(h - 2\,e_f - 2h_{c,fi,v}\right)\left(\left(b - 2b_{c,fi,h}\right)^3 - e_w^3\right)/12\right\} - I_{s,z}\right] \quad (53)$$

Where: $\boldsymbol{A_s}$ is the cross-section and $\boldsymbol{I_{s,z}}$ is the second moment of area of the reinforcing bars related to the central axis Z of the composite cross section.

4-2.4 Reinforcing bars

The only factor that changes in this model is that the temperature will be a linear function. Thus, in this improvement, the average reinforcement bars temperature's value will be calculated assuming equation (54).

Therefore, one equation is presented that may be used for the three types of profiles, varying the temperature and empirical coefficients. These factors depend on the secton factor and fire rating and are based the initial design constraint equal to ***u = 50 mm.***

$$\theta_{f,t} = \theta_{0,s} + k_{t,s}(A_m / V) \quad (54)$$

Where: $k_{t,s}$: is an empirical coefficient affected by the geometrical average u=50 mm given in table 23

$\theta_{0,s}$: is average temperature in ºC given in table 23

HEA / HEB / HD		
Standard fire resistance class	$\boldsymbol{\theta_{0,s}}$ $[ºC]$	$\boldsymbol{k_{t,s}}$ $[m ºC]$
R30	67	5.19
R60	151	14.23
R90	250	18.53
R120	336	20.82

Table 23: Improved parameters for average bars temperature for u =50mm

Then, on last step component for the reinforcing bars, one can determine the design value of the plastic resistance to axial compression and the flexural stiffness in the fire situation from equations (55) and (56):

$$N_{fi,pl,Rd,f} = A_s\, K_{y,t}\, f_{sy} /\ \gamma_{M,fi,s} \tag{55}$$

$$(EI)_{fi,f,z} = K_{E,t}\, E_s\, I_{s,z} \tag{56}$$

Where: $\boldsymbol{K_{sy,\theta}}$ and $\boldsymbol{K_{sE,\theta}}$ the reduction factors for the reinforcing steel following the table 9 corresponding to $\theta = \theta_{s,t}$

4-2.5 The balanced summation model

The balanced summation of the portions of each component of the cross section was performed by equation (57) and (58). This will allow for the calculation of the plastic resistance to axial compression and the effective flexural stifness in fire situation, following the new proposam model, using a factor of 0.6 for the component of effective flexural stiffness for the concrete.

For the comparison, the same formulation as in Annex G was used, removing the reductions in properties and geometry resulting from the increase in temperature:

$$N_{fi,pl,Rd} = N_{fi,pl,Rd,f} + N_{fi,pl,Rd,w} + N_{fi,pl,Rd,c} + N_{fi,pl,Rd,s} \tag{57}$$

$$(EI)_{fi,eff,z} = (EI)_{fi,f,z} + (EI)_{fi,w,z} + 0.6\,(EI)_{fi,c,z} + (EI)_{fi,s,z} \tag{58}$$

The critical axial compression resistance or Euler buckling load ($N_{fi,cr,z}$) using equation59:

$$N_{fi,cr,z} = \pi^2 (EI)_{fi,eff,z} / L_\theta^2 \tag{59}$$

Using $\boldsymbol{\bar{\lambda}_\theta}$ and the buckling **curve c** of EN 1993-1-1[13] to obtain the reduction coefficient $\boldsymbol{\chi_z}$, sequentially the design axial buckling load in the fire situation is determinate following equation (60):

$$N_{fi,Rd,z} = \chi_z\, N_{fi,pl,Rd} \tag{60}$$

4-4 Results

All the results and different part of calculations of this chapter are presented on the Annex B of this work.

5- ADVANCED CALCULATION METHOD

This advanced calculation method is based on performing a numerical simulation using the software ANSYS Mechanical APDL [3], in which a nonlinear transient thermal simulation model has been developed. The three-dimensional study was developed with the aim of determining the buckling resistance of partially encased columns for different fire resistance class (30, 60, 90 and 120 minutes).

30 different steel profile, as described in the previous chapter for 2 heights (3m-4m) will be simulated and analyzed numerically.

5-1 Numerical simulation

5-1-1 Element Type

Different types of elements are going to be used to solve the thermal and the structural analysis. These elements are defined in the data base of the software ANSYS and described thoroughly on this section.

SHELL181 is suitable for analyzing thin to moderately thick shell structures. It is a 4-node element with six degrees of freedom at each node. The element uses linear interpolating functions and full gaus integration method (2x2) in the plane of the shell, with 5 integartion points over the thickness.

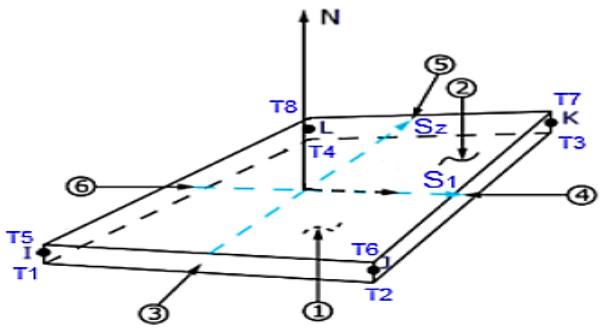

Figure 19: Geometry of SHELL181

LINK180 is a 3-D spar useful in a variety of engineering applications. The element can be used to model trusses, sagging cables, links, springs, and so on. The element is a uniaxial tension-compression element with three degrees of freedom at each node. As in a pin-jointed structure, no bending of the element is considered. The element uses linear interpolating functions and exact integration method (analystical).

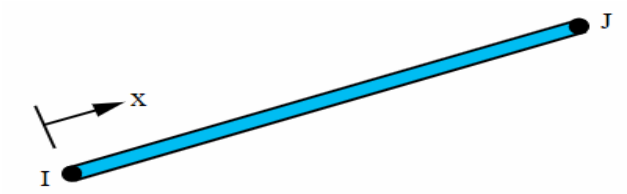

Figure 20: Geometry of LINK180

SOLID65 is used for 3-D modeling of the concrete with the reinforcing bars in this case. The solid is capable of cracking in tension (in three orthogonal directions) and crushing in compression (not consider in this study). The most important feature of this element is the consieration of nonlinear material properties. The element is defined by 8 nodes having 3 degrees of freedom at each node. Linear interpolating functions are used with full gaus integration method (2x2x2).

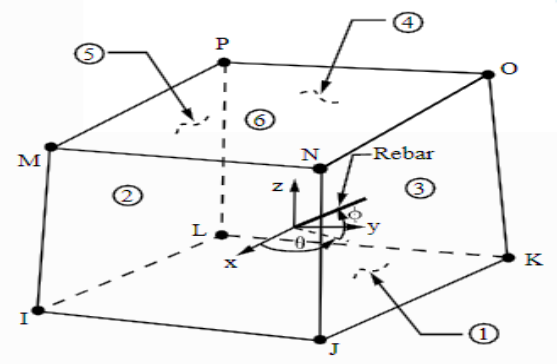

Figure 21: Geometry of SOLID65

To notice that while running a thermal analysis, all these structural elements will be switched automatically from structural type to thermal one, using their equivalents

SHELL 181 ➔ SHELL131
SOLID 65 ➔ SOLID70
LINK 180 ➔ LINK 33

5-1-2 Numerical model of the columns

The model is a full three-Dimensional model, based on perfect contact between materials. For the definition of the models of the cross sections of the PEC on the software ANSYS it was necessary to perform a simplification and start by drawing the geometry of the cross section and create the surface afterwards:

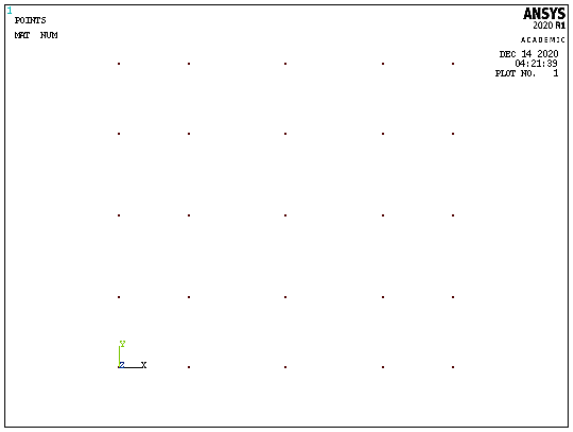

Figure 22: keypoints of HEB240 profile

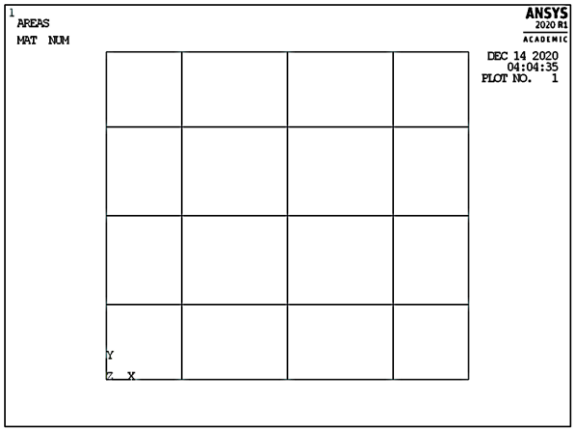

Figure 23: Areas of HEB240 profile

After extruding the area of the profile by the height intended (3m or 4m in each case) and attribute the current mesh consideration of 50 element divisions for columns with a height of 3 meters and 80 element divisions for that of 4m of height. The finite element models require to apply the element type and the materials properties to the different component of the composite column, see figure 24. Special plates with 20mm of thickness were considered in the top and bottom of the column, in order to distribute the axial load and reactions (not represented)

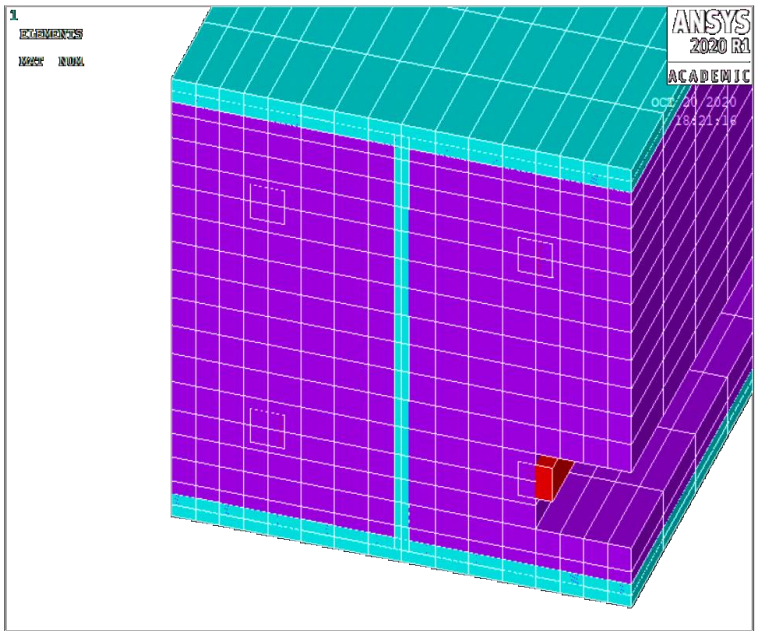

Figure 24: 3D numerical model of PEC on ANSYS

5-1-3 Numerical analysis

To perform a numerical analysis, in order to determine the buckling resistance of PEC under fire situation, it's necessary to go through 4 steps described on this section.

5-1-3.1 Eigen Buckling analysis

Eigen-value buckling analysis predicts the theoretical buckling strength of an ideal elastic structure. This solution method computes the structural eigen-values for the system of loading and constraints. This is known as classical Euler buckling analysis. Buckling loads for several configurations are readily available from tabulated solutions.

The Eigen-value solver uses a reference load (unit force) to determine the buckling load (critical). Applying a load other than 1 will scale the result by a factor that depends on the load level, so its necessary to apply a vertical force (FY) point load of (-1) N to the top of the column.

After applying the necessary boundary conditions on the top and bottom link of the column for the 3 different case of boundary conditions (K =1; K = 0.7; K = 0.5), a static analysis as 1st step of analysis must be ran.

The second step considers an Eigen buckling analysis with Block Lenclos extraction method. The solution of equation (61) must be found primarily:

$$[K]\{d\} = \{F_{ref}\} \tag{61}$$

Where: F_{ref} is an arbitrary reference load for the column
[K] is stiffness matrix of the column
{d} is the displacement vector

When the displacements are known, the stress field can be calculated for the reference load $\{F_{ref}\}$, which can be used to form the stress stiffness matrix $[K_{\sigma,ref}]$. Since the stress stiffness matrix is proportional to the load vector $\{F_{ref}\}$, an arbitrary stress stiffness matrix $[K_{\sigma}]$ and an arbitrary load vector {F} may be defined by a constant λ as shown by Equations (62) and (63):

$$[K_{\sigma}] = \lambda[K_{\sigma,ref}] \tag{62}$$

$$\{F\} = \lambda\{F_{ref}\} \tag{63}$$

Since the stiffness matrix is not changed by the applied load because the solution is linear. A relation between the stiffness matrices, the displacement and the critical load can then be presented as shown in Equations. 64-65, which can be used to predict the bifurcation point.

$$\{F_{cri}\} = \lambda_{cri}\{F_{ref}\} \tag{64}$$

$$\left[[k] + \lambda_{cri}[K_{\sigma,ref}]\right]\{d\} = \lambda_{cri}\{F_{ref}\} \tag{65}$$

Where: F_{cri} is the critical load

Since the buckling mode is defined as a change in displacement for the same load level, Equation 66 are still valid:

$$\left[[k] + \lambda_{cri}[K_{\sigma,ref}]\right]\{\{d\} + \{\delta d\}\} = \lambda_{cri}\{F_{ref}\} \tag{66}$$

Where: $\{\delta d\}$ represents the incremental buckling displacement vector.

The difference between Eq. 65 and Eq. 66 produces an eigenvalue problem, represented by equation 67, where the smallest root λ defines the first buckling load λcri , when bifurcation is expected. The mode of instability can also be determined

$$\left[[k] + \lambda[K_{\sigma,ref}]\right]\{\delta d\} = \{0\} \tag{67}$$

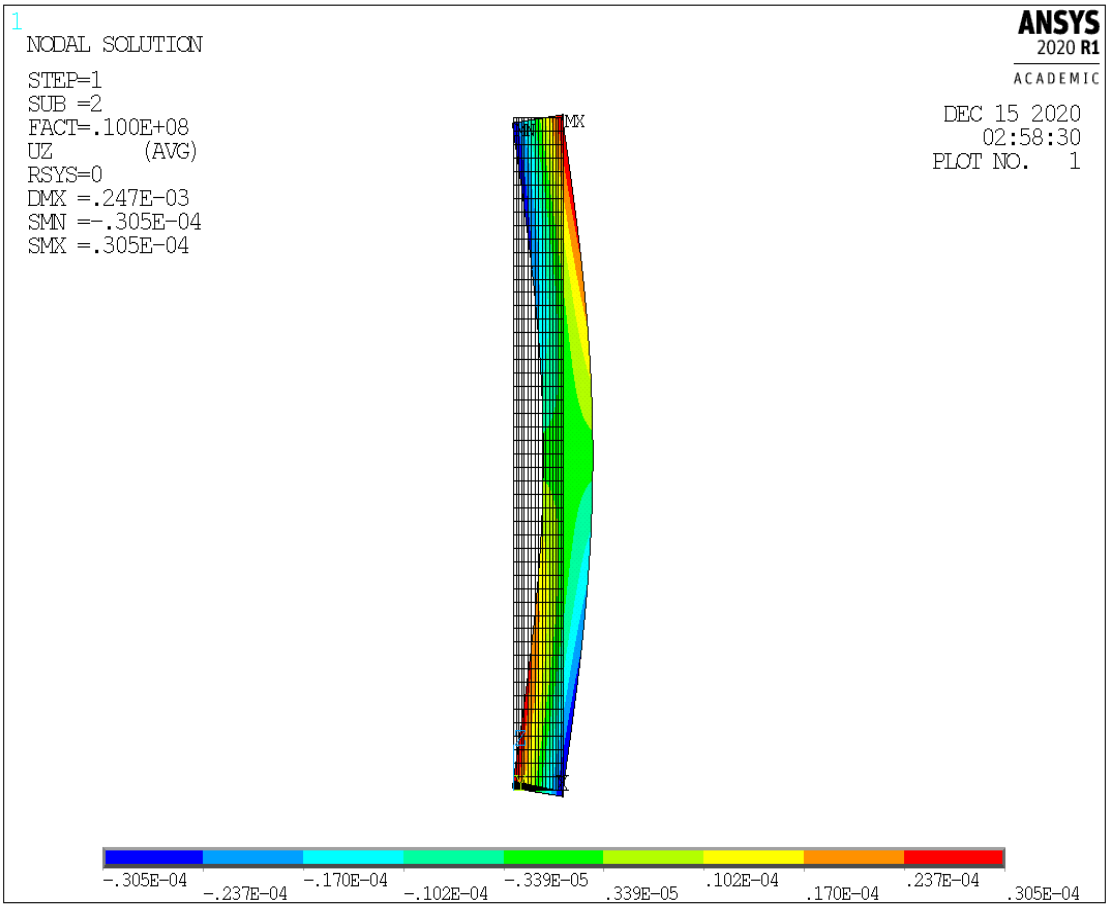

Figure 25: The elastic critical shape of HEA240 profile

The Critical axial compression resistance values or the Euler buckling load for the different steel profile of the partially encased columns are obtained from this analysis and presented on the annex C of this thesis and will be compared to that one calculed by the simplified method from Annex G of EN1994-1.2 [1].

5-1-3.2 The non-linear buckling analysis

The nonlinear buckling analysis is more real than Eigen-value analysis because it considers non-linear, large-deflection, static analysis to predict buckling loads (load bearing). The solution method may be based on increments of the applied load or the applied displacement, until a load level is found whereby the structure becomes unstable (suddenly a very small increase in the load will cause very large deflections).

The nodal position needs to be updated in order to define this geometric imperfection of the column. It is acceptable to introduce a half sine harmonic and consider the maximum imperfection equal to U_{max}= L/150 following equation (68):

$$U = U_{max}\, sin(\pi x/L) \tag{68}$$

The instability mode obtained from eigen buckling analysis will be used to introduce the imperfection on geometry. This means that the geometry must be updated, using the

adequate scale factor ($U_{max}/U_{max,horizental}$) from the analysis, to approximate the maximum imperfection (U_{max}).

The Newton Raphson method with incremental displacement will be used as solution method on this analysis. The Newton Raphson solution method uses incremental displacement with an iterative solution method within each displacement incremental step.

Typical incremental displacement of 1 mm was applied, adjusting to any minimum incremental displacement of 0,01 mm and to maximum incremental displacement of 2 mm, to reach 300 as pseudo time at the end of loadstep, see table 24. The criterion for convergence is based on displacement with tolerance value of 5%.

The solution is based on the tangent elastic modulus, which only gives results up to the region where the tangent stiffness is not negative. The displacement should be applied with "small" increments to update geometry, using a table defined with the Ansys utility menu:

Pseudo Time	Displacement (U_x)
0	0
300	-0.3

Table 24: Displacement parameter to use as disp. variation

The table defines a parameter and should be used when defining the boundary conditions running the analysis, to prevent any kind of instability.

The axial buckling load at room temperature $N_{b,Rd}$ is the result of this simulation.

5-1-3.3 The non-linear transient thermal analysis:

According to EN 1991-1-2 [16], two methods of heat transfer should be considered to simulate fire. The convection and radiation methods. For the first mode of heat transfer, the convection coefficient, $\boldsymbol{\alpha_c}$, may be consider equal to 25$[W/m^2K]$, when this standard nominal curve is considered. For hydrocarbon nominal curve a different convection coefficient should be consider.

For the second mode of heat transfer, the view factor, φ , may be consider equal to unit or may be calculated. The emissivity represents the ratio between the radiative heat absorbed by steel and that of a black body surface.

The program uses the finite element method, solving equation (69) for the nodes of the domain (Ω) of the cross section and equation (70) for the boundary ($\partial\Omega$) that is exposed to the fire conditions:

$$\nabla\left(\lambda_{(T)} \cdot \nabla T\right) = \rho_{(T)} \cdot C_{p(T)} \cdot \partial T/\partial t \;\rightarrow\; (\Omega) \qquad (69)$$

Where: T is the temperature of each node in the cross section
$\rho_{(T)}$ is the specific mass of each node for each material
$C_{p(T)}$ is the specific heat for each material

$$\lambda_{(T)} \cdot \nabla T \cdot \vec{n} = \alpha_c (T_g - T) + \phi \cdot \varepsilon_m \cdot \varepsilon_f \cdot \sigma \cdot \left(T_g^4 - T^4\right) \rightarrow (\partial\Omega) \qquad (70)$$

Where:

$\lambda_{(T)}$	is the thermal conductivity for each material
α_c	is the convection factor = 25
T_g	is the gases temperature in fire situation
ϕ	is the view factor
$\varepsilon_m , \varepsilon_f$	represent respectively the emissivity of the materials and the fire
σ	is Stefan Boltzmann's constant = 5.67x10^{-8}

To run a transient thermal analysis in ANSYS it's necessary to introduce the Boundary condition adequate for the four faces of the column with T_0 = 20ºC , T_g = ISO834 and α_c=25[W/m^2K],

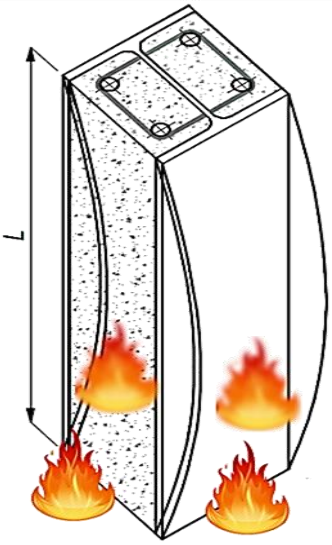

Figure 26: Bondary condition for the column

The nonlinear transient thermal analysis was defined with an integration time step of 60 s, which can decrease to 1 s and increase up to 60 s. The criterion for convergence uses a tolerance value of the heat flow, smaller than 0.1% with a minimum reference value of 1x10.

5-1-3.4 The non-linear thermal buckling analysis:

After running a nonlinear transit thermal analysis, its ncessary to run a non-linear buckling analysis another time to determinate the axial buckling load of the partially encased column of the model studied for different fire rating (30-60-90-120) periodes.

As for the second step of analysis, The Newton Raphson with incremental displacement will be used as solution method on this static analysis.

Typical incremental displacement of 1 mm was applied, adjusting to any minimum incremental displacement of 0,01 mm and to maximum incremental displacement of 2 mm, to reach 300 as pseudo time at the end of loadstep. The criterion for convergence is based on displacement with tolerance value of 5%.

The element type defined before for the thermal analysis will be switched from thermal to a structural element, while maintaining the same number of integration points as the Euler analysis.

Finally, its important to apply the nodal temperature from the previous thermal analysis for each different fire rating time (1800s-3600s-4800s-7200s) and run a static analysis with large displacement and typical incremental displacement to get the axial buckling load bearing under fire $N_{b,Rd,fi,t}$.

This $N_{b,Rd,fi,t}$ which will be compared to the analytic solution from EN1994-1.2 [1] and to that from improved solution method.

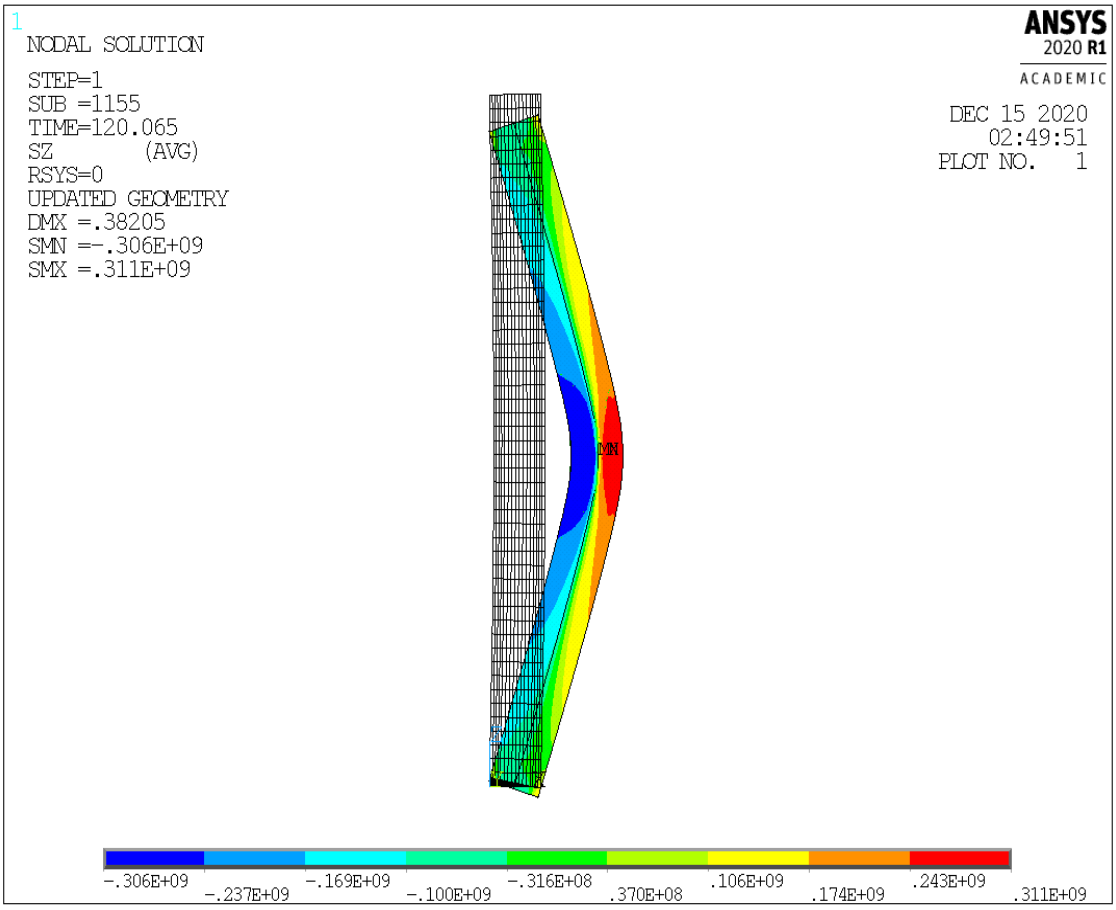

Figure 27: The buckling resistance shape of HEA300 profile for R120

5-2 Results:

All the results from this numerical solution as the critical elastic load deduced from Euler analysis and the design value of the axial buckling load under fire situation will be presented minutely on the annex C of this work.

6- COMPARISON OF THE RESULTS

6-1 The plastic resistance to axial compression:

The values of the plastic resistance to axial compression of partially encased columns for the three series of profiles, calculated with balanced summation method from EN 1994-1-2 annex G are compared with that one calculated with the improved method, shown in Figure 28 The values for fire resistance in 30 minutes are too safe.

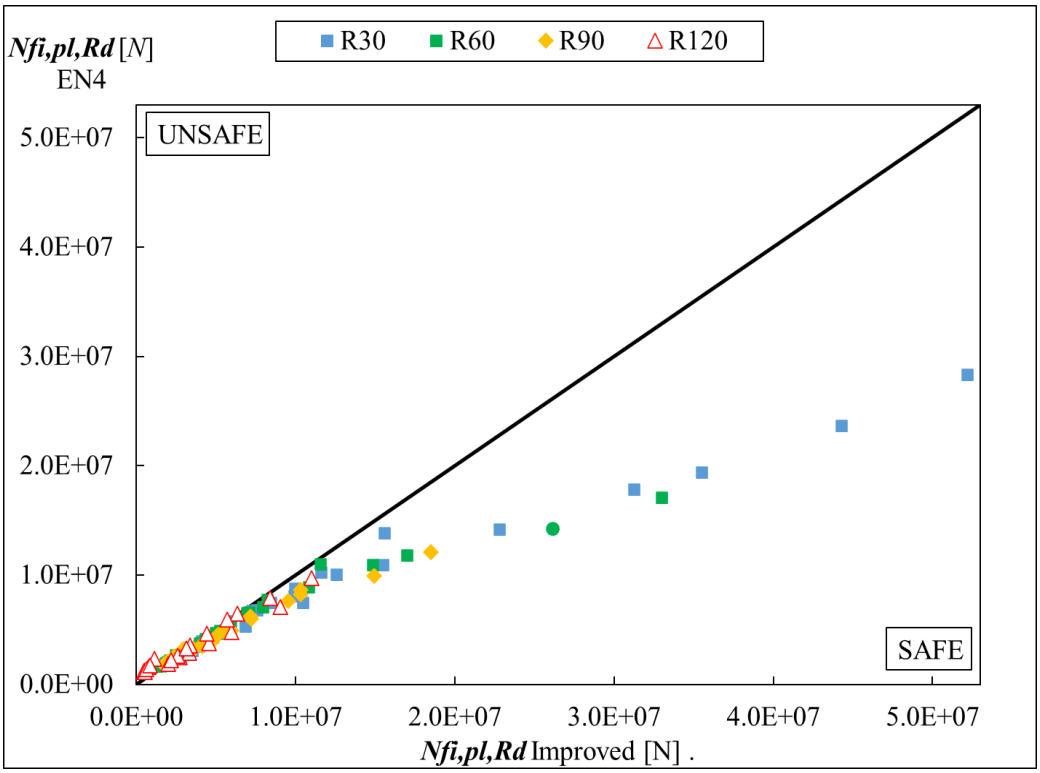

Figure 28: The plastic resistance with two methods

6-2 The effective flexural stiffness:

The values of effective flexural stiffness according to the EN 1994-1.2 are compared to the values obtained by the improvement. In figure 29 the values of effective flexural stifness are divided by the respective value at room temperature, for better visualization in scale.

The values of effective flexural stiffness for R30 are safe. For the last two strength classes, the results of the standard for the three series of profiles show more safe values than unsafe, with the series with the highest section factor being unsafe.

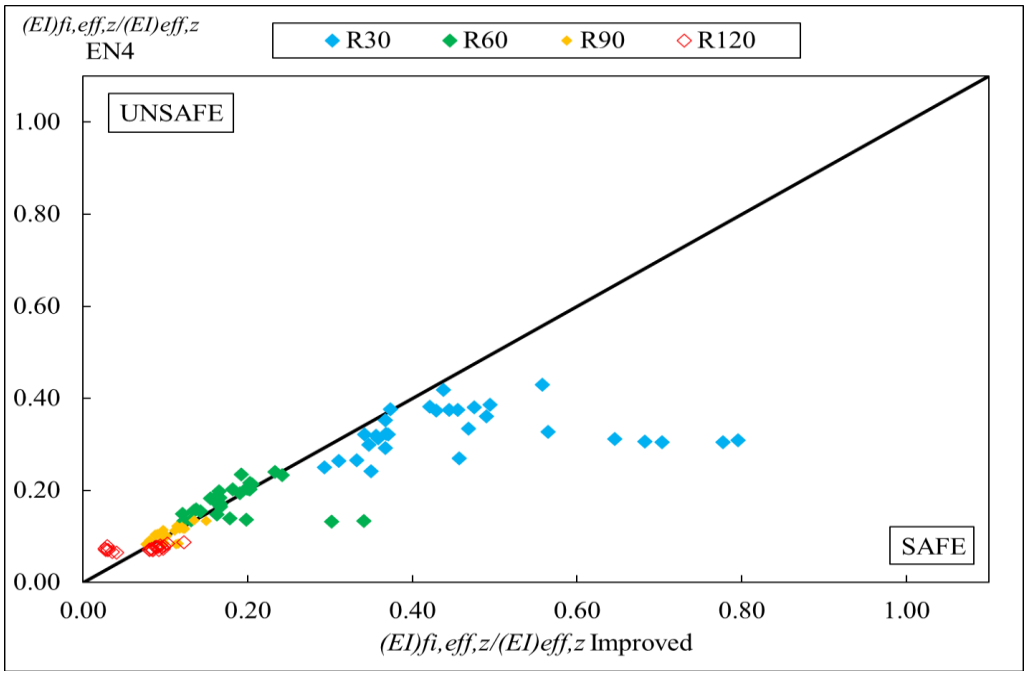

Figure 29: The effective flexural stiffness with two methods

6-3 The critical axial compression resistance:

Figure 30 shows a comparaison between the critical axial compression load or the critical elastic load calculated at room temperature T= 20ºC for two different height of the column (3 and 4 meter) and for the three different bounding conditions for each height K= (1 , 0.7 , 0.5), according to the annex G from EN1994-1.2 and the numerical simulation on Ansys.

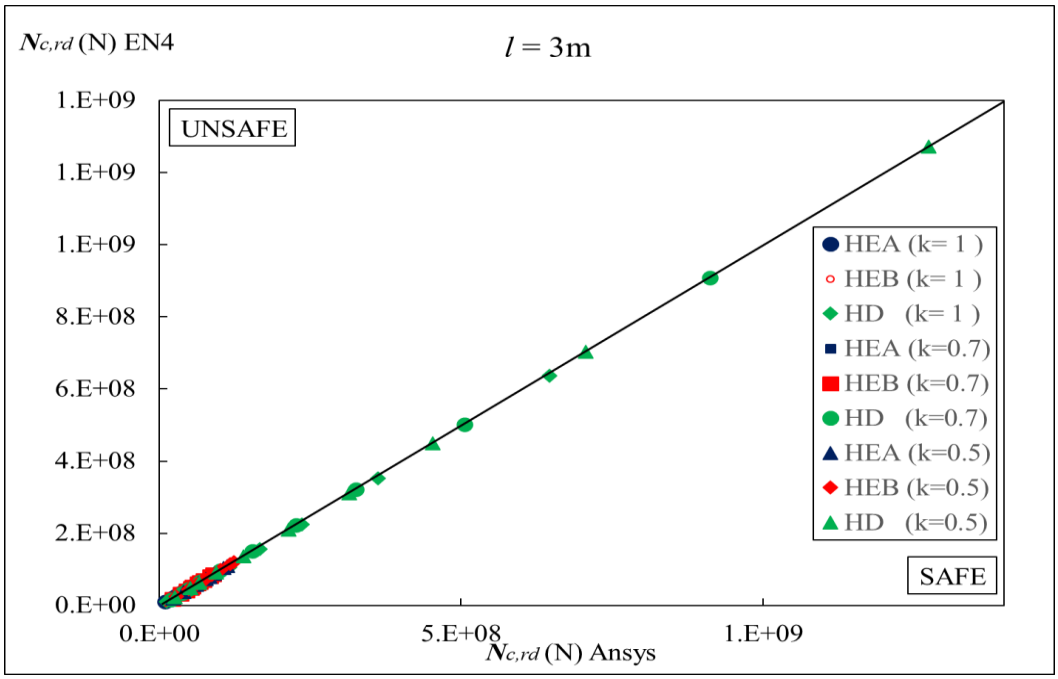

Figure 30: The critical axial compression resistance for steel profiles for l=3m

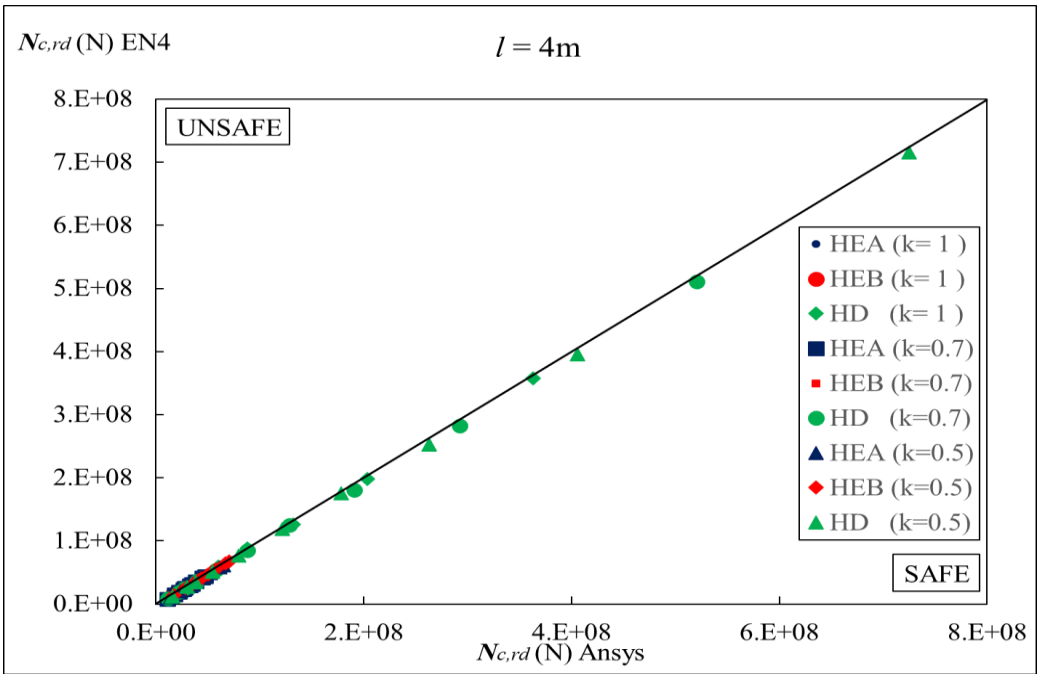

Figure 31: The critical axial compression resistance for steel profiles for l=4m

We can conclude from the figures 30 and 31 that the column with higher height (4m) shows a little safer approximation than the column with 3 m of height and all the steel profile towards to a safe domain.

6-4 The design value of axial Buckling load:

As the aim of the study, Figure 31 presents the comparison of the design values of the axial buckling load, using the results from Eurocode EN 1994-1-2 [1] and results from the non-linear thermal buckling numerical analysis for the different fire resistance classes (30-60-90 and 120 minutes) for the three different series steel profiles and for the buckling length $l_\theta = l = 3$ meter .

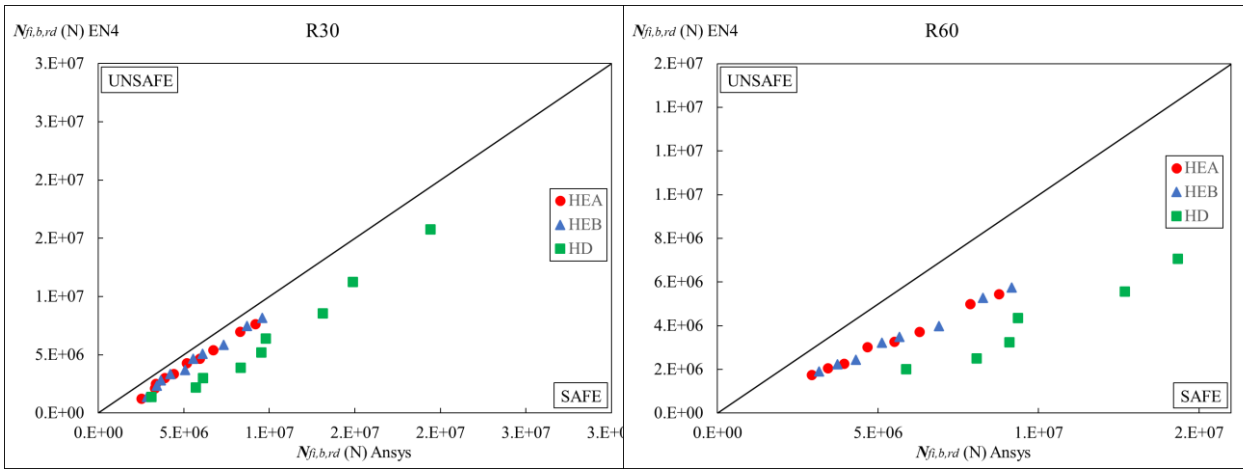

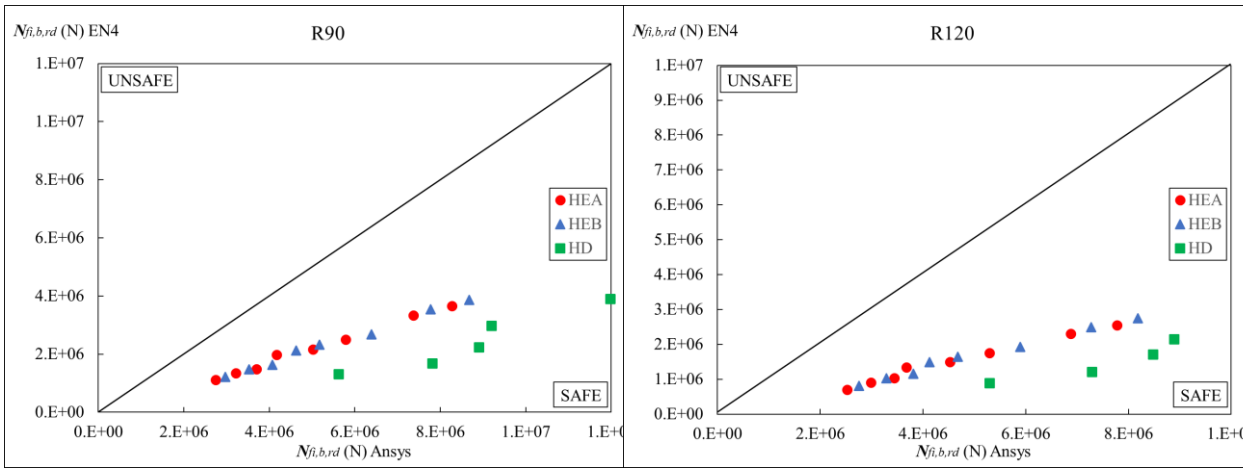

Figure 32: The design values of axial buckling load with two methods

Figure 32 shows a comparaison between the design values of the axial buckling load for the partially encased columns under fire situation, obtained with numerical simulation on ANSYS and that ones calculated with the balanced summation method from EN4.

And we can deduce that in the four classes of fire resistance, The simplified method shows a safe values, we can also coc«nclude that the steel profile with a greater cross-section factor have a greater resistance and this is noticed by the result of HD steel profile.

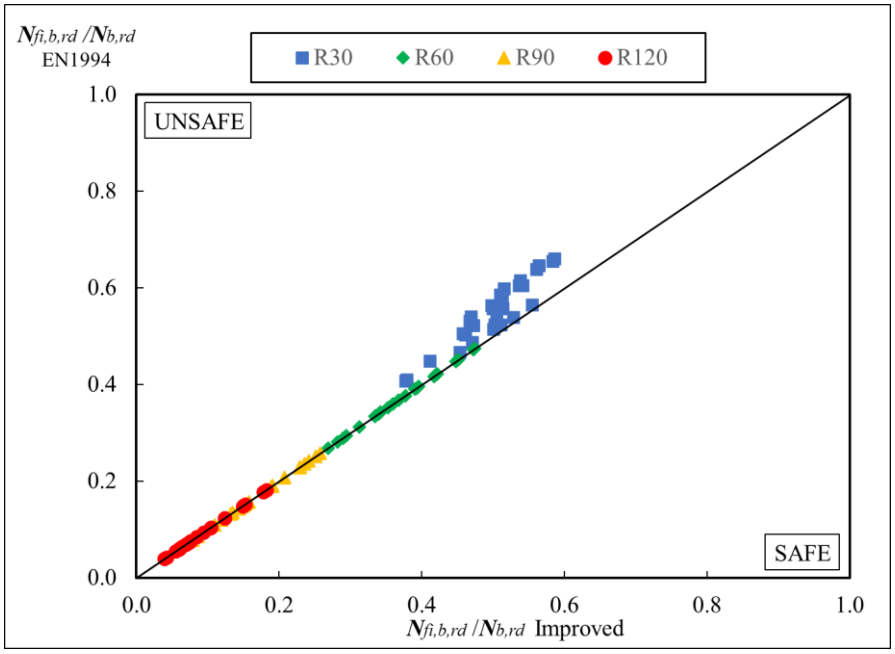

Figure 33: The design values of axial buckling load with two simplified methods

In figure 33 the values of buckling load according to the EN 1994-1.2 are compared to the values obtained by the improvement, whose show an unsafe value for R30.

7- CONCLUSIONS AND FUTURE PROPOSITION

In the present study, the effect of the fire resistance of partially encased columns has been evaluated on its load bearing capacity.

A new improved formula has been presented to the balanced summation model, as an alternative to the annex G of EN1994-1.2, in order to calculate the buckling resistance.

A new multi function, has been developed for the calculation of the average temperature of the four components of the column , so that it is possible to calculate the reduction factor in the elastic modulus of this components, affecting the calculation of flexural stiffness and the plastic resistance to axial compression.

With the aim to present safer results, the new improved solution method showed good results for profiles with a lower section factor, that is, profiles with larger dimensions, as it resulted in safe values for plastic resistance to axial compression and for effective flexural stiffness.Thus the two simplified solution methods show closer results.

Therefore the values of the two analytic method was compared to that one from euler buckling analysis (critical load) from the numerical analysis and it can be concluded that the column with higher height shows a safer value that the shortest one and all the steel profile show a safe values and specially HD profiles which shows a safer values as expected and presents a higher critical load when compared with HEB and HEA steel profile of the partially encased columns.

For the design values of the axial buckling load of PEC in fire situation, it was shown a safe values for all the fire class resistance R30-R60-R90-R120 because the numerical results are always higher that the ones presented by the new formulae or European standard due to the the full resistance of the four components, and the full geometry of column by the numerical model , it was also found that the numerical results is conservative for the HD profiles which show a safer results than HEB or HEA steel profiles.

We can also conclude that the improved method shows an unsafe results in comparison with the European standard while calculating the buckling resistance which decreases with the buckling length and for higher fire rating classes, smaller buckling loads are expected.

This study must be extended for other types of cross section and different configurations of PEC. Experimental tests are also required to validate the results.

REFERENCES

[1] CEN - EN 1994-1-2; "Eurocode 4 - Design of composite steel and concrete structures Part 1-2: General rules - Structural fire design", Brussels, August 2005.

[2] ISO834-1, "Fire-resistance tests - Elements of building construction - Part 1: General requirements", Switzerland, 1999.

[3] ANSYS®, "Academic Research Mechanical APDL". Release 20.R1

[4] R. F. Stevens e H. L. Malhotra, "Fire Resistance of Encased Steel Stanchions", proceedings of the Institution of Civil Engineers, p. 77–98, vol. 27, no 1, 1964.

[5] J. C. Dotreppe, J. M. Franssen, e J. B. Schleich, "Computer aided fire resistance for steel and composite structures", Acier - Stahl - Steel, vol. 3, p. 105–112, 1984.

[6] J. B. Schleich, Computer Assisted analysis of the fire resistance of steel and composite concrete-steel structure. Final Report EUR 10828, Luxembourg, 1987.

[7] Karl Kordina ''Behaviour of Composite Columns and Girders in Fire'' Technical University of Braunschweig - FIRE SAFETY SCIENCE-PROCEEDINGS OF THE SECOND INTERNATIONAL SYMPOSIUM, p. 681-695, 1989, Borehamwood, England.

[8] T. T. Lie e M. Chabot, "A method to predict the fire resistance of circular concrete filled hollow steel columns", Jounal of Fire Protection Engineering, vol. 2, no 4, p. 111–124, 1990.

[9] Stefan Winter and Jörg Lange, "Behavior of Partially Encased Composite Columns Using High-Strength Steel - Ultimate", proceedings of Composite Construction in Steel and Concrete IV, ISBN 0784406162, p. 539–550, 2002.

[10] António J.P. Moura Correia, João Paulo C. Rodrigues "Fire resistance of partially encased steel columns with restrained thermal elongation", Journal of Constructional Steel Research, vol. 67, no 4, p. 593–601, 2011.

[11] S. Huang, B. Davison and I. W. Burgess "High-temperature tests on joints to steel and partially-encased H-section columns", Journal of Constructional Steel Research, vol. 80, p. 243–251, 2013

[12] P. A. G. Piloto et al., "Experimental investigation of the fire resistance of partially encased beams", Journal of Constructional Steel Research, vol. 80, no Oct, p. 121– 137, 2013.

[13] S. Arezki e I. Said, "Practical fire design of partially encased composite steel concrete columns according to Eurocode 4", proceedings of MATEC Web of Conferences., p. 01029, vol. 11, EDP Sciences, 2014.

[14] Paulo Gonçalves Piloto et al., “Partially Encased Section: Strength and Stiffness Under Fire Conditions”, proceedings of IFireSS - International Fire Safety Symposium, p. 15– 18, Coimbra, Portugal, April 2015.

[15] M. Milanović, M. Cvetkovska, e P. Knežević, “Load-bearing capacity of fire exposed composite columns”, Gradjevinar, vol. 67, no 12, p. 1187–1197, 2015.

[16] A. Piquer e D. Hernández-Figueirido, “Protected steel columns vs partially encased columns: Fire resistance and economic considerations”, Journal of Constructional Steel Research, vol. 124, p. 47–56, May, 2016.

[17] J. Kralik, M. Klabnik, e A. Grmanova, “Nonlinear Analysis of Steel Concrete Columns Fire Resistance”, proceedings of Engineering Mechanics 2016, p 22, May 2016, Svratka, Czech Republic.

[18] A. Fellouh, N. Benlakehal, P. Piloto, A. Ramos e L. M. Mesquita, “Load caring capacity of partially encased columns for different fire ratings”, Fire Research 2016, p. 13-19, July 2016 , institute polytechnic of Bragança, Bragança, Portugal.

[19] P. A. G. Piloto et al., “Experimental bending tests of partially encased beams at elevated temperatures”, Fire Safety Journal, vol. 92, no May, p. 23–41, 2017[20] L. Calió, P. Piloto and R. Rigobello , “Balanced Summation model for the calculation of the buckling resistance of partially encased columns under fire : New improvements”, proceedings of Research and advanced technology in fire safety, p. 271–287, October 2017, University of Santander - GIDAI, Santander, Spain.

[21] B. Afredo, P.A.G. Piloto and D. Rossetto, “Partially encased columns: effect of resistance and rigidity on buckling resistance under fire action”, New improvement for the balanced summation method, p. 51-64, July 2018, Institute polytechnic of Bragança, Bragança, Portugal.

[22] Tectonica-online, “Steel profiles partially embedded in concrete for improving fire resistance”. [Online]. Available at: http://www.tectonicaonline.com/products/1710/improving_fire_resistance_concrete_embedded_profil es_partially_steel/. [Access 30-may-2020]

[23] CEN - EN 1993-1-1, “Eurocode 3: Design of steel structures - Part 1-1: General rules and rules for buildings Eurocode”. European Standard, p. 91, 2005, Brussels.

[24] CEN - EN 1992-1-1, “Eurocode 2: Design of concrete structures - Part 1-1: General rules and rules for buildings Eurocode”. European Standard, p. 225, 2004, Brussels.

[25] CEN - EN 1993-1-2, “Eurocode 3: Design of steel structures - Part 1-2: General rules - Structural fire design Eurocode”. European Standard, p. 78, 2005, Brussels.

[26] CEN - EN 1991-1-2, “Eurocode 1: Actions on structures -Part 1-2: General actions - Actions on structures exposed to fire”. European Standard, p. 59, 2002, Brussels.

[27] CEN - EN 1994-1-1, “Eurocode 4: Design of composite steel and concrete structures - Part 1-1: General rules and rules for buildings Eurocode”. European Standard, p. 118, 2004, Brussels.

[28] CEN - EN 1992-1-2, “Eurocode 2: Design of concrete structures - Part 1-2: General rules - Structural fire design Eurocode”. European Standard p. 97, 2004, Brussels.

[29] Valdir. P. e Silva, “Estruturas de aço em situação de incêndio. Determinação de temperatura nos elementos estruturais de aço com proteção térmica”, p. 14-27, May, 2002, Brasília, Brasil.

[30] O. Jungbluth, “Optimierte Verbundbauteile”, 1982, Köeln: Stahlbau Verlags GmbH.

[31] B. Afredo, P.A.G. Piloto and D. Rossetto, “Partially encased columns: effect of resistance and rigidity on buckling resistance under fire action”, Figure 17, July 2018, Institute polytechnic of Bragança, Bragança, Portugal.

ANNEX A:

Balanced summation model - EN 1994-1.2 Annex G

ANNEX A - Balanced summation model - EN 1994-1-2 Annex G

A-1 Average temperature and reduction factor of components:

A-1.1 Flanges of the steel profile:

Performing the calculations presented in equation (23) from the third chapiter, and considering the parameters shown in table 11, the average temperatures are obtained at the edges of the profiles under study, giving rise to the values presented in table AA1.

		$\theta_{f,t}$ [°C]			
Profiles	A_m/V	***R30***	***R60***	***R90***	***R120***
HEA 240	17.029	714.3	842.6	909.7	975.8
HEA 280	14.550	690.4	819.0	894.5	964.7
HEA 300	13.563	680.9	809.5	888.4	960.4
HEA 360	12.381	669.5	798.2	881.1	955.1
HEA 400	11.795	663.8	792.6	877.5	952.5
HEA 450	11.212	658.2	787.1	874.0	949.9
HEA 500	10.748	653.7	782.6	871.1	947.8
HEA 600	10.056	647.0	776.0	866.8	944.8
HEA 700	9.565	642.3	771.3	863.8	942.6
HEA 800	9.198	638.8	767.8	861.6	940.9
HEB 240	16.667	710.8	839.2	907.5	974.2
HEB 280	14.286	687.9	816.4	892.9	963.6
HEB 300	13.333	678.7	807.3	887.0	959.3
HEB 360	12.222	667.9	796.7	880.2	954.4
HEB 400	11.667	662.6	791.4	876.8	951.9
HEB 450	11.111	657.2	786.1	873.3	949.4
HEB 500	10.667	652.9	781.9	870.6	947.5
HEB 600	10.000	646.5	775.5	866.5	944.5
HEB 700	9.524	641.9	771.0	863.6	942.4
HEB 800	9.167	638.5	767.5	861.4	940.8
HD 260x54.1	15.889	703.3	831.7	902.7	970.7
HD 260x142	14.741	692.3	820.8	895.7	965.6
HD 320x127	12.917	674.6	803.4	884.4	957.5
HD 320x198	12.367	669.3	798.1	881.1	955.0
HD 320x300	11.723	663.1	792.0	877.1	952.2
HD 400x237	10.326	649.7	778.6	868.5	946.0
HD 400x382	9.734	643.9	773.0	864.9	943.3
HD 400x551	9.180	638.6	767.7	861.5	940.9
HD 400x818	8.468	631.7	760.9	857.1	937.7
HD 400x1299	7.535	622.7	752.0	851.3	933.5

Table AA1: The average temperature of the flanges for different fire class

A-1.2 Web of the steel profile:

The height reduction $h_{w,fi}$ of the web is calculating following equation 28 and considering the parameters shown in table 12.

	$h_{w,fi}$ [m]				
Profiles	***Am/v***	***R30***	***R60***	***R90***	***R120***
HEA 240	17.029	0.01341	0.03281	0.05309	0.06580
HEA 280	14.550	0.01339	0.03204	0.05002	0.05988
HEA 300	13.563	0.01333	0.03165	0.04887	0.05802
HEA 360	12.381	0.01315	0.03071	0.04645	0.05439
HEA 400	11.795	0.01313	0.03043	0.04563	0.05316
HEA 450	11.212	0.01309	0.03014	0.04486	0.05203
HEA 500	10.748	0.01307	0.02993	0.04429	0.05121
HEA 600	10.056	0.01313	0.02984	0.04383	0.05048
HEA 700	9.565	0.01318	0.02978	0.04354	0.05002
HEA 800	9.198	0.01325	0.02983	0.04345	0.04984
HEB 240	16.667	0.01281	0.03115	0.04981	0.06095
HEB 280	14.286	0.01288	0.03070	0.04765	0.05679
HEB 300	13.333	0.01286	0.03043	0.04678	0.05537
HEB 360	12.222	0.01277	0.02976	0.04490	0.05250
HEB 400	11.667	0.01278	0.02959	0.04429	0.05155
HEB 450	11.111	0.01279	0.02941	0.04372	0.05067
HEB 500	10.667	0.01280	0.02928	0.04329	0.05004
HEB 600	10.000	0.01291	0.02931	0.04303	0.04955
HEB 700	9.524	0.01299	0.02934	0.04287	0.04924
HEB 800	9.167	0.01308	0.02944	0.04287	0.04917
HD 260x54.1	15.889	0.01375	0.03334	0.05311	0.06473
HD 260x142	14.741	0.01197	0.02855	0.04436	0.05291
HD 320x127	12.917	0.01279	0.03010	0.04592	0.05407
HD 320x198	12.367	0.01189	0.02783	0.04216	0.04943
HD 320x300	11.723	0.01084	0.02519	0.03788	0.04420
HD 400x237	10.326	0.01211	0.02811	0.04223	0.04926
HD 400x382	9.734	0.01116	0.02577	0.03847	0.04471
HD 400x551	9.180	0.01016	0.02335	0.03469	0.04019
HD 400x818	8.468	0.00897	0.02049	0.03025	0.03494
HD 400x1299	7.535	0.00765	0.01737	0.02550	0.02936

Table AA2: The height reduction of the web for different fire class

A-1.3 Concrete:

The thickness reduction of the area of the concrete $b_{c,fi}$ are obtained from the table 13 with linear interpolation, giving rise to the values presented in table 26.

	$b_{c,fi}$ [m]				
Profiles	***Am/v***	***R30***	***R60***	***R90***	***R120***
HEA 240	17.029	0.004	0.015	0.031	0.058
HEA 280	14.550	0.004	0.015	0.030	0.053
HEA 300	13.563	0.004	0.015	0.029	0.051
HEA 360	12.381	0.004	0.015	0.029	0.049
HEA 400	11.795	0.004	0.015	0.028	0.048
HEA 450	11.212	0.004	0.015	0.028	0.046
HEA 500	10.748	0.004	0.015	0.028	0.045
HEA 600	10.056	0.004	0.015	0.028	0.044
HEA 700	9.565	0.004	0.015	0.027	0.043
HEA 800	9.198	0.004	0.015	0.027	0.042
HEB 240	16.667	0.004	0.015	0.031	0.057
HEB 280	14.286	0.004	0.015	0.030	0.053
HEB 300	13.333	0.004	0.015	0.029	0.051
HEB 360	12.222	0.004	0.015	0.029	0.048
HEB 400	11.667	0.004	0.015	0.028	0.047
HEB 450	11.111	0.004	0.015	0.028	0.046
HEB 500	10.667	0.004	0.015	0.028	0.045
HEB 600	10.000	0.004	0.015	0.028	0.044
HEB 700	9.524	0.004	0.015	0.027	0.043
HEB 800	9.167	0.004	0.015	0.027	0.042
HD 260x54.1	15.889	0.004	0.015	0.030	0.056
HD 260x142	14.741	0.004	0.015	0.030	0.053
HD 320x127	12.917	0.004	0.015	0.029	0.050
HD 320x198	12.367	0.004	0.015	0.029	0.049
HD 320x300	11.723	0.004	0.015	0.028	0.047
HD 400x237	10.326	0.004	0.015	0.028	0.045
HD 400x382	9.734	0.004	0.015	0.027	0.043
HD 400x551	9.180	0.004	0.015	0.027	0.042
HD 400x818	8.468	0.004	0.015	0.027	0.041
HD 400x1299	7.535	0.004	0.015	0.026	0.039

Table AA3: The thickness reduction of the concrete for different fire class

The average temperatures for the concrete $\boldsymbol{\theta_{c,t}}$ for different fire rating are obtained from table 14 with linear interpolation, giving rise to the values presented in table AA4.

$\boldsymbol{\theta_{c,t}}$ [°C]					
Profiles	***Am/v***	***R30***	***R60***	***R90***	***R120***
HEA 240	17.029	248.5	366.9	440.3	514.7
HEA 280	14.550	227.1	346.3	415.5	479.3
HEA 300	13.563	218.5	338.0	405.6	465.2
HEA 360	12.381	208.3	328.2	391.2	448.3
HEA 400	11.795	203.3	323.3	382.8	439.9
HEA 450	11.212	198.3	318.4	374.5	431.6
HEA 500	10.748	194.2	314.6	367.8	425.0
HEA 600	10.056	188.3	308.8	357.9	415.1
HEA 700	9.565	184.0	304.7	350.9	408.1
HEA 800	9.198	180.9	301.7	345.7	402.8
HEB 240	16.667	245.3	363.9	436.7	509.5
HEB 280	14.286	224.8	344.0	412.9	475.5
HEB 300	13.333	216.6	336.1	403.3	461.9
HEB 360	12.222	207.0	326.9	388.9	446.0
HEB 400	11.667	202.2	322.2	381.0	438.1
HEB 450	11.111	197.4	317.6	373.0	430.2
HEB 500	10.667	193.5	313.9	366.7	423.8
HEB 600	10.000	187.8	308.3	357.1	414.3
HEB 700	9.524	183.7	304.4	350.3	407.5
HEB 800	9.167	180.6	301.4	345.2	402.4
HD 260x54.1	15.889	238.6	357.4	428.9	498.4
HD 260x142	14.741	228.7	347.8	417.4	482.0
HD 320x127	12.917	213.0	332.6	398.8	456.0
HD 320x198	12.367	208.2	328.1	391.0	448.1
HD 320x300	11.723	202.7	322.7	381.8	438.9
HD 400x237	10.326	190.6	311.1	361.8	418.9
HD 400x382	9.734	185.5	306.1	353.3	410.5
HD 400x551	9.180	180.7	301.5	345.4	402.6
HD 400x818	8.468	174.6	289.4	335.3	386.7
HD 400x1299	7.535	166.5	270.7	321.9	363.4

Table AA 4: The average temperature of the concrete for different fire class

A-2 The design value of the plastic resistance to axial compression:

After calculating the design value of the plastic for the four components of the steel profile, so that all can be added in a balanced summation according to equation 18:

	$N_{fi,pl,Rd}$ (N)				
Profiles	T = 20ºC	R 30	R 60	R 90	R 120
HEA 240	3439373	2004742	1506357	933414	496935
HEA 280	4628305	2924060	2244045	1469221	876939
HEA 300	5184016	3291347	2485607	1676894	1051748
HEA 360	6272946	4021731	2998912	2129361	1456207
HEA 400	6897497	4502464	3369371	2452283	1748688
HEA 450	8251794	5665477	4387398	3164186	2248783
HEA 500	9012762	6229889	4822661	3545332	2594724
HEA 600	10274319	7305485	5709250	4341574	3326598
HEA 700	12541009	9374439	7572733	5750681	4416647
HEA 800	13672635	10409459	8467225	6573854	5182482
HEB 240	4232140	2275705	1670285	1058625	607043
HEB 280	5524112	3252985	2427219	1611225	1001685
HEB 300	6177875	3692467	2713644	1856406	1209828
HEB 360	7300963	4476216	3270594	2346640	1650923
HEB 400	7949361	4989875	3669640	2694999	1968164
HEB 450	9333305	6190813	4721853	3437714	2498250
HEB 500	10123920	6792282	5190480	3849536	2874211
HEB 600	11447349	7940405	6144223	4708948	3668266
HEB 700	13775911	10079065	8073685	6181215	4820787
HEB 800	14970698	11182982	9034242	7068241	5649934
HD 260x54.1	3348437	2103779	1601112	1021417	567862
HD 260x142	6393707	3256011	2286845	1555253	1037910
HD 320x127	6597267	3960467	2893834	2016012	1352595
HD 320x198	9096680	5077365	3548860	2541074	1818697
HD 320x300	12655207	6719743	4523533	3308521	2502682
HD 400x237	12191752	7372978	5245073	3740012	2713835
HD 400x382	16964568	9794046	6707376	4867718	3713959
HD 400x551	22856304	12773265	8452978	6182837	4871403
HD 400x818	32263369	17667716	11311425	8298054	6734155
HD 400x1299	49074667	27071944	17028116	12594909	10554597

Table AA5: The plastic resistance of the steel profile for different fire class

A-3 The effective flexural stiffness:

After calculating the effective flexural stiffness for each component of the steel profile, so that all can be added in a balanced summation with the reduction coefficient depending on the effect of thermal stress according to equation 19:

	$(EI)_{fi,eff,z}$				
Profiles	T = 20ºC	R 30	R 60	R 90	R 120
HEA 240	8950255	2334457	1403671	780669	521774
HEA 280	16774761	5389295	3246833	1796226	1139861
HEA 300	21915938	7148588	4181668	2336022	1493992
HEA 360	26180032	8379328	4662531	2650513	1742592
HEA 400	28266116	9067929	4939851	2820428	1870314
HEA 450	33520110	12243839	6906160	3879260	2481938
HEA 500	36240836	13106888	7261363	4100999	2652277
HEA 600	39865892	14422235	7816884	4443723	2894900
HEA 700	47155612	19028023	10697297	6002214	3784178
HEA 800	49873674	20064940	11165260	6296539	3982135
HEB 240	11371460	2653534	1588509	913353	648373
HEB 280	20618366	6028320	3556217	2016636	1349932
HEB 300	26644099	8009619	4571249	2612901	1757807
HEB 360	30910085	9325060	5069143	2933815	2013171
HEB 400	32997808	10054676	5355650	3107624	2144737
HEB 450	38253305	13270774	7331032	4170193	2760064
HEB 500	40975706	14167525	7694046	4395451	2933890
HEB 600	44604771	15533269	8262394	4744738	3183012
HEB 700	51900572	20178769	11155094	6310850	4079807
HEB 800	54623192	21245377	11632392	6611091	4283627
HD 260x54.1	10106437	2927845	1759877	960687	608990
HD 260x142	21794075	4834422	2758201	1655662	1250392
HD 320x127	28368872	8500235	4756504	2736506	1858846
HD 320x198	41656481	11399578	6053784	3611587	2645763
HD 320x300	61811620	16049645	8072858	4959574	3874117
HD 400x237	96185243	32357865	17262295	10033392	7009595
HD 400x382	142065405	44678825	22405833	13339853	9956095
HD 400x551	205200767	62153411	29512435	17915894	14098367
HD 400x818	320773524	95748337	43003108	26596526	22056907
HD 400x1299	579830834	176572776	76047420	48322638	42178266

Table AA6: The effective flexural stiffness of the steel profile for different fire class

A-4 The critical axial compression resistance:

The critical axial compression resistance or Euler buckling load ($N_{fi,cr,z}$) is calculated around the Z axis for the different buckling length at room temperature and for different fire resistance class following equation (20):

T = 20 °C						
$N_{fi,cr,z}$ **(N)**						
	l = 3m			***l = 4m***		
Profiles	***lθ = l***	***lθ = 0.7l***	***lθ = 0.5l***	***lθ = l***	***lθ = 0.7l***	***lθ = 0.5l***
HEA 240	9815053	14021504	19630106	-	7887096	11041934
HEA 280	18395584	26279406	36791168	-	14782166	20695032
HEA 300	24033515	34333593	48067030	13518852	19312646	27037704
HEA 360	28709617	41013739	57419234	16149160	23070228	32298319
HEA 400	30997264	44281806	61994529	17435961	24908516	34871922
HEA 450	36758914	52512735	73517828	20676889	29538413	41353778
HEA 500	39742524	56775034	79485048	22355170	31935957	44710339
HEA 600	43717842	62454060	87435684	24591286	35130409	49182572
HEA 700	51711915	73874164	103423830	29087952	41554218	58175905
HEA 800	54692603	78132291	109385207	30764589	43949413	61529179
HEB 240	12470201	17814573	24940402	-	10020697	14028976
HEB 280	22610568	32300811	45221136	-	18169206	25436889
HEB 300	29218524	41740749	58437049	16435420	23479171	32870840
HEB 360	33896702	48423860	67793404	19066895	27238421	38133789
HEB 400	36186145	51694493	72372290	20354707	29078152	40709413
HEB 450	41949443	59927775	83898886	23596562	33709374	47193123
HEB 500	44934890	64192700	89869780	25275876	36108394	50551751
HEB 600	48914605	69878007	97829210	27514465	39306379	55028930
HEB 700	56915346	81307637	113830692	32014882	45735546	64029764
HEB 800	59901033	85572904	119802066	33694331	48134759	67388662
HD 260x54.1	11082949	15832784	22165897	-	8905941	12468317
HD 260x142	23899878	34142682	47799755	-	19205259	26887362
HD 320x127	31109949	44442785	62219898	17499346	24999066	34998693
HD 320x198	45681443	65259204	91362886	25695812	36708302	51391623
HD 320x300	67784026	96834323	135568052	38128515	54469307	76257029
HD 400x237	105478922	150684174	210957843	59331893	84759848	118663787
HD 400x382	155792150	222560214	311584300	87633084	125190120	175266168
HD 400x551	225027821	321468316	450055643	126578149	180825928	253156299
HD 400x818	351767531	502525045	703535063	197869236	282670338	395738473
HD 400x1299	635855661	908365230	1271711322	357668809	510955442	715337619

Table AA7: The critical axial compression resistance of the steel profile at room temperature

R 30						
$N_{fi,cr,z}$ (N)						
	l = 3m			*l = 4m*		
Profiles	***lθ = l***	***lθ = 0.7l***	***lθ = 0.5l***	***lθ = l***	***lθ = 0.7l***	***lθ = 0.5l***
HEA 240	2560019	3657169	5120037	-	2057158	2880021
HEA 280	5910024	8442891	11820047	-	4749126	6648777
HEA 300	7839304	11199006	15678608	4409609	6299441	8819217
HEA 360	9188962	13127088	18377924	5168791	7383987	10337582
HEA 400	9944097	14205852	19888193	5593554	7990792	11187109
HEA 450	13426872	19181246	26853744	7552615	10789451	15105231
HEA 500	14373311	20533302	28746622	8084987	11549982	16169975
HEA 600	15815750	22593929	31631500	8896359	12709085	17792719
HEA 700	20866562	29809375	41733125	11737441	16767773	23474883
HEA 800	22003669	31433813	44007338	12377064	17681520	24754128
HEB 240	2909926	4157037	5819851	-	2338333	3273666
HEB 280	6610793	9443990	13221586	-	5312244	7437142
HEB 300	8783530	12547900	17567060	4940736	7058194	9881471
HEB 360	10226073	14608675	20452145	5752166	8217380	11504332
HEB 400	11026186	15751694	22052371	6202229	8860328	12404459
HEB 450	14553032	20790045	29106064	8186080	11694401	16372161
HEB 500	15536430	22194900	31072860	8739242	12484631	17478484
HEB 600	17034136	24334479	34068271	9581701	13688145	19163403
HEB 700	22128496	31612137	44256992	12447279	17781827	24894558
HEB 800	23298163	33283090	46596326	13105217	18721738	26210433
HD 260x54.1	3210741	4586773	6421482	-	2580060	3612084
HD 260x142	5301536	7573624	10603073	-	4260163	5964229
HD 320x127	9321551	13316501	18643101	5243372	7490532	10486744
HD 320x198	12501037	17858624	25002073	7031833	10045476	14063666
HD 320x300	17600405	25143436	35200810	9900228	14143182	19800455
HD 400x237	35484370	50691957	70968740	19959958	28514226	39919916
HD 400x382	48995814	69994020	97991628	27560145	39371636	55120291
HD 400x551	68158842	97369774	136317684	38339349	54770498	76678697
HD 400x818	104999801	149999716	209999603	59062388	84374840	118124777
HD 400x1299	193633717	276619595	387267433	108918966	155598522	217837931

Table AA8: The critical axial compression resistance of the steel profile for R30

R 60						
$N_{fi,cr,z}$ (N)						
	$l = 3m$			$l = 4m$		
Profiles	$l\theta = l$	$l\theta = 0.7l$	$l\theta = 0.5l$	$l\theta = l$	$l\theta = 0.7l$	$l\theta = 0.5l$
HEA 240	-	2198997	3078596	-	-	1731710
HEA 280	-	5086501	7121101	-	2861157	4005620
HEA 300	4585713	6551018	9171425	2579463	3684948	5158927
HEA 360	5113038	7304340	10226076	2876084	4108691	5752168
HEA 400	5417153	7738790	10834306	3047149	4353069	6094297
HEA 450	7573452	10819217	15146903	4260067	6085809	8520133
HEA 500	7962976	11375680	15925952	4479174	6398820	8958348
HEA 600	8572173	12245961	17144346	4821847	6888353	9643694
HEA 700	11730899	16758427	23461798	6598631	9426615	13197261
HEA 800	12244078	17491540	24488155	6887294	9838991	13774587
HEB 240	-	2488564	3483990	-	-	1959744
HEB 280	-	5571184	7799657	-	3133791	4387307
HEB 300	5012935	7161336	10025870	2819776	4028251	5639552
HEB 360	5558937	7941339	11117875	3126902	4467003	6253805
HEB 400	5873128	8390183	11746256	3303634	4719478	6607269
HEB 450	8039377	11484824	16078753	4522149	6460213	9044299
HEB 500	8437466	12053522	16874931	4746074	6780106	9492149
HEB 600	9060729	12943898	18121458	5096660	7280943	10193320
HEB 700	12232930	17475614	24465859	6881023	9830033	13762046
HEB 800	12756345	18223350	25512690	7175444	10250635	14350888
HD 260x54.1	-	2757030	3859843	-	-	2171162
HD 260x142	-	4321008	6049412	-	-	3402794
HD 320x127	5216091	7451558	10432181	2934051	4191501	5868102
HD 320x198	6638717	9483882	13277434	3734278	5334683	7468557
HD 320x300	8852880	12646971	17705760	4979745	7113921	9959490
HD 400x237	18930224	27043178	37860449	10648251	15211787	21296502
HD 400x382	24570745	35101065	49141491	13821044	19744349	27642088
HD 400x551	32364007	46234295	64728013	18204754	26006791	36409507
HD 400x818	47158185	67368836	94316370	26526479	37894970	53052958
HD 400x1299	83395327	119136182	166790655	46909872	67014102	93819743

Table AA9: The critical axial compression resistance of the steel profile for R60

R 90						
$N_{fi,cr,z}$ (N)						
	l = 3m			*l = 4m*		
Profiles	***lθ = l***	***lθ = 0.7l***	***lθ = 0.5l***	***lθ = l***	***lθ = 0.7l***	***lθ = 0.5l***
HEA 240	-	-	-	-	-	-
HEA 280	-	-	-	-	-	-
HEA 300	2561735	3659621	5123470	1440976	2058537	2881952
HEA 360	2906613	4152305	5813227	1634970	2335671	3269940
HEA 400	3092945	4418493	6185890	1739782	2485402	3479563
HEA 450	4254085	6077264	8508170	2392923	3418461	4785845
HEA 500	4497249	6424641	8994498	2529703	3613861	5059405
HEA 600	4873087	6961553	9746174	2741112	3915874	5482223
HEA 700	6582164	9403092	13164329	3702467	5289239	7404935
HEA 800	6904927	9864182	13809854	3884022	5548602	7768043
HEB 240	-	-	-	-	-	-
HEB 280	-	-	-	-	-	-
HEB 300	2865366	4093380	5730732	1611768	2302526	3223537
HEB 360	3217288	4596126	6434576	1809724	2585321	3619449
HEB 400	3407891	4868415	6815781	1916938	2738483	3833877
HEB 450	4573129	6533041	9146258	2572385	3674836	5144770
HEB 500	4820151	6885931	9640303	2711335	3873336	5422670
HEB 600	5203187	7433124	10406374	2926793	4181132	5853585
HEB 700	6920621	9886601	13841242	3892849	5561213	7785699
HEB 800	7249873	10356961	14499746	4078054	5825791	8156107
HD 260x54.1	-	-	-	-	-	-
HD 260x142	-	-	-	-	-	-
HD 320x127	3000914	4287020	6001829	1688014	2411449	3376029
HD 320x198	3960548	5657926	7921097	2227809	3182584	4455617
HD 320x300	5438782	7769688	10877564	3059315	4370450	6118630
HD 400x237	11002845	15718350	22005690	6189100	8841572	12378201
HD 400x382	14628786	20898266	29257572	8228692	11755275	16457384
HD 400x551	19646976	28067108	39293951	11051424	15787748	22102848
HD 400x818	29166354	41666220	58332708	16406074	23437249	32812148
HD 400x1299	52991702	75702432	105983405	29807833	42582618	59615665

Table AA10: The critical axial compression resistance of the steel profile for R90

R 120						
$N_{fi,cr,z}$ (N)						
	$l = 3m$			$l = 4m$		
Profiles	$l\theta = l$	$l\theta = 0.7l$	$l\theta = 0.5l$	$l\theta = l$	$l\theta = 0.7l$	$l\theta = 0.5l$
HEA 240	572190	817414	1144379	321857	459795	643713
HEA 280	1249998	1785711	2499996	703124	1004463	1406248
HEA 300	1638346	2340494	3276692	921570	1316528	1843139
HEA 360	1910966	2729952	3821933	1074919	1535598	2149837
HEA 400	2051029	2930041	4102058	1153704	1648148	2307407
HEA 450	2721749	3888213	5443499	1530984	2187120	3061968
HEA 500	2908548	4155068	5817095	1636058	2337226	3272116
HEA 600	3174614	4535162	6349227	1785720	2551029	3571440
HEA 700	4149815	5928307	8299630	2334271	3334673	4668542
HEA 800	4366899	6238428	8733799	2456381	3509115	4912762
HEB 240	711020	1015743	1422041	399949	571356	799898
HEB 280	1480366	2114808	2960731	832706	1189580	1665411
HEB 300	1927651	2753788	3855303	1084304	1549006	2168608
HEB 360	2207689	3153841	4415377	1241825	1774036	2483650
HEB 400	2351967	3359953	4703935	1322982	1889974	2645963
HEB 450	3026749	4323928	6053499	1702547	2432209	3405093
HEB 500	3217370	4596243	6434740	1809771	2585387	3619541
HEB 600	3490563	4986519	6981126	1963442	2804917	3926883
HEB 700	4474009	6391441	8948018	2516630	3595186	5033260
HEB 800	4697523	6710747	9395046	2642357	3774795	5284713
HD 260x54.1	667832	954046	1335665	375656	536651	751311
HD 260x142	1371208	1958869	2742417	771305	1101864	1542609
HD 320x127	2038453	2912076	4076906	1146630	1638043	2293260
HD 320x198	2901403	4144862	5802807	1632039	2331485	3264079
HD 320x300	4248445	6069207	8496890	2389750	3413929	4779501
HD 400x237	7686881	10981258	15373762	4323870	6176958	8647741
HD 400x382	10918080	15597257	21836160	6141420	8773457	12282840
HD 400x551	15460589	22086556	30921178	8696581	12423688	17393163
HD 400x818	24188105	34554435	48376209	13605809	19436870	27211618
HD 400x1299	46253644	66076634	92507288	26017675	37168107	52035350

Table AA11: The critical axial compression resistance of the steel profile for R120

A-5 The reduction coefficient χ_z

Using $\bar{\lambda}_\theta$ and the buckling curve c of EN 1993-1-1[13], the reduction coefficient χ_z for the axial buckling load of the steel profile is calculated for different fire resistance class in tables below:

$T = 20\ ^oC$						
	χ_z					
Profiles	***l = 3m***			***l = 4m***		
	$l\theta = l$	$l\theta = 0.7l$	$l\theta = 0.5l$	$l\theta = l$	$l\theta = 0.7l$	$l\theta = 0.5l$
HEA 240	0.7901	0.8456	0.8875	-	0.7491	0.8099
HEA 280	0.8421	0.8869	0.9210	-	0.8091	0.8580
HEA 300	0.8627	0.9033	0.9346	0.7739	0.8328	0.8771
HEA 360	0.8610	0.9020	0.9335	0.7715	0.8309	0.8756
HEA 400	0.8587	0.9001	0.9320	0.7681	0.8282	0.8734
HEA 450	0.8575	0.8992	0.9312	0.7664	0.8269	0.8723
HEA 500	0.8562	0.8982	0.9303	0.7645	0.8254	0.8711
HEA 600	0.8515	0.8944	0.9272	0.7576	0.8199	0.8667
HEA 700	0.8472	0.8909	0.9244	0.7513	0.8150	0.8627
HEA 800	0.8430	0.8876	0.9216	0.7452	0.8101	0.8588
HEB 240	0.7957	0.8500	0.8910	-	0.7554	0.8150
HEB 280	0.8462	0.8901	0.9237	-	0.8138	0.8618
HEB 300	0.8652	0.9054	0.9363	0.7776	0.8357	0.8794
HEB 360	0.8629	0.9035	0.9347	0.7742	0.8330	0.8773
HEB 400	0.8603	0.9015	0.9331	0.7705	0.8301	0.8749
HEB 450	0.8587	0.9002	0.9320	0.7681	0.8282	0.8734
HEB 500	0.8571	0.8988	0.9309	0.7657	0.8263	0.8719
HEB 600	0.8520	0.8948	0.9276	0.7584	0.8205	0.8672
HEB 700	0.8475	0.8912	0.9246	0.7517	0.8153	0.8630
HEB 800	0.8430	0.8876	0.9217	0.7453	0.8102	0.8589
HD 260x54.1	0.8148	0.8652	0.9033	-	0.7776	0.8327
HD 260x142	0.8333	0.8799	0.9153	-	0.7989	0.8499
HD 320x127	0.8648	0.9051	0.9360	0.7771	0.8353	0.8791
HD 320x198	0.8726	0.9113	0.9412	0.7883	0.8442	0.8863
HD 320x300	0.8802	0.9175	0.9463	0.7994	0.8530	0.8934
HD 400x237	0.9286	0.9571	0.9794	0.8687	0.9082	0.9386
HD 400x382	0.9338	0.9613	0.9830	0.8760	0.9141	0.9435
HD 400x551	0.9396	0.9661	0.9871	0.8841	0.9206	0.9489
HD 400x818	0.9477	0.9729	0.9928	0.8953	0.9297	0.9565
HD 400x1299	0.9604	0.9835	1.0018	0.9129	0.9441	0.9685

Table AA12: The reduction coefficient of the buckling load at room temperature

R 30						
χ_z						
Profiles	*l = 3m*			*l = 4m*		
	lθ = l	*lθ = 0.7l*	*lθ = 0.5l*	*lθ = l*	*lθ = 0.7l*	*lθ = 0.5l*
HEA 240	0.6091	0.6996	0.7700	-	0.5474	0.6406
HEA 280	0.7226	0.7922	0.8445	-	0.6718	0.7473
HEA 300	0.7566	0.8191	0.8661	0.6221	0.7105	0.7789
HEA 360	0.7483	0.8126	0.8608	0.6109	0.7010	0.7712
HEA 400	0.7414	0.8071	0.8564	0.6016	0.6931	0.7648
HEA 450	0.7556	0.8184	0.8655	0.6208	0.7094	0.7780
HEA 500	0.7503	0.8141	0.8621	0.6135	0.7033	0.7730
HEA 600	0.7373	0.8038	0.8538	0.5960	0.6884	0.7610
HEA 700	0.7430	0.8084	0.8574	0.6037	0.6950	0.7663
HEA 800	0.7322	0.7998	0.8506	0.5894	0.6827	0.7563
HEB 240	0.6037	0.6999	0.7703	-	0.5478	0.6410
HEB 280	0.7238	0.7931	0.8452	-	0.6731	0.7485
HEB 300	0.7564	0.8189	0.8659	0.6218	0.7102	0.7787
HEB 360	0.7483	0.8126	0.8608	0.6108	0.7010	0.7712
HEB 400	0.7415	0.8072	0.8565	0.6017	0.6933	0.7649
HEB 450	0.7540	0.8171	0.8644	0.6186	0.7075	0.7765
HEB 500	0.7485	0.8128	0.8610	0.6112	0.7013	0.7714
HEB 600	0.7353	0.8023	0.8526	0.5935	0.6862	0.7592
HEB 700	0.7402	0.8061	0.8556	0.5999	0.6917	0.7637
HEB 800	0.7291	0.7974	0.8486	0.5853	0.6792	0.7534
HD 260x54.1	0.6562	0.7387	0.8016	-	0.5980	0.6853
HD 260x142	0.6724	0.7519	0.8122	-	0.6157	0.7005
HD 320x127	0.7543	0.8173	0.8646	0.6189	0.7078	0.7767
HD 320x198	0.7631	0.8242	0.8702	0.6310	0.7179	0.7849
HD 320x300	0.7747	0.8335	0.8776	0.6472	0.7313	0.7957
HD 400x237	0.8674	0.9071	0.9377	0.7808	0.8382	0.8815
HD 400x382	0.8721	0.9110	0.9409	0.7877	0.8437	0.8859
HD 400x551	0.8798	0.9171	0.9460	0.7988	0.8525	0.8930
HD 400x818	0.8919	0.9270	0.9542	0.8164	0.8664	0.9043
HD 400x1299	0.9110	0.9426	0.9673	0.8438	0.8882	0.9222

Table AA13: The reduction coefficient of the buckling load for R30

R 60						
χ_z						
Profiles	*l = 3m*			*l = 4m*		
	lθ = l	*lθ = 0.7l*	*lθ = 0.5l*	*lθ = l*	*lθ = 0.7l*	*lθ = 0.5l*
HEA 240	-	0.6448	0.7250	-	-	0.5799
HEA 280	-	0.7467	0.8080	-	0.6087	0.6945
HEA 300	0.7022	0.7759	0.8314	0.5507	0.6488	0.7283
HEA 360	0.6836	0.7610	0.8195	0.5278	0.6281	0.7110
HEA 400	0.6693	0.7494	0.8102	0.5106	0.6123	0.6976
HEA 450	0.6866	0.7634	0.8214	0.5314	0.6314	0.7138
HEA 500	0.6758	0.7547	0.8144	0.5184	0.6195	0.7037
HEA 600	0.6520	0.7353	0.7989	0.4906	0.5935	0.6814
HEA 700	0.6600	0.7418	0.8041	0.4997	0.6021	0.6888
HEA 800	0.6423	0.7273	0.7925	0.4796	0.5829	0.6722
HEB 240	-	0.6501	0.7294	-	-	0.5856
HEB 280	-	0.7492	0.8101	-	0.6121	0.6974
HEB 300	0.7024	0.7761	0.8316	0.5510	0.6491	0.7286
HEB 360	0.6829	0.7604	0.8190	0.5269	0.6273	0.7103
HEB 400	0.6682	0.7485	0.8094	0.5093	0.6111	0.6965
HEB 450	0.6833	0.7607	0.8193	0.5274	0.6277	0.7107
HEB 500	0.6720	0.7516	0.8120	0.5138	0.6153	0.7001
HEB 600	0.6474	0.7315	0.7958	0.4853	0.5884	0.6770
HEB 700	0.6544	0.7372	0.8004	0.4933	0.5960	0.6835
HEB 800	0.6361	0.7222	0.7883	0.4726	0.5762	0.6663
HD 260x54.1	-	0.6860	0.7590	-	-	0.6254
HD 260x142	-	0.7076	0.7766	-	-	0.6497
HD 320x127	0.6968	0.7716	0.8280	0.5439	0.6428	0.7233
HD 320x198	0.7053	0.7784	0.8334	0.5547	0.6523	0.7313
HD 320x300	0.7155	0.7865	0.8399	0.5676	0.6638	0.7408
HD 400x237	0.8281	0.8757	0.9119	0.7236	0.7929	0.8451
HD 400x382	0.8303	0.8775	0.9134	0.7268	0.7955	0.8471
HD 400x551	0.8368	0.8826	0.9176	0.7362	0.8030	0.8531
HD 400x818	0.8487	0.8921	0.9254	0.7535	0.8167	0.8641
HD 400x1299	0.8695	0.9089	0.9392	0.7839	0.8407	0.8835

Table AA14: The reduction coefficient of the buckling load for R60

R 90						
χ_z						
Profiles	*l = 3m*			*l = 4m*		
	lθ = l	*lθ = 0.7l*	*lθ = 0.5l*	*lθ = l*	*lθ = 0.7l*	*lθ = 0.5l*
HEA 240	-	-	-	-	-	-
HEA 280	-	-	-	-	-	-
HEA 300	0.6565	0.7389	0.8018	0.4957	0.5983	0.6855
HEA 360	0.6271	0.7147	0.7823	0.4628	0.5666	0.6578
HEA 400	0.6057	0.6967	0.7677	0.4399	0.5438	0.6374
HEA 450	0.6231	0.7113	0.7795	0.4584	0.5622	0.6539
HEA 500	0.6073	0.6980	0.7688	0.4416	0.5455	0.6389
HEA 600	0.5731	0.6686	0.7447	0.4068	0.5098	0.6060
HEA 700	0.5787	0.6734	0.7487	0.4123	0.5156	0.6114
HEA 800	0.5541	0.6519	0.7309	0.3884	0.4904	0.5876
HEB 240	-	-	-	-	-	-
HEB 280	-	-	-	-	-	-
HEB 300	0.6591	0.7411	0.8035	0.4987	0.6011	0.6880
HEB 360	0.6283	0.7157	0.7831	0.4641	0.5678	0.6589
HEB 400	0.6064	0.6973	0.7682	0.4406	0.5446	0.6381
HEB 450	0.6202	0.7089	0.7776	0.4553	0.5592	0.6512
HEB 500	0.6037	0.6950	0.7663	0.4378	0.5417	0.6355
HEB 600	0.5687	0.6647	0.7415	0.4024	0.5053	0.6017
HEB 700	0.5724	0.6680	0.7442	0.4061	0.5091	0.6054
HEB 800	0.5473	0.6458	0.7258	0.3819	0.4835	0.5810
HD 260x54.1	-	-	-	-	-	-
HD 260x142	-	-	-	-	-	-
HD 320x127	0.6498	0.7335	0.7974	0.4881	0.5910	0.6793
HD 320x198	0.6615	0.7431	0.8051	0.5015	0.6038	0.6903
HD 320x300	0.6747	0.7538	0.8137	0.5171	0.6183	0.7027
HD 400x237	0.7954	0.8498	0.8908	0.6764	0.7551	0.8148
HD 400x382	0.7990	0.8527	0.8931	0.6815	0.7593	0.8181
HD 400x551	0.8083	0.8600	0.8991	0.6948	0.7700	0.8267
HD 400x818	0.8241	0.8726	0.9093	0.7177	0.7883	0.8414
HD 400x1299	0.8499	0.8931	0.9262	0.7554	0.8181	0.8653

Table AA15: The reduction coefficient of the buckling load for R90

R 120						
χ_z						
Profiles	*l = 3m*			*l = 4m*		
	lθ = l	*lθ = 0.7l*	*lθ = 0.5l*	*lθ = l*	*lθ = 0.7l*	*lθ = 0.5l*
HEA 240	-	-	-	-	-	-
HEA 280	-	-	-	-	-	-
HEA 300	0.6614	0.7430	0.8050	0.5014	0.6036	0.6902
HEA 360	0.6165	0.7058	0.7751	0.4513	0.5553	0.6477
HEA 400	0.5855	0.6794	0.7536	0.4192	0.5227	0.6180
HEA 450	0.5943	0.6870	0.7598	0.4281	0.5319	0.6265
HEA 500	0.5728	0.6683	0.7445	0.4064	0.5095	0.6057
HEA 600	0.5263	0.6268	0.7099	0.3625	0.4624	0.5604
HEA 700	0.5218	0.6226	0.7064	0.3584	0.4579	0.5560
HEA 800	0.4899	0.5928	0.6808	0.3304	0.4266	0.5244
HEB 240	-	-	-	-	-	-
HEB 280	-	-	-	-	-	-
HEB 300	0.6670	0.7476	0.8087	0.5080	0.6098	0.6955
HEB 360	0.6216	0.7101	0.7786	0.4568	0.5607	0.6525
HEB 400	0.5908	0.6839	0.7573	0.4245	0.5281	0.6231
HEB 450	0.5946	0.6872	0.7600	0.4284	0.5322	0.6267
HEB 500	0.5724	0.6679	0.7442	0.4060	0.5091	0.6053
HEB 600	0.5255	0.6260	0.7092	0.3618	0.4616	0.5596
HEB 700	0.5182	0.6193	0.7035	0.3552	0.4543	0.5524
HEB 800	0.4860	0.5891	0.6776	0.3271	0.4227	0.5205
HD 260x54.1	-	-	-	-	-	-
HD 260x142	-	-	-	-	-	-
HD 320x127	0.6530	0.7361	0.7995	0.4917	0.5945	0.6823
HD 320x198	0.6674	0.7478	0.8089	0.5084	0.6102	0.6958
HD 320x300	0.6826	0.7601	0.8188	0.5265	0.6270	0.7100
HD 400x237	0.7888	0.8446	0.8866	0.6670	0.7476	0.8087
HD 400x382	0.7953	0.8497	0.8907	0.6762	0.7550	0.8147
HD 400x551	0.8081	0.8598	0.8990	0.6945	0.7698	0.8265
HD 400x818	0.8274	0.8752	0.9115	0.7225	0.7921	0.8444
HD 400x1299	0.8554	0.8975	0.9298	0.7633	0.8244	0.8703

Table AA16: The reduction coefficient of the buckling load for R120

A-6 The design axial buckling load:

Finally, as last step of the work and final result for the simplified calculation method of EN4 part 1-2 annex G[1], the design axial buckling load in the fire situation $N_{fi,Rd,z}$ is determinate following equation(22):

T = 20 °C						
$N_{fi,Rd,z}$ **(N)**						
Profiles	***l = 3m***			***l = 4m***		
	lθ = l	***lθ = 0.7l***	***lθ = 0.5l***	***lθ = l***	***lθ = 0.7l***	***lθ = 0.5l***
HEA 240	2717583	2908443	3052272	-	2576300	2785648
HEA 280	3897487	4104707	4262862	-	3744719	3971160
HEA 300	4472081	4682963	4845005	4012009	4317335	4546896
HEA 360	5401148	5658354	5855879	4839708	5212329	5492415
HEA 400	5922676	6208687	6428157	5297894	5712587	6024190
HEA 450	7076138	7420169	7684058	6324353	6823359	7198261
HEA 500	7716697	8094826	8384740	6890077	7438774	7850943
HEA 600	8748178	9188902	9526278	7783495	8423893	8904725
HEA 700	10624709	11173347	11592753	9422630	10220648	10819671
HEA 800	11525981	12135663	12601116	10189059	11076585	11742723
HEB 240	3367390	3597341	3770799	-	3197143	3449384
HEB 280	4674405	4917195	5102736	-	4495557	4760690
HEB 300	5345028	5593289	5784219	4803883	5162974	5433079
HEB 360	6299640	6596376	6824402	5652305	6081904	6404911
HEB 400	6839067	7166095	7417181	6125056	6598948	6955118
HEB 450	8014396	8401377	8698328	7169052	7730140	8151747
HEB 500	8676730	9099763	9424199	7752177	8365868	8826904
HEB 600	9753429	10243183	10618162	8681576	9393113	9927381
HEB 700	11674611	12276533	12736711	10355864	11231333	11888502
HEB 800	12620802	13288253	13797816	11157210	12128827	12858080
HD 260x54.1	2728330	2896929	3024634	-	2603580	2788397
HD 260x142	5327945	5625588	5852157	-	5108182	5433848
HD 320x127	5705430	5971024	6175258	5126428	5510647	5799632
HD 320x198	7937533	8290026	8561827	7171364	7679576	8062442
HD 320x300	11139301	11611112	11975920	10117194	10794816	11306335
HD 400x237	11321824	11668407	11941178	10591483	11072970	11443729
HD 400x382	15841353	16308460	16676746	14860280	15506582	16005537
HD 400x551	21475423	22082002	22561195	20206154	21041594	21688468
HD 400x818	30575777	31387658	32030740	28885709	29996767	30860631
HD 400x1299	47133706	48264588	49163827	44798247	46330650	47529867

Table AA17: The design axial buckling load of the column at room temperature

R 30						
$N_{fi,Rd,z}$ (N)						
Profiles	***l = 3m***			***l = 4m***		
	lθ = l	***lθ = 0.7l***	***lθ = 0.5l***	***lθ = l***	***lθ = 0.7l***	***lθ = 0.5l***
HEA 240	1221130	1402425	1543703	-	1097423	1284292
HEA 280	2112887	2316378	2469245	-	1964340	2185290
HEA 300	2490258	2696070	2850592	2047652	2338534	2563642
HEA 360	3009561	3268013	3462003	2456781	2819389	3101684
HEA 400	3338115	3633961	3856012	2708514	3120824	3443528
HEA 450	4280979	4636414	4903260	3517077	4019008	4407709
HEA 500	4674177	5071986	5370587	3822193	4381325	4815985
HEA 600	5385971	5872290	6237328	4354306	5029213	5559206
HEA 700	6965248	7578085	8038052	5659487	6514936	7183628
HEA 800	7622040	8325821	8854184	6135066	7106564	7872648
HEB 240	1373876	1592682	1752924	-	1246633	1458674
HEB 280	2354424	2580015	2749467	-	2189673	2434699
HEB 300	2792826	3023914	3197411	2295942	2622478	2875222
HEB 360	3349548	3637231	3853161	2734258	3137868	3452090
HEB 400	3700003	4027767	4273773	3002422	3459262	3816789
HEB 450	4667977	5058455	5351590	3829622	4380277	4807193
HEB 500	5084356	5520536	5847927	4151302	4763390	5239830
HEB 600	5838883	6370614	6769762	4712585	5449039	6028270
HEB 700	7460198	8125046	8624062	6046626	6972056	7697072
HEB 800	8153861	8917072	9490145	6545468	7595428	8425566
HD 260x54.1	1380525	1554108	1686460	-	1258042	1441681
HD 260x142	2189350	2448243	2644588	-	2004853	2280843
HD 320x127	2987227	3236826	3424204	2451255	2803316	3076217
HD 320x198	3874333	4184957	4418265	3203751	3645062	3985110
HD 320x300	5205969	5600604	5897341	4348876	4914195	5346726
HD 400x237	6395072	6688225	6913853	5756582	6180226	6499019
HD 400x382	8541505	8921897	9215162	7714540	8263095	8676309
HD 400x551	11237616	11714898	12083877	10203448	10889089	11406596
HD 400x818	15758070	16377689	16858847	14423493	15307360	15977099
HD 400x1299	24663429	25517689	26185762	22843358	24046143	24964624

Table AA18: The design axial buckling load of the column for R30

R 60						
$N_{fi,Rd,z}$ (N)						
Profiles	***l* = 3m**			***l* = 4m**		
	lθ* = *l	***lθ* = 0.7*l***	***lθ* = 0.5*l***	***lθ* = *l***	***lθ* = 0.7*l***	***lθ* = 0.5*l***
HEA 240	-	971296	1092107	-	-	873535
HEA 280	-	1675649	1813286	-	1365941	1558460
HEA 300	1745270	1928525	2066548	1368735	1612627	1810327
HEA 360	2050061	2282094	2457533	1582752	1883665	2132216
HEA 400	2255050	2524936	2729812	1720489	2063072	2350375
HEA 450	3012227	3349171	3603751	2331370	2770215	3131583
HEA 500	3259307	3639633	3927789	2500140	2987737	3393795
HEA 600	3722693	4198054	4561064	2800930	3388174	3890027
HEA 700	4997897	5617517	6089319	3784420	4559638	5216364
HEA 800	5438816	6158339	6709954	4060851	4935760	5691566
HEB 240	-	1085794	1218286	-	-	978192
HEB 280	-	1818586	1966237	-	1485756	1692786
HEB 300	1906198	2106103	2256660	1495325	1761483	1977168
HEB 360	2233339	2486864	2678590	1723174	2051603	2323093
HEB 400	2451872	2746586	2970386	1868927	2242376	2555945
HEB 450	3226285	3591931	3868417	2490159	2964119	3355741
HEB 500	3487998	3901100	4214435	2667117	3193676	3633978
HEB 600	3977886	4494527	4889776	2981962	3615431	4159573
HEB 700	5283160	5952016	6462342	3982393	4811765	5518720
HEB 800	5746671	6524094	7121721	4269906	5205486	6019372
HD 260x54.1	-	1098326	1215200	-	-	1001286
HD 260x142	-	1618186	1775859	-	-	1485841
HD 320x127	2016322	2232771	2395955	1574071	1860051	2093108
HD 320x198	2503104	2762494	2957760	1968409	2315082	2595225
HD 320x300	3236563	3557909	3799481	2567562	3002624	3350819
HD 400x237	4343575	4593298	4783109	3795078	4159057	4432464
HD 400x382	5569392	5885701	6126274	4874722	5335744	5681963
HD 400x551	7073328	7460868	7756170	6222732	6787351	7211176
HD 400x818	9600016	10091459	10467323	8523610	9238194	9774627
HD 400x1299	14806317	15476224	15992214	13348453	14315649	15043792

Table AA19: The design axial buckling load of the column for R60

R 90						
$N_{fi,Rd,z}$ (N)						
Profiles	*l = 3m*			*l = 4m*		
	lθ = l	*lθ = 0.7l*	*lθ = 0.5l*	*lθ = l*	*lθ = 0.7l*	*lθ = 0.5l*
HEA 240	-	-	-	-	-	-
HEA 280	-	-	-	-	-	-
HEA 300	1100813	1239099	1344527	831174	1003221	1149536
HEA 360	1335392	1521837	1665765	985418	1206435	1400652
HEA 400	1485406	1708444	1882586	1078770	1333619	1563040
HEA 450	1971511	2250673	2466608	1450351	1779000	2069125
HEA 500	2153066	2474670	2725547	1565450	1933930	2265056
HEA 600	2488262	2902842	3233344	1766134	2213518	2631189
HEA 700	3327715	3872747	4305585	2370908	2964838	3515939
HEA 800	3642856	4285404	4804847	2553326	3223900	3863026
HEB 240	-	-	-	-	-	-
HEB 280	-	-	-	-	-	-
HEB 300	1223505	1375711	1491644	925758	1115911	1277161
HEB 360	1474400	1679415	1837588	1088965	1332477	1546180
HEB 400	1634342	1879164	2070238	1187550	1467637	1719575
HEB 450	2132146	2437025	2673195	1565161	1922346	2238676
HEB 500	2324080	2675355	2949938	1685408	2085396	2446283
HEB 600	2677800	3130083	3491784	1894958	2379201	2833507
HEB 700	3538215	4129018	4600239	2510170	3146922	3741850
HEB 800	3868359	4564436	5130181	2699464	3417201	4106325
HD 260x54.1	-	-	-	-	-	-
HD 260x142	-	-	-	-	-	-
HD 320x127	1310065	1478720	1607623	983948	1191553	1369406
HD 320x198	1680993	1888190	2045874	1274441	1534300	1754069
HD 320x300	2232423	2494021	2692283	1710910	2045746	2324910
HD 400x237	2974814	3178236	3331674	2529650	2824209	3047349
HD 400x382	3889418	4150493	4347554	3317568	3696125	3982500
HD 400x551	4997372	5317075	5558862	4295876	4760724	5111313
HD 400x818	6838689	7240559	7545681	5955928	6541603	6981777
HD 400x1299	10704943	11249025	11665316	9513583	10304473	10898233

Table AA20: The design axial buckling load of the column for R90

R 120						
$N_{fi,Rd,z}$ (N)						
Profiles	***l = 3m***			***l = 4m***		
	lθ = l	***lθ = 0.7l***	***lθ = 0.5l***	***lθ = l***	***lθ = 0.7l***	***lθ = 0.5l***
HEA 240	-	-	-		-	-
HEA 280	-	-	-		-	-
HEA 300	695613	781399	846688	527317	634883	725868
HEA 360	897815	1027817	1128714	657255	808603	943197
HEA 400	1023939	1188065	1317808	733011	914041	1080737
HEA 450	1336515	1544816	1708563	962708	1196034	1408787
HEA 500	1486129	1734024	1931696	1054567	1321900	1571581
HEA 600	1750901	2085105	2361496	1206030	1538256	1864330
HEA 700	2304584	2749955	3119743	1583079	2022350	2455501
HEA 800	2539010	3072240	3528231	1712422	2210595	2717610
HEB 240	-	-	-	-	-	-
HEB 280	-	-	-	-	-	-
HEB 300	807003	904417	978418	614576	737803	841396
HEB 360	1026259	1172299	1285345	754151	925657	1077306
HEB 400	1162747	1346046	1490460	835439	1039484	1226279
HEB 450	1485484	1716793	1898594	1070228	1329452	1565745
HEB 500	1645072	1919812	2138951	1167043	1463119	1739766
HEB 600	1927638	2296428	2601646	1327091	1693163	2052769
HEB 700	2498090	2985581	3391631	1712322	2190156	2663067
HEB 800	2745903	3328243	3828135	1847978	2388494	2940668
HD 260x54.1	-	-	-	-	-	-
HD 260x142	-	-	-	-	-	-
HD 320x127	883245	995633	1081426	665055	804108	922815
HD 320x198	1213708	1360042	1471193	924538	1109737	1265376
HD 320x300	1708217	1902361	2049191	1317677	1569070	1776945
HD 400x237	2140754	2292097	2406121	1810211	2028730	2194728
HD 400x382	2953618	3155722	3308163	2511354	2803990	3025684
HD 400x551	3936408	4188502	4379149	3383275	3749803	4026254
HD 400x818	5571878	5893488	6137891	4865466	5334220	5686362
HD 400x1299	9028203	9472724	9813450	8056217	8701418	9186033

Table AA21: The design axial buckling load of the column for R120

ANNEX B:

New proposal formulas for balanced summation model

ANNEX B - New proposal formula for balanced summation model

B-1 Average temperature and reduction factor of components:

B-1.1 Flanges of the steel profile:

Performing the calculations presented in equation (38) from the fourth chapiter, and taking into account the new proposed parameters shown in table 17, the average temperatures are obtained at the edges of the profiles under study, giving rise to the values presented in table AB1.

	$\theta_{f,t}$ [°C]				
Profiles	***Am/v***	***R30***	***R60***	***R90***	***R120***
HEA 240	17.029	745.4	944.1	995.2	1041.3
HEA 280	14.550	736.9	939.0	991.7	1037.9
HEA 300	13.563	733.5	936.9	990.3	1036.6
HEA 360	12.381	729.5	934.5	988.6	1035.0
HEA 400	11.795	727.5	933.3	987.7	1034.2
HEA 450	11.212	725.5	932.1	986.9	1033.4
HEA 500	10.748	723.9	931.1	986.3	1032.7
HEA 600	10.056	721.5	929.7	985.3	1031.8
HEA 700	9.565	719.8	928.7	984.6	1031.1
HEA 800	9.198	718.6	927.9	984.1	1030.6
HEB 240	16.667	744.2	943.3	994.7	1040.8
HEB 280	14.286	736.0	938.4	991.3	1037.6
HEB 300	13.333	732.7	936.5	989.9	1036.3
HEB 360	12.222	728.9	934.2	988.4	1034.7
HEB 400	11.667	727.0	933.0	987.6	1034.0
HEB 450	11.111	725.1	931.9	986.8	1033.2
HEB 500	10.667	723.6	931.0	986.1	1032.6
HEB 600	10.000	721.3	929.6	985.2	1031.7
HEB 700	9.524	719.7	928.6	984.5	1031.0
HEB 800	9.167	718.4	927.9	984.0	1030.6
HD 260x54.1	15.889	731.7	923.7	1017.3	1071.4
HD 260x142	14.741	712.3	913.7	1013.5	1070.8
HD 320x127	12.917	681.4	897.8	1007.5	1069.8
HD 320x198	12.367	672.1	893.0	1005.7	1069.6
HD 320x300	11.723	661.2	887.3	1003.6	1069.2
HD 400x237	10.326	637.6	875.1	999.0	1068.5
HD 400x382	9.734	627.6	870.0	997.0	1068.2
HD 400x551	9.180	618.2	865.1	995.2	1067.9
HD 400x818	8.468	606.2	858.9	992.9	1067.5
HD 400x1299	7.535	590.4	850.8	989.8	1067.0

Table AB1: The average temperature of the flanges for different fire class

B-1.2 Web of the steel profile:

Performing the calculations presented in equation (44) from the fourth chapiter, and considering the new proposed parameters shown in table 18, the average temperatures for the web of the steel profile are obtained, giving rise to the values presented in table AB2:

	$\theta_{w,t}$ [°C]				
Profiles	***Am/v***	***R30***	***R60***	***R90***	***R120***
HEA 240	17.029	412.7	714.7	926.2	1075.2
HEA 280	14.550	357.2	622.9	813.5	952.6
HEA 300	13.563	325.0	569.5	748.8	881.5
HEA 360	12.381	264.3	468.8	628.0	747.8
HEA 400	11.795	233.4	417.4	566.5	679.6
HEA 450	11.212	215.4	387.5	530.2	639.8
HEA 500	10.748	199.8	361.7	499.0	605.5
HEA 600	10.056	174.1	319.1	447.6	548.8
HEA 700	9.565	147.3	274.6	394.3	489.8
HEA 800	9.198	136.4	256.6	372.4	465.8
HEB 240	16.667	324.3	567.3	752.3	880.7
HEB 280	14.286	291.0	512.6	683.3	806.9
HEB 300	13.333	254.9	452.8	611.1	727.3
HEB 360	12.222	212.1	381.7	525.4	632.9
HEB 400	11.667	189.5	344.2	480.3	583.1
HEB 450	11.111	175.1	320.4	451.2	551.3
HEB 500	10.667	162.7	299.9	426.3	524.0
HEB 600	10.000	142.3	266.0	385.1	478.8
HEB 700	9.524	121.4	231.3	343.4	432.8
HEB 800	9.167	112.2	216.1	324.8	412.5
HD 260x54.1	15.889	467.5	525.9	446.3	778.8
HD 260x142	14.741	390.2	552.4	652.8	825.4
HD 320x127	12.917	346.2	461.2	702.4	718.6
HD 320x198	12.367	314.7	464.7	596.9	728.4
HD 320x300	11.723	286.5	453.9	607.9	719.8
HD 400x237	10.326	252.2	385.2	600.3	639.5
HD 400x382	9.734	225.1	377.2	521.1	634.1
HD 400x551	9.180	203.8	362.9	516.7	619.9
HD 400x818	8.468	179.0	340.3	503.3	595.9
HD 400x1299	7.535	147.9	308.3	480.1	561.1

Table AB2: The average temperature of the web for different fire class

B-1.3 Concrete:

The average temperature of the concrete for different fire rating, can be obtained from the new proposed equation (49) and considering the new proposed parameters from table 19, giving rise to the values presented in table AB3:

	$\theta_{c,t}$ [ºC]				
Profiles	***Am/v***	***R30***	***R60***	***R90***	***R120***
HEA 240	17.029	250.4	386.7	555.7	650.7
HEA 280	14.550	215.6	319.0	489.4	584.8
HEA 300	13.563	202.7	295.9	457.5	549.9
HEA 360	12.381	189.2	276.6	407.4	489.2
HEA 400	11.795	182.7	267.4	382.0	458.4
HEA 450	11.212	174.9	253.4	363.7	438.6
HEA 500	10.748	168.9	242.7	348.5	421.9
HEA 600	10.056	160.1	227.6	324.5	394.7
HEA 700	9.565	154.7	220.2	302.8	368.2
HEA 800	9.198	149.8	211.2	291.5	356.1
HEB 240	16.667	252.7	407.3	502.5	572.3
HEB 280	14.286	217.4	334.7	449.6	526.1
HEB 300	13.333	205.4	314.3	416.2	488.2
HEB 360	12.222	191.5	290.8	376.7	443.3
HEB 400	11.667	184.6	279.5	356.4	419.9
HEB 450	11.111	177.0	265.0	340.5	403.4
HEB 500	10.667	171.0	253.8	327.2	389.5
HEB 600	10.000	162.2	237.7	306.4	367.1
HEB 700	9.524	156.4	228.6	288.1	345.6
HEB 800	9.167	151.5	219.3	277.9	335.1
HD 260x54.1	15.889	231.7	361.5	468.7	494.0
HD 260x142	14.741	235.2	383.7	493.9	551.9
HD 320x127	12.917	198.8	320.5	418.9	466.8
HD 320x198	12.367	197.6	324.3	423.0	482.2
HD 320x300	11.723	191.5	317.8	415.1	480.7
HD 400x237	10.326	164.0	270.2	358.6	416.9
HD 400x382	9.734	159.0	265.6	352.9	418.0
HD 400x551	9.180	152.2	256.3	341.7	410.0
HD 400x818	8.468	142.0	241.3	323.6	394.0
HD 400x1299	7.535	128.0	219.7	297.9	369.9

Table AB3: The average temperature of the concrete for different fire class

The vertical reduction $b_{c,fi,v}$ and horizontal reduction $b_{c,fi,h}$ of the concrete must be total. They are obtained from equations (50) and (51), considering the new proposed parameters from table (20) and (21):

Profiles	*Am/v*	$b_{c,fi,v}$				$b_{c,fi,h}$			
		R30	***R60***	***R90***	***R120***	***R30***	***R60***	***R90***	***R120***
HEA 240	17.029	0.00725	0.03116	-	-	0.01168	0.01265	-	-
HEA 280	14.550	0.00537	0.02637	-	-	0.01168	0.01338	-	-
HEA 300	13.563	0.00476	0.02471	0.03768	0.07364	0.01168	0.01408	0.02346	0.04889
HEA 360	12.381	0.00427	0.02301	0.03271	0.05818	0.01168	0.01582	0.02549	0.04537
HEA 400	11.795	0.00404	0.02223	0.03013	0.05041	0.01168	0.01672	0.02702	0.04468
HEA 450	11.212	0.00386	0.02151	0.02907	0.04620	0.01168	0.01709	0.02551	0.03938
HEA 500	10.748	0.00377	0.02100	0.02942	0.04559	0.01168	0.01744	0.02476	0.03598
HEA 600	10.056	0.00357	0.02023	0.02794	0.04027	0.01168	0.01806	0.02452	0.03246
HEA 700	9.565	0.00349	0.01975	0.02853	0.04027	0.01168	0.01884	0.02669	0.03376
HEA 800	9.198	0.00340	0.01939	0.02792	0.03796	0.01168	0.01906	0.02608	0.03131
HEB 240	16.667	0.00734	0.03070	-	-	0.01168	0.01603	-	-
HEB 280	14.286	0.00558	0.02619	-	-	0.01168	0.01591	-	-
HEB 300	13.333	0.00500	0.02462	0.04694	0.09371	0.01168	0.01679	0.03862	0.07136
HEB 360	12.222	0.00457	0.02307	0.04296	0.08081	0.01168	0.01785	0.03703	0.06267
HEB 400	11.667	0.00436	0.02234	0.04077	0.07404	0.01168	0.01843	0.03682	0.05944
HEB 450	11.111	0.00421	0.02167	0.04004	0.07067	0.01168	0.01867	0.03471	0.05336
HEB 500	10.667	0.00412	0.02119	0.04061	0.07063	0.01168	0.01890	0.03337	0.04914
HEB 600	10.000	0.00394	0.02046	0.03940	0.06600	0.01168	0.01932	0.03207	0.04408
HEB 700	9.524	0.00387	0.02000	0.04014	0.06639	0.01168	0.01988	0.03290	0.04336
HEB 800	9.167	0.00378	0.01965	0.03962	0.06431	0.01168	0.02003	0.03197	0.04044
HD 260x54.1	15.889	0.01001	0.03033	-	-	0.01168	0.02087	-	-
HD 260x142	14.741	0.00859	0.02624	-	-	0.01168	0.02174	-	-
HD 320x127	12.917	0.00626	0.02341	0.05032	0.09827	0.01168	0.02147	0.04173	0.06022
HD 320x198	12.367	0.00575	0.02131	0.04639	0.08969	0.01168	0.02177	0.04252	0.06198
HD 320x300	11.723	0.00521	0.01866	0.04169	0.08025	0.01168	0.02193	0.04201	0.06083
HD 400x237	10.326	0.00367	0.01816	0.03713	0.05959	0.01168	0.02174	0.03650	0.04859
HD 400x382	9.734	0.00329	0.01575	0.03315	0.05251	0.01168	0.02192	0.03654	0.04868
HD 400x551	9.180	0.00302	0.01308	0.02910	0.04648	0.01168	0.02200	0.03595	0.04738
HD 400x818	8.468	0.00275	0.00929	0.02364	0.03949	0.01168	0.02205	0.03487	0.04499
HD 400x1299	7.535	0.00250	0.00397	0.01636	0.03150	0.01168	0.02210	0.03341	0.04174

Table AB4: The vertical and horizontal reduction of the concrete for different fire class

B-1.4 Reinforcing bars:

The average reinforcement bars temperature's value will be calculated assuming equation (55), considering the new proposed parameters from table 22:

	$\theta_{s,t}$ [°C]				
Profiles	***Am/v***	***R30***	***R60***	***R90***	***R120***
HEA 240	17.029	155.4	393.3	565.5	685.6
HEA 280	14.550	142.5	358.1	519.6	634.7
HEA 300	13.563	137.4	344.0	501.3	614.5
HEA 360	12.381	131.3	327.2	479.4	590.2
HEA 400	11.795	128.2	318.8	468.6	578.1
HEA 450	11.212	125.2	310.5	457.8	566.2
HEA 500	10.748	122.8	303.9	449.2	556.7
HEA 600	10.056	119.2	294.1	436.3	542.5
HEA 700	9.565	116.6	287.1	427.2	532.4
HEA 800	9.198	114.7	281.9	420.4	524.8
HEB 240	16.667	153.5	388.2	558.8	678.2
HEB 280	14.286	141.1	354.3	514.7	629.3
HEB 300	13.333	136.2	340.7	497.1	609.7
HEB 360	12.222	130.4	324.9	476.5	586.9
HEB 400	11.667	127.6	317.0	466.2	575.5
HEB 450	11.111	124.7	309.1	455.9	564.1
HEB 500	10.667	122.4	302.8	447.7	555.0
HEB 600	10.000	118.9	293.3	435.3	541.3
HEB 700	9.524	116.4	286.5	426.5	531.5
HEB 800	9.167	114.6	281.4	419.9	524.2
HD 260x54.1	15.889	149.5	377.1	544.4	662.2
HD 260x142	14.741	143.5	360.8	523.2	638.6
HD 320x127	12.917	134.0	334.8	489.3	601.2
HD 320x198	12.367	131.2	327.0	479.2	589.9
HD 320x300	11.723	127.8	317.8	467.2	576.7
HD 400x237	10.326	120.6	297.9	441.3	548.0
HD 400x382	9.734	117.5	289.5	430.4	535.8
HD 400x551	9.180	114.6	281.6	420.1	524.5
HD 400x818	8.468	110.9	271.5	406.9	509.8
HD 400x1299	7.535	106.1	258.2	389.6	490.7

Table AB5: The average temperature of the rebars for different fire class

B-2 The design value of the plastic resistance to axial compression:

After calculating the design value of the plastic for the four components of the steel profile, so that all can be added in a summation according to equation (58):

	$N_{fi,pl,Rd}$ (N)			
Profiles	R 30	R 60	R 90	R 120
HEA 240	1945835	1104157	471121	351103
HEA 280	2838180	1880402	1104445	482181
HEA 300	3160611	2176143	1401705	667068
HEA 360	3795123	2826563	1968651	1080898
HEA 400	4225057	3285047	2433356	1445001
HEA 450	5319148	4347035	3430742	2186454
HEA 500	5817379	4770840	3915033	2585227
HEA 600	6815566	5664753	4928491	3585813
HEA 700	8814995	7557270	6944568	5356802
HEA 800	9809674	8475378	7847834	6322796
HEB 240	2208365	1361026	570342	526077
HEB 280	3105748	2181184	1237486	537850
HEB 300	3482501	2552529	1640087	757062
HEB 360	4154678	3191905	2320998	1251742
HEB 400	4609292	3583357	2812910	1675489
HEB 450	5733478	4631775	3820010	2464002
HEB 500	6261616	5082941	4308775	2913552
HEB 600	7321678	6035001	5327812	3912394
HEB 700	9382988	7988657	7163321	5628460
HEB 800	10440061	8966109	8091853	6627192
HD 260x54.1	1967694	1397550	691164	323663
HD 260x142	3158670	1873215	937126	406251
HD 320x127	3887758	2724647	1810575	792766
HD 320x198	4959577	3304278	2066142	998740
HD 320x300	6520732	4187869	2604513	1315446
HD 400x237	7211822	5143796	3864823	2404533
HD 400x382	9507384	6498657	4879703	3061494
HD 400x551	12292109	8035066	6128750	3873715
HD 400x818	16829846	10446254	8166536	5284584
HD 400x1299	25585414	15295952	12450573	8496506

Table AB6: The plastic resistance of the steel profile for different fire class

B-3 The effective flexural stiffness:

After calculating the effective flexural stiffness for each component of the steel profile, so that all can be added in a balanced summation according to equation (59):

	$(EI)_{fi,eff,z}$			
Profiles	R 30	R 60	R 90	R 120
HEA 240	2004768	1253377	740656	385255
HEA 280	4604619	3108356	2144660	1098435
HEA 300	5943842	4049613	2965900	1487238
HEA 360	6626357	4473576	3322560	1921867
HEA 400	6992118	4701693	3506651	2147041
HEA 450	9716821	6835424	5239884	3365097
HEA 500	10193122	7152119	5496328	3682287
HEA 600	10929069	7660572	5913200	4194004
HEA 700	14935231	10837762	8536936	6288270
HEA 800	15564384	11297223	8904649	6737259
HEB 240	2280865	1381485	872735	487705
HEB 280	5052958	3306229	2349165	1263481
HEB 300	6496988	4275341	3167552	1735706
HEB 360	7186849	4710079	3501780	2100268
HEB 400	7556461	4939113	3679595	2311912
HEB 450	10284486	7068945	5402742	3523079
HEB 500	10762528	7378651	5647954	3817677
HEB 600	11502430	7877303	6048749	4282141
HEB 700	15517592	11062205	8650004	6367153
HEB 800	16149963	11511637	8995150	6829753
HD 260x54.1	2514867	1592027	961610	457296
HD 260x142	4124683	2440551	1591267	882732
HD 320x127	7646903	4528666	3181758	1707579
HD 320x198	10576323	5668324	3936439	2279189
HD 320x300	15518549	7425540	5075590	3121498
HD 400x237	32468399	17060074	12393641	8357999
HD 400x382	46505070	21584432	15406441	10698734
HD 400x551	66936765	27761235	19485242	13742527
HD 400x818	107124410	39340994	27104564	19268408
HD 400x1299	211059967	67571541	45923896	32297517

Table AB7: The effective flexural stiffness of the steel profile for different fire class

B-4 The critical axial compression resistance:

The critical axial compression resistance or Euler buckling load ($N_{fi,cr,z}$) is calculated around the Z axis for the different buckling length for different fire resistance class following equation (20) as same of simplified calculation method:

R 30						
$N_{fi,cr,z}$ **(N)**						
Profiles	***l = 3m***			***l = 4m***		
	lθ = l	***lθ = 0.7l***	***lθ = 0.5l***	***lθ = l***	***lθ = 0.7l***	***lθ = 0.5l***
HEA 240	2198474	3140678	4396949	-	1766631	2473284
HEA 280	5049530	7213614	10099059	-	4057658	5680721
HEA 300	6518152	9311646	13036305	3666461	5237801	7332921
HEA 360	7266614	10380877	14533228	4087470	5839243	8174941
HEA 400	7667716	10953880	15335432	4313090	6161557	8626180
HEA 450	10655686	15222409	21311373	5993824	8562605	11987647
HEA 500	11178009	15968585	22356019	6287630	8982329	12575260
HEA 600	11985065	17121522	23970131	6741599	9630856	13483199
HEA 700	16378314	23397591	32756628	9212802	13161145	18425603
HEA 800	17068257	24383224	34136514	9600895	13715564	19201789
HEB 240	2501248	3573212	5002497	-	2009932	2813904
HEB 280	5541189	7915984	11082378	-	4452741	6233838
HEB 300	7124745	10178207	14249490	4007669	5725241	8015338
HEB 360	7881262	11258946	15762525	4433210	6333157	8866420
HEB 400	8286587	11837982	16573174	4661205	6658865	9322411
HEB 450	11278201	16111715	22556402	6343988	9062840	12687976
HEB 500	11802432	16860618	23604865	6638868	9484097	13277736
HEB 600	12613826	18019751	25227652	7095277	10136110	14190554
HEB 700	17016944	24309920	34033889	9572031	13674330	19144062
HEB 800	17710416	25300595	35420832	9962109	14231584	19924218
HD 260x54.1	2757860	3939800	5515720	-	2216138	3102593
HD 260x142	4523221	6461744	9046441	-	3634731	5088623
HD 320x127	8385767	11979667	16771534	4716994	6738563	9433988
HD 320x198	11598236	16568908	23196471	6524007	9320011	13048015
HD 320x300	17017994	24311420	34035988	9572621	13675174	19145243
HD 400x237	35605584	50865120	71211168	20028141	28611630	40056282
HD 400x382	50998516	72855023	101997032	28686665	40980950	57373330
HD 400x551	73404376	104863395	146808752	41289962	58985659	82579923
HD 400x818	117475061	167821516	234950123	66079722	94399603	132159444
HD 400x1299	231453153	330647362	462906306	130192399	185989141	260384797

Table AB8: The critical axial compression resistance of the steel profile for R30

R 60						
$N_{fi,cr,z}$ (N)						
Profiles	***l = 3m***			***l = 4m***		
	lθ = l	***lθ = 0.7l***	***lθ = 0.5l***	***lθ = l***	***lθ = 0.7l***	***lθ = 0.5l***
HEA 240	-	1963545	2748963	-	-	1546292
HEA 280	-	4869563	6817388	-	2739129	3834781
HEA 300	4440897	6344139	8881794	2498005	3568578	4996009
HEA 360	4905825	7008322	9811651	2759527	3942181	5519053
HEA 400	5155983	7365690	10311966	2900241	4143201	5800481
HEA 450	7495882	10708402	14991763	4216433	6023476	8432867
HEA 500	7843177	11204538	15686353	4411787	6302553	8823574
HEA 600	8400757	12001082	16801515	4725426	6750609	9450852
HEA 700	11884936	16978479	23769871	6685276	9550395	13370553
HEA 800	12388791	17698273	24777583	6968695	9955279	13937390
HEB 240	-	-	3029935	-	-	1704339
HEB 280	-	5179551	7251371	-	2913497	4078896
HEB 300	4688436	6697766	9376873	2637245	3767494	5274491
HEB 360	5165179	7378827	10330358	2905413	4150590	5810826
HEB 400	5416343	7737633	10832686	3046693	4352419	6093386
HEB 450	7751966	11074237	15503931	4360481	6229258	8720961
HEB 500	8091596	11559423	16183192	4551523	6502175	9103045
HEB 600	8638429	12340613	17276859	4859117	6941595	9718233
HEB 700	12131066	17330094	24262131	6823724	9748178	13647449
HEB 800	12623922	18034174	25247844	7100956	10144223	14201912
HD 260x54.1	-	2494075	3491705	-	-	1964084
HD 260x142	-	3823376	5352727	-	-	3010909
HD 320x127	4966237	7094625	9932475	2793509	3990727	5587017
HD 320x198	6216013	8880019	12432026	3496507	4995011	6993015
HD 320x300	8143016	11632880	16286032	4580447	6543495	9160893
HD 400x237	18708464	26726378	37416929	10523511	15033587	21047022
HD 400x382	23669978	33814254	47339956	13314363	19020518	26628725
HD 400x551	30443601	43490859	60887202	17124526	24463608	34249051
HD 400x818	43142227	61631753	86284454	24267503	34667861	48535006
HD 400x1299	74100486	105857838	148200973	41681524	59545034	83363047

Table AB9: The critical axial compression resistance of the steel profile for R60

R 90						
$N_{fi,cr,z}$ (N)						
Profiles	***l = 3m***			***l = 4m***		
	lθ = l	***lθ = 0.7l***	***lθ = 0.5l***	***lθ = l***	***lθ = 0.7l***	***lθ = 0.5l***
HEA 240	-	-	-	-	-	-
HEA 280	-	-	-	-	-	-
HEA 300	3252474	4646391	6504948	1829517	2613595	3659033
HEA 360	3643595	5205136	7287190	2049522	2927889	4099044
HEA 400	3845473	5493533	7690946	2163079	3090112	4326157
HEA 450	5746176	8208823	11492352	3232224	4617463	6464448
HEA 500	6027398	8610568	12054796	3390411	4843445	6780822
HEA 600	6484550	9263643	12969100	3647559	5210799	7295119
HEA 700	9361797	13373996	18723595	5266011	7522873	10532022
HEA 800	9765040	13950058	19530081	5492835	7846907	10985670
HEB 240	-	-	-	-	-	-
HEB 280	-	-	-	-	-	-
HEB 300	3473610	4962300	6947220	1953906	2791294	3907811
HEB 360	3840132	5485902	7680263	2160074	3085820	4320148
HEB 400	4035127	5764468	8070255	2269759	3242513	4539518
HEB 450	5924769	8463956	11849539	3332683	4760975	6665365
HEB 500	6193675	8848107	12387349	3483942	4977060	6967884
HEB 600	6633195	9475993	13266390	3731172	5330246	7462345
HEB 700	9485790	13551129	18971581	5335757	7622510	10671514
HEB 800	9864286	14091837	19728572	5548661	7926658	11097322
HD 260x54.1	-	-	-	-	-	-
HD 260x142	-	-	-	-	-	-
HD 320x127	3489188	4984554	6978376	1962668	2803812	3925337
HD 320x198	4316788	6166840	8633576	2428193	3468848	4856387
HD 320x300	5566008	7951439	11132015	3130879	4472685	6261759
HD 400x237	13591149	19415927	27182297	7645021	10921459	15290042
HD 400x382	16895053	24135791	33790107	9503468	13576382	19006935
HD 400x551	21367959	30525656	42735918	12019477	17170681	24038954
HD 400x818	29723481	42462115	59446962	16719458	23884940	33438916
HD 400x1299	50361187	71944553	100722374	28328168	40468811	56656336

Table AB10: The critical axial compression resistance of the steel profile for R90

R 120						
$N_{fi,cr,z}$ (N)						
Profiles	***l = 3m***			***l = 4m***		
	lθ = l	***lθ = 0.7l***	***lθ = 0.5l***	***lθ = l***	***lθ = 0.7l***	***lθ = 0.5l***
HEA 240	-	-	-	-	-	-
HEA 280	-	-	-	-	-	-
HEA 300	1630939	2329913	3261878	917403	1310576	1834807
HEA 360	2107563	3010804	4215125	1185504	1693577	2371008
HEA 400	2354494	3363562	4708987	1324403	1892004	2648805
HEA 450	3690242	5271774	7380483	2075761	2965373	4151522
HEA 500	4038080	5768686	8076160	2271420	3244886	4542840
HEA 600	4599240	6570343	9198481	2587073	3695818	5174145
HEA 700	6895860	9851229	13791720	3878921	5541316	7757843
HEA 800	7388231	10554616	14776462	4155880	5936971	8311760
HEB 240	-	-	-	-	-	-
HEB 280	-	-	-	-	-	-
HEB 300	1903414	2719163	3806828	1070670	1529529	2141341
HEB 360	2303201	3290287	4606402	1295551	1850787	2591101
HEB 400	2535295	3621850	5070590	1426103	2037291	2852207
HEB 450	3863488	5519269	7726977	2173212	3104589	4346425
HEB 500	4186551	5980788	8373103	2354935	3364193	4709870
HEB 600	4695893	6708419	9391787	2641440	3773486	5282880
HEB 700	6982365	9974807	13964730	3927580	5610829	7855161
HEB 800	7489662	10699518	14979325	4212935	6018479	8425870
HD 260x54.1	-	-	-	-	-	-
HD 260x142	-	-	-	-	-	-
HD 320x127	1872570	2675100	3745140	1053321	1504744	2106641
HD 320x198	2499411	3570587	4998821	1405918	2008455	2811837
HD 320x300	3423106	4890151	6846211	1925497	2750710	3850994
HD 400x237	9165571	13093673	18331143	5155634	7365191	10311268
HD 400x382	11732475	16760678	23464950	6599517	9427882	13199034
HD 400x551	15070367	21529096	30140734	8477081	12110116	16954163
HD 400x818	21130174	30185963	42260348	11885723	16979604	23771446
HD 400x1299	35418190	50597415	70836380	19922732	28461046	39845464

Table AB11: The critical axial compression resistance of the steel profile for R120

A-5 The reduction coefficient χ_z

Using $\bar{\lambda}_\theta$ and the buckling curve c of EN 1993-1-1[13], the reduction coefficient χ_z for the axial buckling load of the steel profile is calculated for different fire resistance class in tables below:

R 30						
	χz					
Profiles	***l = 3m***			***l = 4m***		
	lθ = l	***lθ = 0.7l***	***lθ = 0.5l***	***lθ = l***	***lθ = 0.7l***	***lθ = 0.5l***
HEA 240	0.5750	0.6702	0.7461	-	0.5118	0.6078
HEA 280	0.6937	0.7691	0.8260	-	0.6394	0.7205
HEA 300	0.7270	0.7956	0.8472	0.5824	0.6767	0.7514
HEA 360	0.7106	0.7826	0.8368	0.5613	0.6583	0.7362
HEA 400	0.6984	0.7728	0.8290	0.5459	0.6445	0.7248
HEA 450	0.7206	0.7906	0.8432	0.5742	0.6696	0.7455
HEA 500	0.7114	0.7833	0.8373	0.5624	0.6592	0.7369
HEA 600	0.6910	0.7669	0.8242	0.5368	0.6363	0.7179
HEA 700	0.7038	0.7772	0.8324	0.5527	0.6506	0.7298
HEA 800	0.6885	0.7649	0.8226	0.5337	0.6335	0.7155
HEB 240	0.5757	0.6709	0.7466	-	0.5125	0.6085
HEB 280	0.6944	0.7696	0.8264	-	0.6401	0.7211
HEB 300	0.7252	0.7943	0.8461	0.5802	0.6748	0.7498
HEB 360	0.7085	0.7810	0.8355	0.5587	0.6559	0.7342
HEB 400	0.6962	0.7711	0.8276	0.5432	0.6421	0.7227
HEB 450	0.7166	0.7874	0.8407	0.5691	0.6651	0.7418
HEB 500	0.7071	0.7798	0.8345	0.5568	0.6543	0.7329
HEB 600	0.6861	0.7630	0.8211	0.5308	0.6309	0.7133
HEB 700	0.6982	0.7727	0.8289	0.5457	0.6444	0.7246
HEB 800	0.6824	0.7600	0.8187	0.5263	0.6268	0.7099
HD 260x54.1	0.6341	0.7205	0.7870	-	0.5741	0.6644
HD 260x142	0.6398	0.7252	0.7908	-	0.5802	0.6698
HD 320x127	0.7365	0.8032	0.8533	0.5950	0.6875	0.7602
HD 320x198	0.7530	0.8163	0.8638	0.6172	0.7064	0.7755
HD 320x300	0.7741	0.8329	0.8772	0.6463	0.7305	0.7951
HD 400x237	0.8705	0.9097	0.9398	0.7853	0.8418	0.8844
HD 400x382	0.8804	0.9176	0.9464	0.7997	0.8532	0.8936
HD 400x551	0.8924	0.9274	0.9546	0.8171	0.8670	0.9048
HD 400x818	0.9086	0.9406	0.9656	0.8404	0.8855	0.9199
HD 400x1299	0.9325	0.9603	0.9821	0.8742	0.9126	0.9423

Table AB12: The reduction coefficient of the buckling load for R30

R 60						
	χ_z					
Profiles	***l = 3m***			***l = 4m***		
	lθ = l	***lθ = 0.7l***	***lθ = 0.5l***	***lθ = l***	***lθ = 0.7l***	***lθ = 0.5l***
HEA 240	-	0.6936	0.7652	-	-	0.6339
HEA 280	-	0.7726	0.8288	-	0.6442	0.7245
HEA 300	0.7247	0.7938	0.8458	0.5795	0.6742	0.7493
HEA 360	0.6879	0.7644	0.8222	0.5330	0.6328	0.7150
HEA 400	0.6633	0.7445	0.8063	0.5036	0.6057	0.6919
HEA 450	0.6863	0.7632	0.8212	0.5311	0.6311	0.7135
HEA 500	0.6748	0.7538	0.8138	0.5171	0.6183	0.7027
HEA 600	0.6489	0.7327	0.7968	0.4870	0.5900	0.6784
HEA 700	0.6638	0.7449	0.8066	0.5042	0.6063	0.6924
HEA 800	0.6451	0.7296	0.7943	0.4828	0.5860	0.6748
HEB 240	-	0.6665	0.7430	-	-	0.6038
HEB 280	-	0.7560	0.8155	-	0.6213	0.7052
HEB 300	0.7011	0.7751	0.8308	0.5494	0.6476	0.7274
HEB 360	0.6709	0.7507	0.8112	0.5125	0.6141	0.6991
HEB 400	0.6538	0.7367	0.8000	0.4926	0.5953	0.6830
HEB 450	0.6791	0.7574	0.8166	0.5224	0.6232	0.7068
HEB 500	0.6668	0.7474	0.8086	0.5077	0.6096	0.6953
HEB 600	0.6397	0.7251	0.7907	0.4766	0.5801	0.6697
HEB 700	0.6549	0.7377	0.8008	0.4939	0.5966	0.6841
HEB 800	0.6353	0.7215	0.7878	0.4718	0.5754	0.6656
HD 260x54.1	-	0.6944	0.7659	-	-	0.6349
HD 260x142	-	0.7247	0.7904	-	-	0.6692
HD 320x127	0.6994	0.7736	0.8296	0.5472	0.6457	0.7257
HD 320x198	0.7066	0.7794	0.8343	0.5563	0.6538	0.7325
HD 320x300	0.7141	0.7854	0.8390	0.5658	0.6622	0.7394
HD 400x237	0.8293	0.8767	0.9127	0.7252	0.7943	0.8461
HD 400x382	0.8295	0.8768	0.9128	0.7255	0.7945	0.8463
HD 400x551	0.8353	0.8814	0.9166	0.7340	0.8012	0.8517
HD 400x818	0.8474	0.8911	0.9245	0.7517	0.8152	0.8629
HD 400x1299	0.8682	0.9078	0.9383	0.7820	0.8392	0.8822

Table AB13: The reduction coefficient of the buckling load for R60

R 90						
χ_z						
Profiles	*l = 3m*			*l = 4m*		
	$l_\theta = l$	*$l_\theta = 0.7l$*	*$l_\theta = 0.5l$*	*$l_\theta = l$*	*$l_\theta = 0.7l$*	*$l_\theta = 0.5l$*
HEA 240	-	-	-	-	-	-
HEA 280	-	-	-	-	-	-
HEA 300	0.7514	0.8150	0.8628	0.6151	0.7046	0.7741
HEA 360	0.7029	0.7765	0.8319	0.5516	0.6496	0.7290
HEA 400	0.6650	0.7459	0.8074	0.5056	0.6076	0.6935
HEA 450	0.6793	0.7575	0.8167	0.5226	0.6234	0.7070
HEA 500	0.6584	0.7405	0.8031	0.4979	0.6004	0.6874
HEA 600	0.6173	0.7064	0.7756	0.4521	0.5560	0.6484
HEA 700	0.6238	0.7119	0.7800	0.4591	0.5630	0.6546
HEA 800	0.6020	0.6935	0.7651	0.4360	0.5399	0.6338
HEB 240	-	-	-	-	-	-
HEB 280	-	-	-	-	-	-
HEB 300	0.7326	0.8002	0.8509	0.5899	0.6832	0.7567
HEB 360	0.6763	0.7551	0.8148	0.5190	0.6201	0.7042
HEB 400	0.6402	0.7256	0.7911	0.4773	0.5807	0.6702
HEB 450	0.6603	0.7421	0.8043	0.5001	0.6024	0.6891
HEB 500	0.6408	0.7260	0.7914	0.4779	0.5812	0.6707
HEB 600	0.6022	0.6936	0.7652	0.4362	0.5401	0.6340
HEB 700	0.6190	0.7079	0.7768	0.4540	0.5579	0.6500
HEB 800	0.5963	0.6887	0.7612	0.4302	0.5339	0.6284
HD 260x54.1	-	-	-	-	-	-
HD 260x142	-	-	-	-	-	-
HD 320x127	0.7121	0.7838	0.8377	0.5632	0.6599	0.7375
HD 320x198	0.7297	0.7979	0.8490	0.5861	0.6799	0.7540
HD 320x300	0.7345	0.8017	0.8521	0.5924	0.6853	0.7584
HD 400x237	0.8242	0.8726	0.9094	0.7179	0.7884	0.8414
HD 400x382	0.8218	0.8707	0.9078	0.7144	0.7857	0.8392
HD 400x551	0.8229	0.8716	0.9085	0.7160	0.7869	0.8402
HD 400x818	0.8294	0.8767	0.9127	0.7254	0.7944	0.8462
HD 400x1299	0.8445	0.8888	0.9226	0.7475	0.8119	0.8603

Table AB14: The reduction coefficient of the buckling load for R90

R 120						
χ_z						
Profiles	***l = 3m***			***l = 4m***		
	lθ = l	***lθ = 0.7l***	***lθ = 0.5l***	***lθ = l***	***lθ = 0.7l***	***lθ = 0.5l***
HEA 240	-	-	-	-	-	-
HEA 280	-	-	-	-	-	-
HEA 300	0.7617	0.8232	0.8693	0.6291	0.7164	0.7836
HEA 360	0.7147	0.7859	0.8394	0.5665	0.6628	0.7400
HEA 400	0.6726	0.7521	0.8123	0.5145	0.6159	0.7007
HEA 450	0.6812	0.7590	0.8179	0.5248	0.6254	0.7087
HEA 500	0.6621	0.7435	0.8055	0.5022	0.6044	0.6908
HEA 600	0.6103	0.7006	0.7709	0.4447	0.5487	0.6418
HEA 700	0.6113	0.7014	0.7715	0.4458	0.5497	0.6427
HEA 800	0.5845	0.6785	0.7529	0.4181	0.5216	0.6170
HEB 240	-	-	-	-	-	-
HEB 280	-	-	-	-	-	-
HEB 300	0.7671	0.8274	0.8727	0.6365	0.7225	0.7886
HEB 360	0.7015	0.7754	0.8310	0.5499	0.6481	0.7278
HEB 400	0.6540	0.7369	0.8002	0.4929	0.5956	0.6832
HEB 450	0.6630	0.7443	0.8061	0.5033	0.6054	0.6917
HEB 500	0.6407	0.7259	0.7914	0.4777	0.5811	0.6706
HEB 600	0.5920	0.6850	0.7581	0.4257	0.5294	0.6242
HEB 700	0.6012	0.6928	0.7645	0.4352	0.5390	0.6330
HEB 800	0.5751	0.6703	0.7461	0.4087	0.5118	0.6079
HD 260x54.1	-	-	-	-	-	-
HD 260x142	-	-	-	-	-	-
HD 320x127	0.7550	0.8178	0.8650	0.6199	0.7086	0.7774
HD 320x198	0.7662	0.8267	0.8722	0.6353	0.7215	0.7878
HD 320x300	0.7735	0.8325	0.8768	0.6455	0.7299	0.7946
HD 400x237	0.8361	0.8821	0.9171	0.7352	0.8022	0.8525
HD 400x382	0.8369	0.8827	0.9177	0.7364	0.8031	0.8532
HD 400x551	0.8391	0.8845	0.9191	0.7395	0.8056	0.8552
HD 400x818	0.8429	0.8875	0.9216	0.7451	0.8101	0.8588
HD 400x1299	0.8487	0.8921	0.9254	0.7535	0.8167	0.8641

Table AB15: The reduction coefficient of the buckling load for R120

A-6 The design axial buckling load:

Finally, as last step of the work and final result for the new formulas proposed for the balanced summation method of EN4 part 1-2 annex G[1], the design axial buckling load in the fire situation $N_{fi,Rd,z}$ is also determinate following equation(22):

R 30						
N fi,rd,z (N)						
Profiles	***l = 3m***			***l = 4m***		
	lθ = l	***lθ = 0.7l***	***lθ = 0.5l***	***lθ = l***	***lθ = 0.7l***	***lθ = 0.5l***
HEA 240	1118840	1304186	1451751	-	995817	1182775
HEA 280	1968892	2182887	2344317	-	1814625	2044775
HEA 300	2297611	2514733	2677786	1840897	2138864	2374893
HEA 360	2696823	2970184	3175809	2130378	2498218	2793966
HEA 400	2950573	3265266	3502445	2306516	2723200	3062236
HEA 450	3833205	4205491	4485208	3054460	3561637	3965641
HEA 500	4138453	4556545	4871004	3271438	3834595	4287042
HEA 600	4709323	5226890	5617551	3658397	4336730	4892782
HEA 700	6203766	6850805	7338007	4872085	5735082	6433515
HEA 800	6753510	7503263	8069495	5235315	6214462	7019171
HEB 240	1271335	1481491	1648726	-	1131764	1343845
HEB 280	2156564	2390328	2566648	-	1987990	2239466
HEB 300	2525595	2766066	2946675	2020525	2349885	2611175
HEB 360	2943583	3244606	3471103	2321106	2725079	3050531
HEB 400	3208796	3554109	3814475	2503703	2959563	3331287
HEB 450	4108759	4514739	4819897	3262664	3813073	4253124
HEB 500	4427279	4882781	5225586	3486708	4096852	4589082
HEB 600	5023372	5586329	6011721	3886408	4619125	5222774
HEB 700	6551150	7250310	7777270	5120469	6046028	6799228
HEB 800	7124181	7934396	8547184	5494660	6543537	7410995
HD 260x54.1	1247804	1417783	1548567	-	1129640	1307401
HD 260x142	2020881	2290693	2497768	-	1832573	2115605
HD 320x127	2863260	3122684	3317416	2313256	2672994	2955666
HD 320x198	3734481	4048372	4284004	3061010	3503262	3846387
HD 320x300	5047460	5431317	5719928	4214034	4763678	5184373
HD 400x237	6277951	6560292	6777839	5663753	6071210	6378027
HD 400x382	8370163	8724307	8998151	7603023	8111603	8495536
HD 400x551	10969926	11399816	11733706	10044256	10657279	11121877
HD 400x818	15292141	15830523	16251192	14143420	14902776	15482026
HD 400x1299	23858634	24568782	25128444	22365870	23349443	24108288

Table AB16: The design axial buckling load of the column for R30

R 60						
N fi,rd,z (N)						
Profiles	l = 3m			l = 4m		
	lθ = l	lθ = 0.7l	lθ = 0.5l	lθ = l	lθ = 0.7l	lθ = 0.5l
HEA 240	-	765852	844893	-	-	699958
HEA 280	-	1452838	1558477	-	1211429	1362412
HEA 300	1577004	1727513	1840560	1261035	1467050	1630566
HEA 360	1944285	2160646	2324068	1506458	1788777	2020942
HEA 400	2178911	2445710	2648633	1654286	1989817	2273040
HEA 450	2983423	3317479	3569893	2308589	2743516	3101751
HEA 500	3219201	3596407	3882284	2467202	2950024	3352562
HEA 600	3675679	4150548	4513630	2758580	3342206	3842727
HEA 700	5016356	5629434	6095653	3810087	4581703	5232676
HEA 800	5467805	6183867	6732188	4091493	4966213	5719496
HEB 240	-	907183	1011288	-	-	821724
HEB 280	-	1649012	1778764	-	1355224	1538280
HEB 300	1789664	1978371	2120525	1402334	1653141	1856648
HEB 360	2141388	2396099	2589360	1635920	1960033	2231379
HEB 400	2342639	2639894	2866746	1764993	2133223	2447314
HEB 450	3145558	3507918	3782213	2419487	2886337	3273764
HEB 500	3389400	3798881	4109965	2580742	3098553	3533965
HEB 600	3860449	4376073	4771821	2876387	3500611	4041466
HEB 700	5232050	5893044	6397265	3945659	4766026	5464869
HEB 800	5696570	6469282	7063489	4230209	5158949	5967570
HD 260x54.1	-	970508	1070336	-	-	887250
HD 260x142	-	1357550	1480532	-	-	1253583
HD 320x127	1905501	2107895	2260408	1490840	1759196	1977326
HD 320x198	2334822	2575488	2756621	1838090	2160275	2420307
HD 320x300	2990355	3289082	3513689	2369291	2773009	3096553
HD 400x237	4265623	4509313	4694599	3730404	4085589	4352357
HD 400x382	5390554	5698150	5932039	4714987	5163315	5500032
HD 400x551	6711488	7082332	7364784	5897396	6437763	6843414
HD 400x818	8852291	9308838	9657868	7852034	8516069	9014524
HD 400x1299	13279631	13885384	14351740	11960701	12835786	13494399

Table AB17: The design axial buckling load of the column for R60

R 90						
N fi,rd,z (N)						
Profiles	***l = 3m***			***l = 4m***		
	lθ = l	***lθ = 0.7l***	***lθ = 0.5l***	***lθ = l***	***lθ = 0.7l***	***lθ = 0.5l***
HEA 240	-	-	-	-	-	-
HEA 280	-	-	-	-	-	-
HEA 300	354013	383984	406481	289776	331944	364698
HEA 360	776297	857562	918761	609196	717456	805149
HEA 400	932127	1045523	1131722	708682	851673	972147
HEA 450	1337321	1491267	1607793	1028790	1227182	1391790
HEA 500	1602181	1801979	1954196	1211648	1461002	1672604
HEA 600	2117631	2423522	2660843	1551053	1907604	2224433
HEA 700	2442171	2787115	3053837	1797575	2204169	2562809
HEA 800	2966946	3417950	3770847	2148915	2660916	3123768
HEB 240	-	-	-	-	-	-
HEB 280	-	-	-	-	-	-
HEB 300	417853	456365	485278	336456	389642	431567
HEB 360	836946	934420	1008262	642266	767326	871417
HEB 400	1050057	1190023	1297423	782735	952340	1099200
HEB 450	1532538	1722317	1866807	1160729	1398281	1599455
HEB 500	1802463	2042257	2226214	1344159	1634990	1886667
HEB 600	2300247	2649724	2923154	1666226	2063078	2421772
HEB 700	2667087	3050070	3346931	1956041	2403784	2800865
HEB 800	3177097	3669076	4055349	2291759	2844769	3347892
HD 260x54.1	-	-	-	-	-	-
HD 260x142	-	-	-	-	-	-
HD 320x127	492145	541726	579015	389259	456100	509767
HD 320x198	683858	747697	795631	549255	637138	706586
HD 320x300	1329929	1451476	1542719	1072637	1240838	1373218
HD 400x237	1702933	1802962	1878911	1483205	1628986	1738548
HD 400x382	2140465	2267832	2364478	1860688	2046283	2185822
HD 400x551	3180352	3368503	3511311	2767052	3041239	3247350
HD 400x818	4047131	4278205	4453903	3539624	3876421	4129374
HD 400x1299	5176007	5447387	5654668	4581090	4976034	5272468

Table AB18: The design axial buckling load of the column for R90

R 120						
N fi,rd,z (N)						
Profiles	***l = 3m***			***l = 4m***		
	lθ = l	***lθ = 0.7l***	***lθ = 0.5l***	***lθ = l***	***lθ = 0.7l***	***lθ = 0.5l***
HEA 240	-	-	-	-	-	-
HEA 280	-	-	-	-	-	-
HEA 300	267439	289018	305224	220889	251515	275134
HEA 360	344600	378934	404748	273176	319613	356807
HEA 400	448657	501675	541881	343232	410871	467394
HEA 450	736265	820405	884063	567277	676006	766045
HEA 500	956694	1074374	1163916	725635	873350	998203
HEA 600	1334447	1531769	1685434	972407	1199679	1403216
HEA 700	1580402	1813314	1994595	1152479	1421205	1661596
HEA 800	2095886	2432951	2699589	1499289	1870384	2212496
HEB 240	-	-	-	-	-	-
HEB 280	-	-	-	-	-	-
HEB 300	403534	435277	459126	334857	380090	414855
HEB 360	377322	417041	446960	295761	348580	391421
HEB 400	495142	557906	605800	373133	450918	517245
HEB 450	829946	931665	1009037	629989	757863	865831
HEB 500	1073461	1216321	1325920	800457	973694	1123626
HEB 600	1458695	1687748	1868069	1048986	1304511	1538114
HEB 700	1751527	2018505	2227510	1267842	1570488	1844338
HEB 800	2249895	2622523	2919179	1599055	2002548	2378437
HD 260x54.1	-	-	-	-	-	-
HD 260x142	-	-	-	-	-	-
HD 320x127	244355	264706	279983	200637	229359	251611
HD 320x198	311261	335849	354321	258089	293104	320030
HD 320x300	613223	659981	695134	511728	578657	629900
HD 400x237	835093	881011	915994	734302	801206	851427
HD 400x382	1100922	1161195	1207124	968633	1056446	1122361
HD 400x551	2017579	2126704	2209914	1778136	1937084	2056387
HD 400x818	2580647	2717200	2821447	2281208	2479993	2629192
HD 400x1299	3287560	3455873	3584601	2918904	3163640	3347362

Table AB19: The design axial buckling load of the column for R120

ANNEX C:

Advanced calculation method – Numerical solution

ANNEX C – Advanced calculation method – Numerical solution

C-1 The critical axial compression resistance:

The critical axial compression resistance for the partially encased column is deduced from the first analysis the Euler buckling analysis for the different buckling length for each steel profile at room temperature:

T = 20 °C						
N cr,rd (N)						
	l = 3m			*l = 4m*		
Profiles	***lθ = l***	***lθ = 0.7l***	***lθ = 0.5l***	***lθ = l***	***lθ = 0.7l***	***lθ = 0.5l***
HEA 240	10000933	17506504	22815106	-	11072096	14226934
HEA 280	19380584	29764406	39976168	-	17967166	23880032
HEA 300	25018515	37818593	51252030	14368852	22497646	30222704
HEA 360	29694617	44498739	60604234	16999160	26255228	35483319
HEA 400	31982264	47766806	65179529	18285961	28093516	38056922
HEA 450	37743914	55997735	76702828	21526889	32723413	44538778
HEA 500	40827524	60260034	82670048	23205170	35120957	47895339
HEA 600	44802842	65939060	90620684	25841286	38315409	52367572
HEA 700	52796915	77359164	106608830	30337952	44739218	61360905
HEA 800	55777603	81617291	112570207	32014589	47134413	64714179
HEB 240	13455201	21299573	28125402	-	13205697	17213976
HEB 280	23595568	35785811	48406136	-	21354206	28621889
HEB 300	30203524	45225749	61622049	16685420	26664171	36055840
HEB 360	34881702	51908860	70978404	19316895	30423421	41318789
HEB 400	37171145	55179493	75557290	21104707	32263152	43894413
HEB 450	42934443	63412775	87083886	24346562	36894374	50378123
HEB 500	45989890	67677700	93054780	26025876	39293394	53736751
HEB 600	49969605	73363007	101014210	28264465	42491379	58213930
HEB 700	57970346	84792637	117015692	33264882	48920546	67214764
HEB 800	60956033	89057904	122987066	34944331	51319759	70573662
HD 260x54.1	12367949	19317784	25350897	-	12090941	15653317
HD 260x142	25184878	37627682	50984755	-	22390259	30072362
HD 320x127	32394949	47927785	65404898	18149346	28184066	38183693
HD 320x198	46966443	68744204	94547886	26345812	39893302	54576623
HD 320x300	69069026	100319323	138753052	38778515	57654307	79442029
HD 400x237	116463922	154169174	214142843	59981893	87944848	121848787
HD 400x382	166777150	226045214	314769300	88283084	128375120	178451168
HD 400x551	236012821	324953316	453240643	132328149	190575928	262906299
HD 400x818	362752531	506010045	706720063	203619236	292420338	405488473
HD 400x1299	646840661	911850230	1274896322	363418809	520705442	725087619

Table AC1: The critical axial compression resistance for the steel profiles at room temperature

C-2 The axial buckling load under fire:

Following the results obtained on the numerical solution on ANSYS [3] which is presented on the table C2 below, the axial buckling load $N_{fi,b,Rd}$ in [N] will be drawn for each steel profile for L= 3m and K=1, for all the fire resistance class R(30-60-90-120), in function of the vertical displacement (deformation) ε_z [m]:

ANSYS				
	N fi,b,rd (N)			
Profiles	***R30***	***R60***	***R90***	***R120***
HEA 240	2517406	-	-	-
HEA 280	3304009	-	-	-
HEA 300	3375060	2934012	2744033	2528683
HEA 360	3888495	3438803	3224135	2986566
HEA 400	4401929	3943595	3704236	3444449
HEA 450	5169730	4673157	4178201	3684900
HEA 500	5941147	5518230	5021656	4526701
HEA 600	6711939	6289647	5793073	5298118
HEA 700	8291215	7868923	7372350	6877394
HEA 800	9193104	8770196	8273622	7778667
HEB 240	2832471	-	-	-
HEB 280	3423811	-	-	-
HEB 300	3652930	3162731	2972752	2757458
HEB 360	4198303	3738803	3524143	3286485
HEB 400	5058890	4314876	4075535	3815511
HEB 450	5541147	5118149	4621656	4126701
HEB 500	6091066	5668089	5171656	4675739
HEB 600	7311939	6889647	6388730	5887812
HEB 700	8691215	8268915	7771312	7273578
HEB 800	9592824	9166501	8672584	8178283
HD 260x54.1	3104009	-	-	-
HD 260x142	5703615	-	-	-
HD 320x127	6121016	5874396	5619385	5295029
HD 320x198	8313211	8066583	7811572	7287599
HD 320x300	9532190	9088309	8907887	8479623
HD 400x237	9795734	9351853	9201853	8889211
HD 400x382	13128715	12684834	11979337	11453043
HD 400x551	14872533	14340877	13678890	12818955
HD 400x818	19422710	18791054	17929067	16753754
HD 400x1299	31430453	30798806	29607506	28488035

Table AC2: The design value of the axial buckling load for the steel profiles under fire

The HEA profiles:

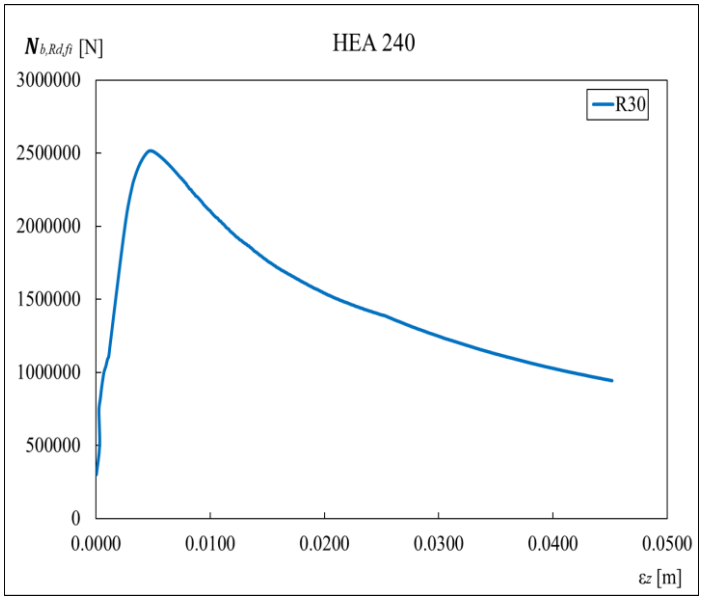

Figure AC1: Axial buckling load of HEA240 profile for R30

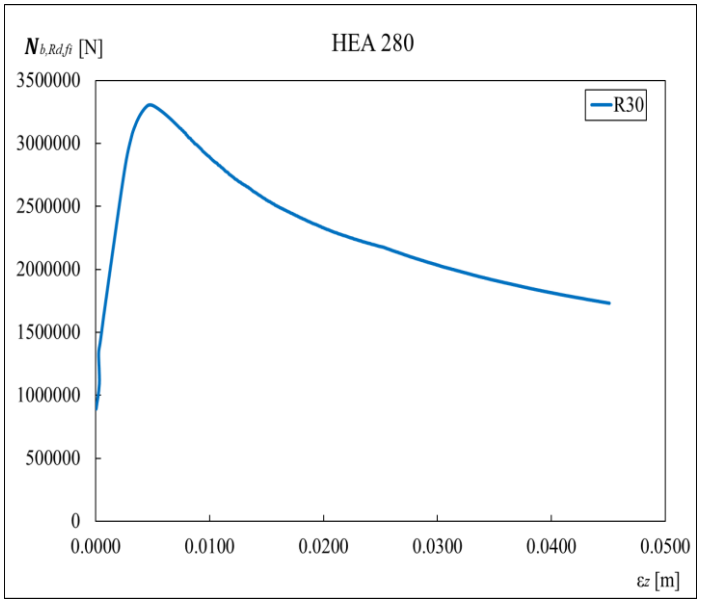

Figure AC4: Axial buckling load of HEA280 profile for R30

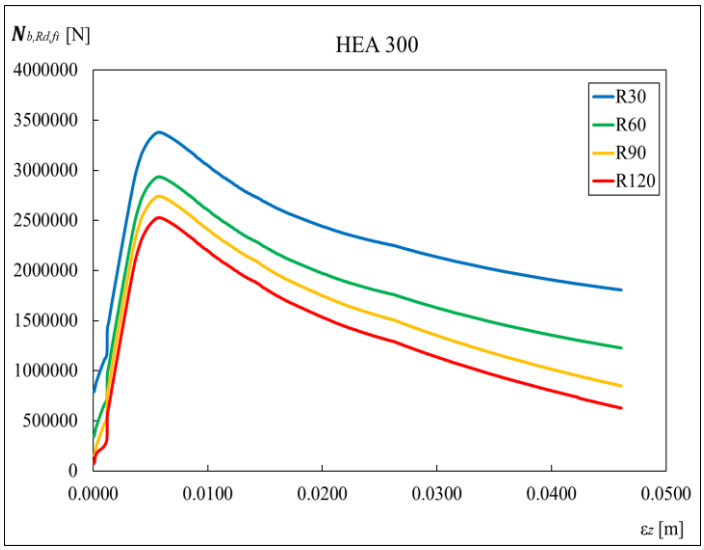

Figure AC7: Axial buckling load of HEA300 profile under fire

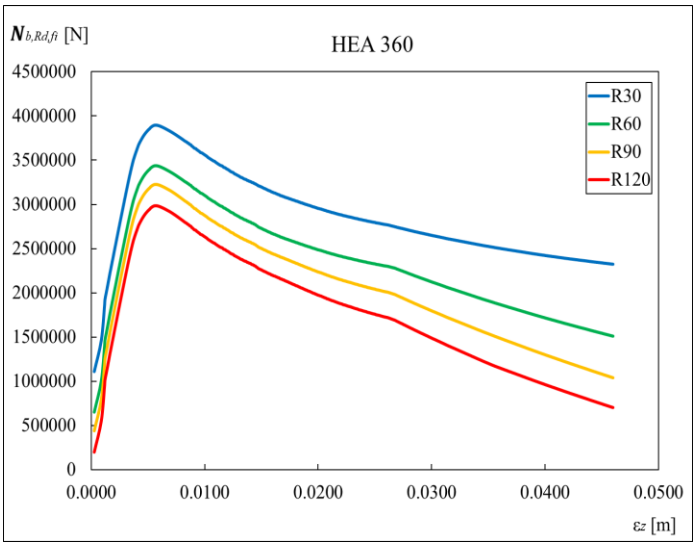

Figure AC10: Axial buckling load of HEA360 profile under fire

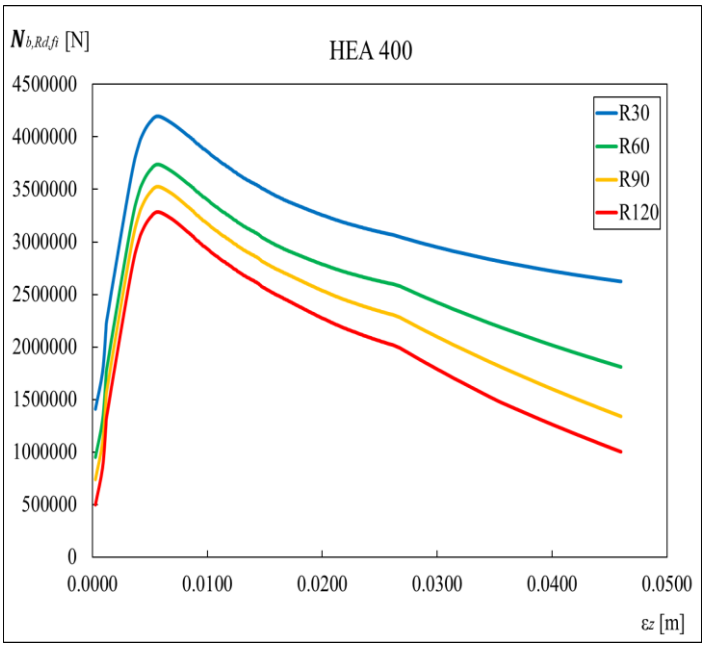

Figure AC13: Axial buckling load of HEA400 profile under fire

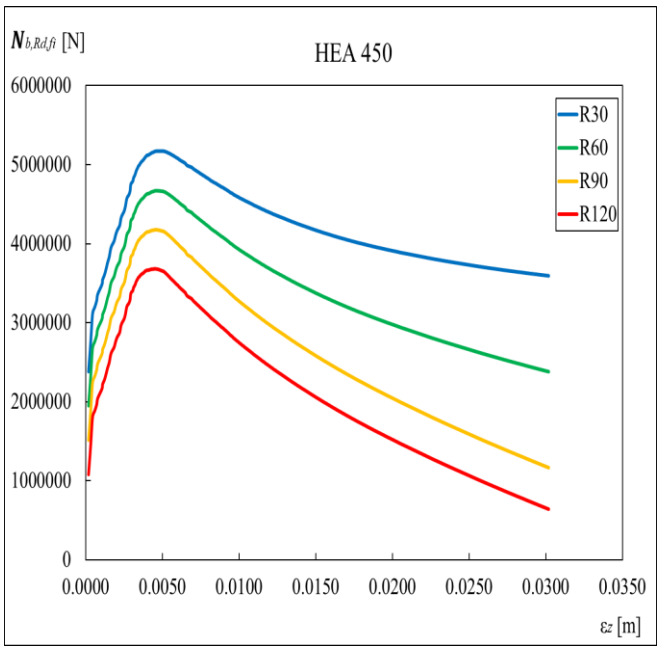

Figure AC16: Axial buckling load of HEA450 profile under

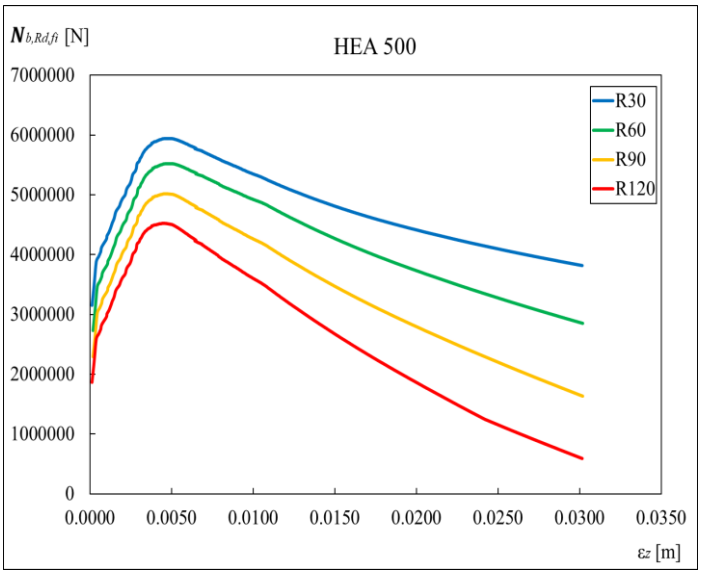

Figure AC19: Axial buckling load of HEA500 profile under

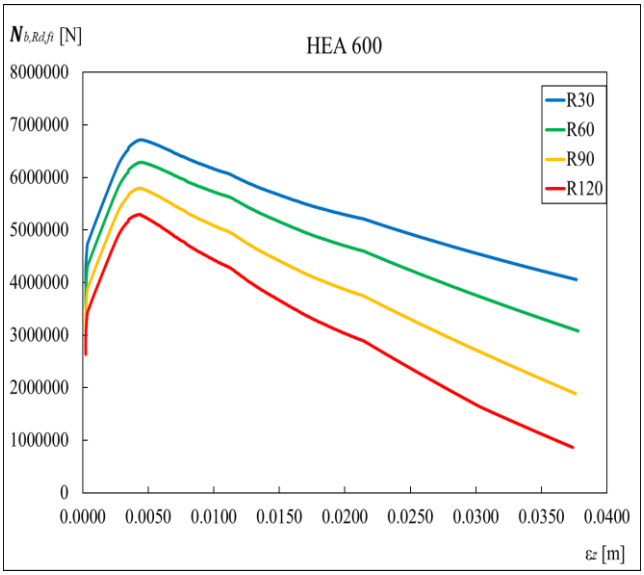

Figure AC22: Axial buckling load of HEA600 profile under

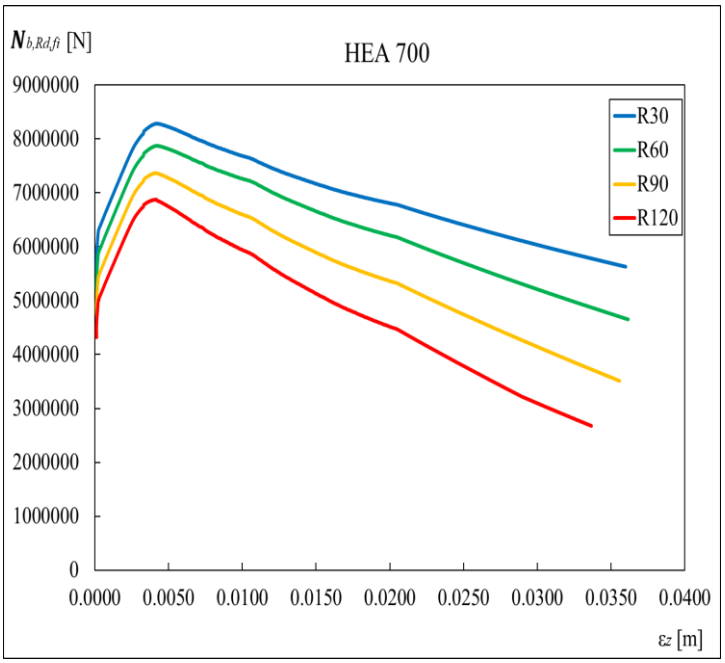

Figure AC25: Axial buckling load of HEA700 profile under fire

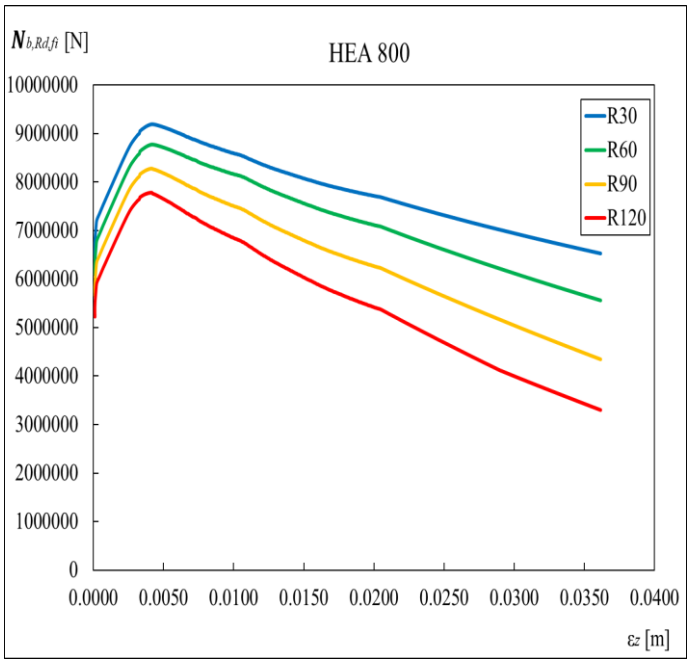

Figure AC28: Axial buckling load of HEA800 profile under fire

The HEB profiles:

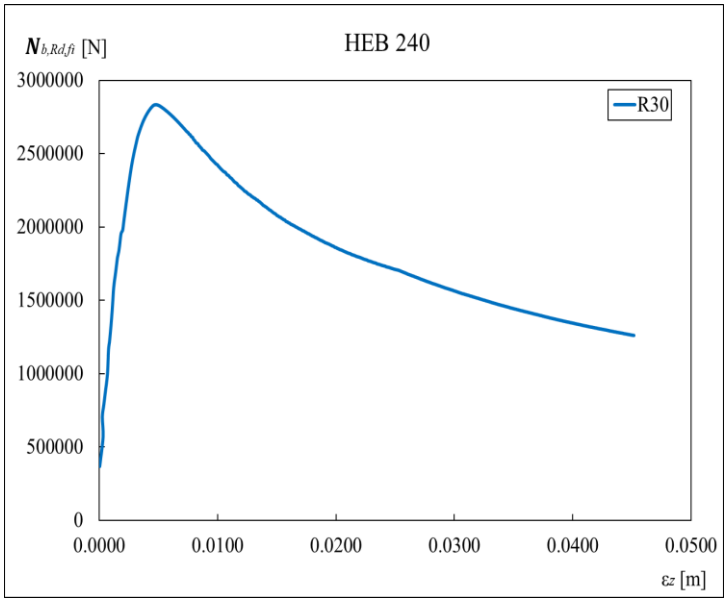

Figure AC31: Axial buckling load of HEB240 profile for R30

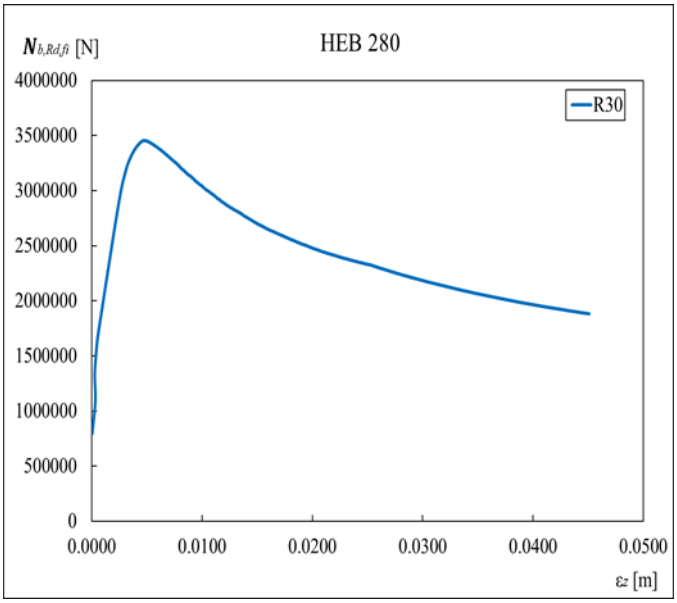

Figure AC34: Axial buckling load of HEB280 profile for R30

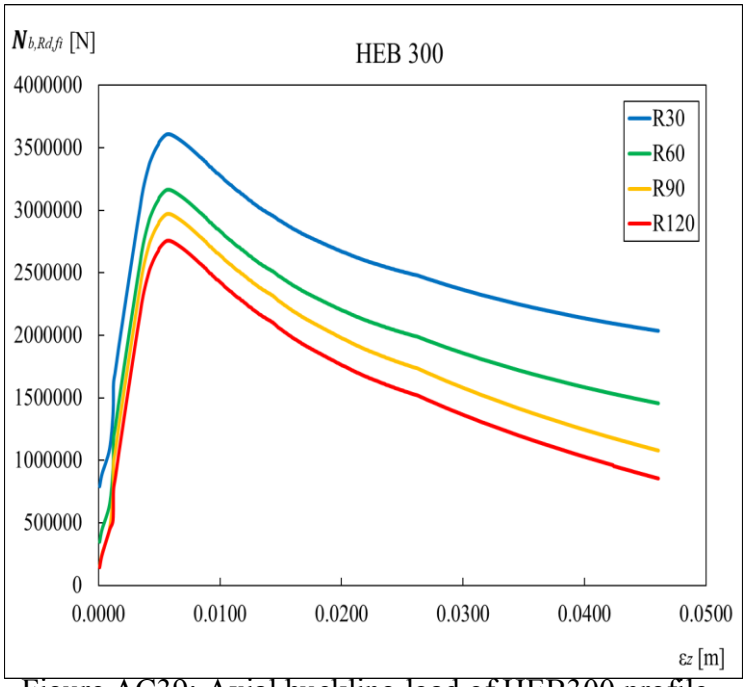

Figure AC39: Axial buckling load of HEB300 profile under fire

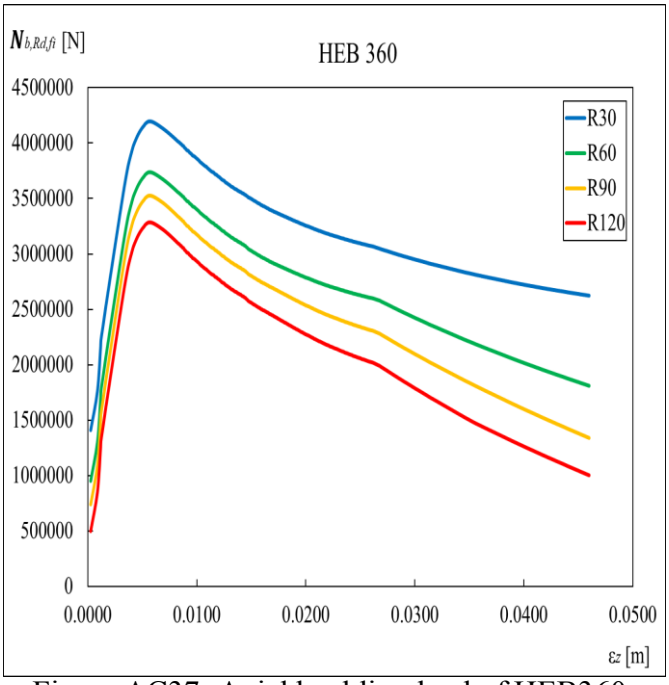

Figure AC37: Axial buckling load of HEB360 profile under fire

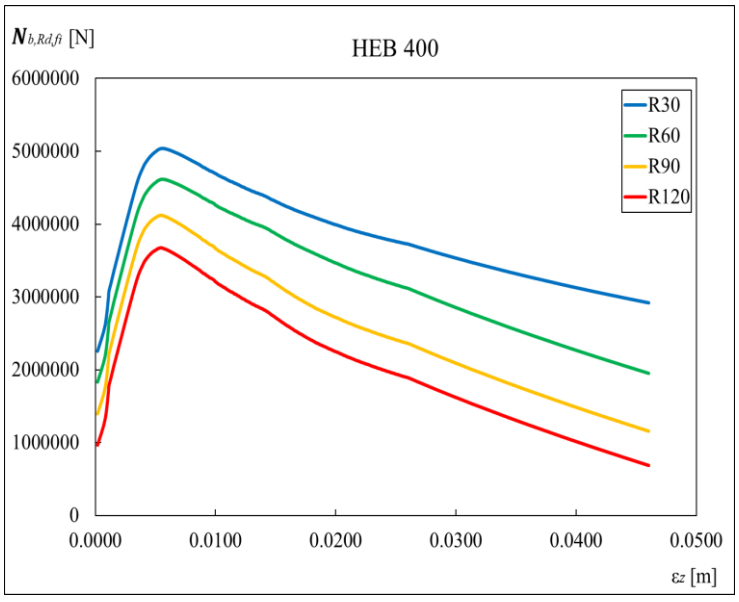

Figure AC42: Axial buckling load of HEB400 profile under fire

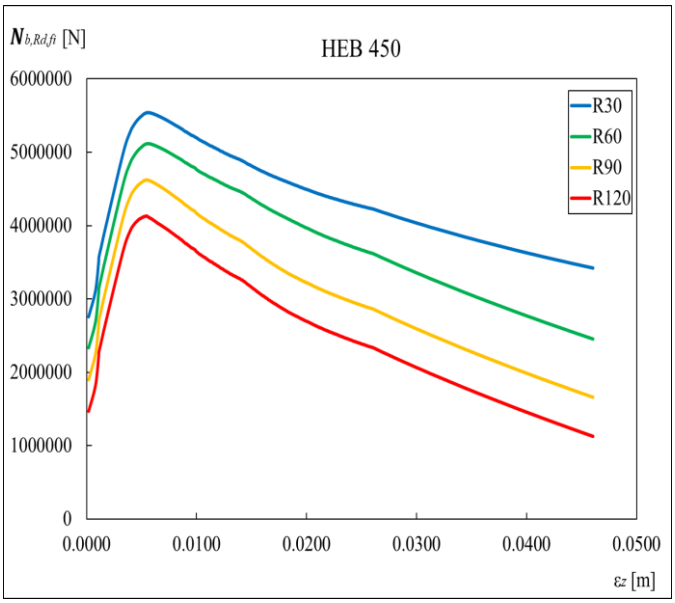

Figure AC16: Axial buckling load of HEB450 profile under fire

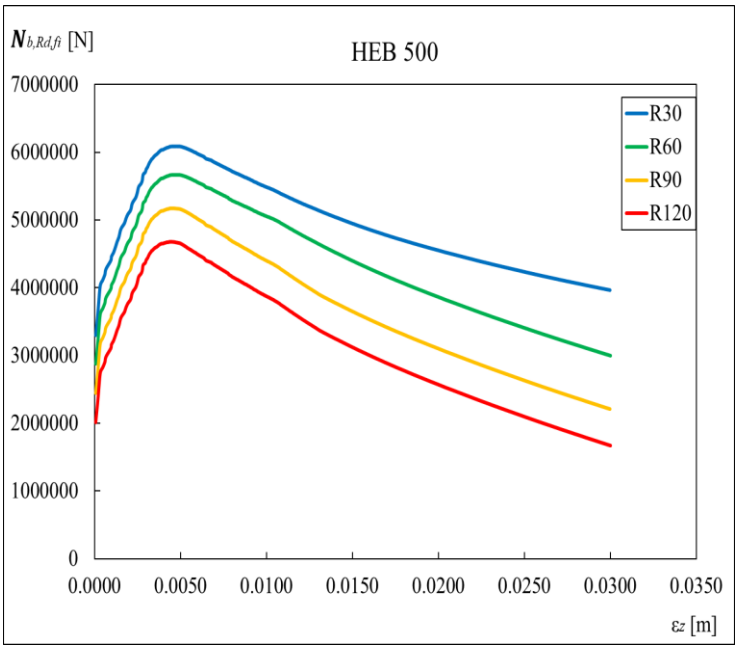

Figure AC46: Axial buckling load of HEB600 profile under fire

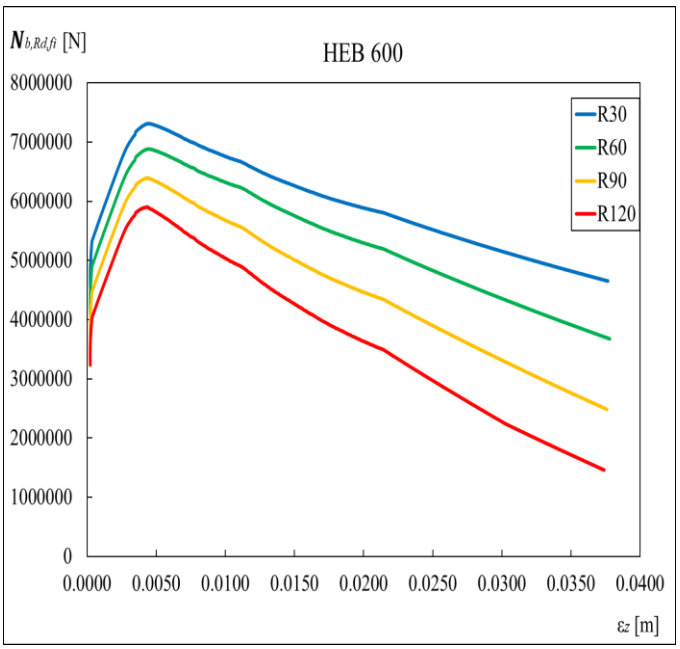

Figure AC49: Axial buckling load of HEB500 profile under fire

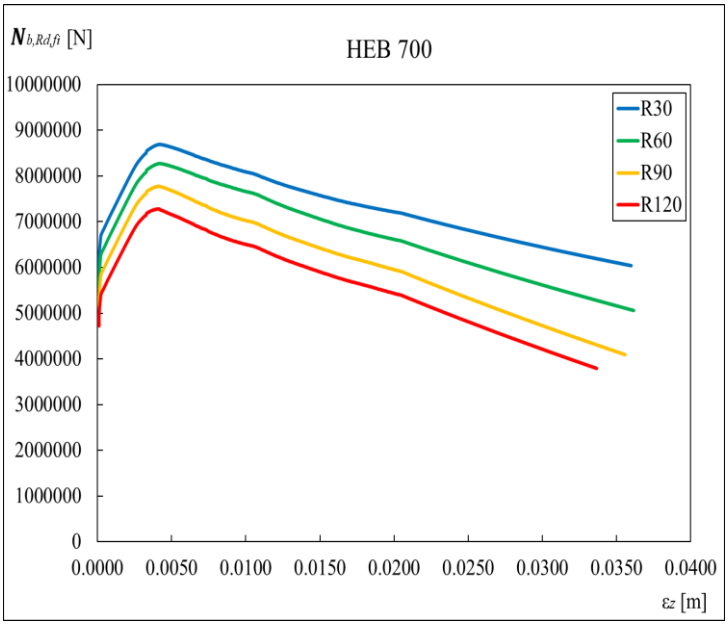

Figure AC52: Axial buckling load of HEB700 profile under fire

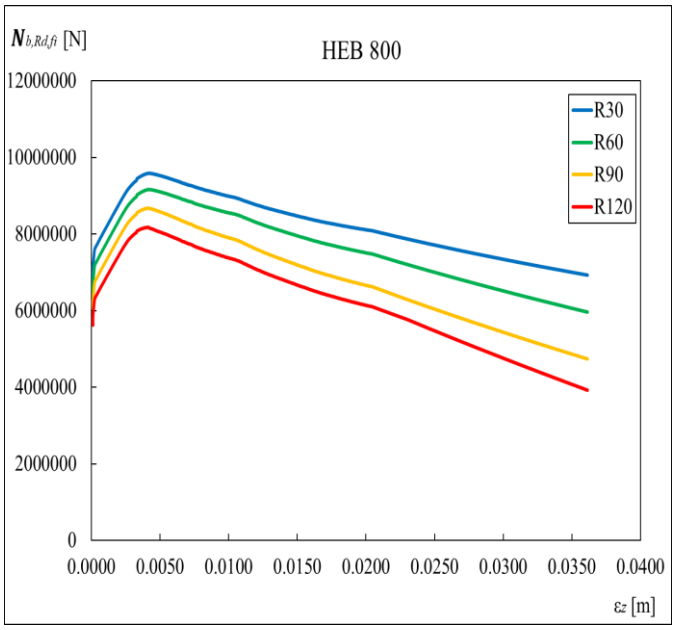

Figure AC55: Axial buckling load of HEB800 profile under fire

The HD profiles:

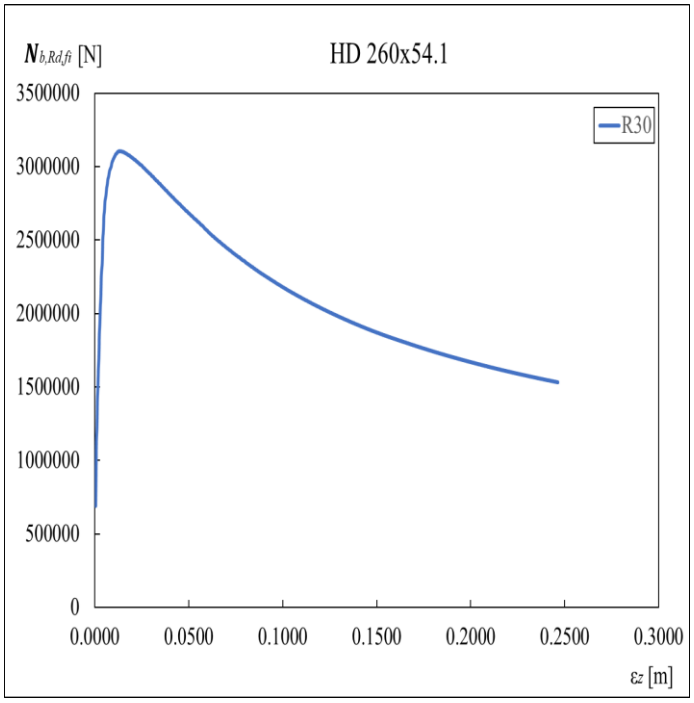

Figure AC58: Axial buckling load of HD260x54.1 profile for R30

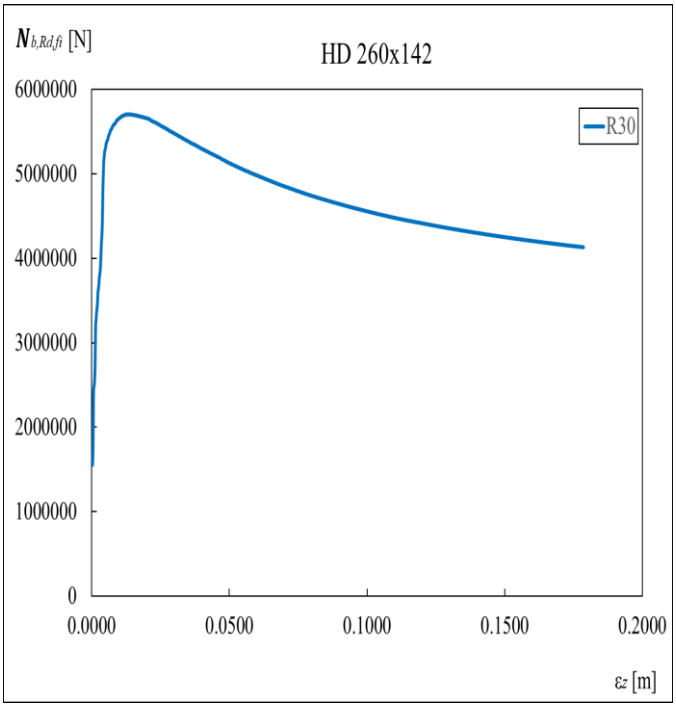

Figure AC61: Axial buckling load of HD260x142 profile for R30

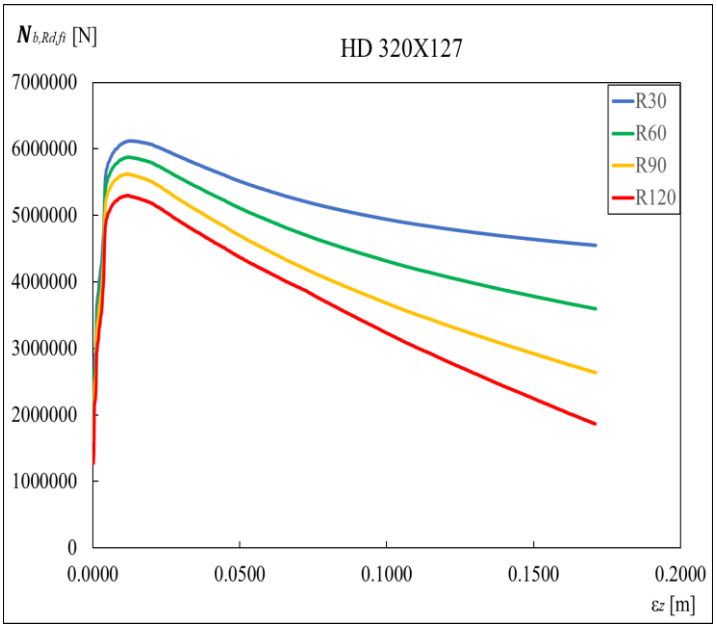

Figure AC64: Axial buckling load of HD320x127 profile under fire

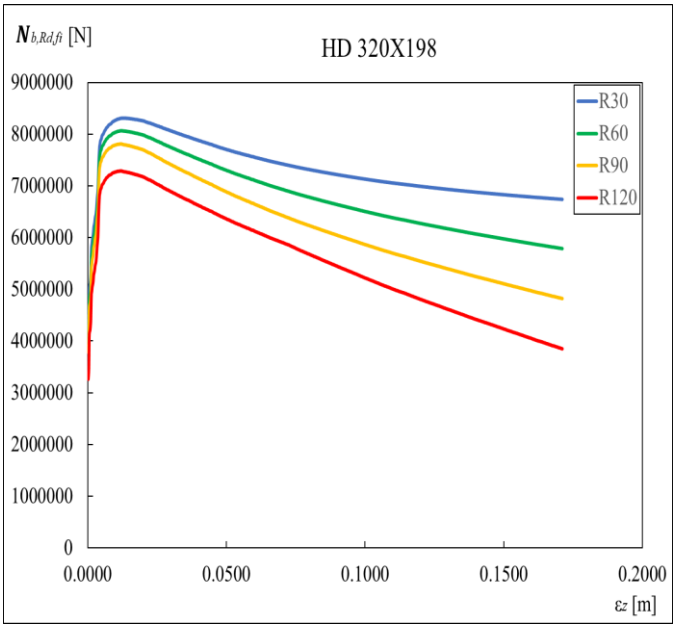

Figure AC67: Axial buckling load of HD320x198 profile under fire

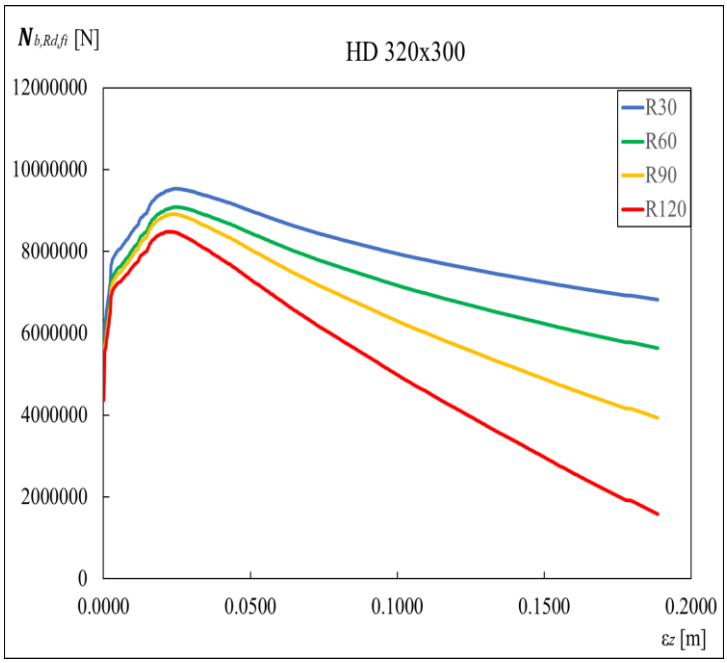

Figure AC70: Axial buckling load of HD320x300 profile under fire

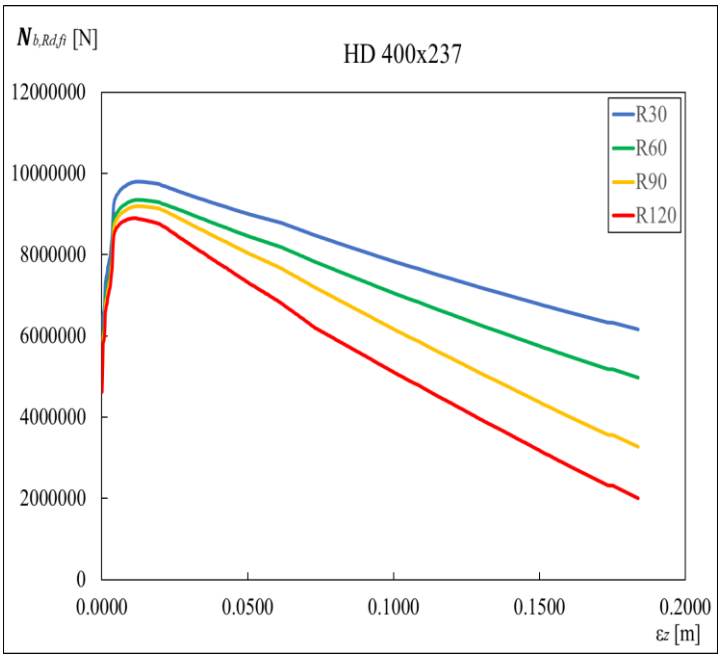

Figure AC76: Axial buckling load of HD400x237 profile under fire

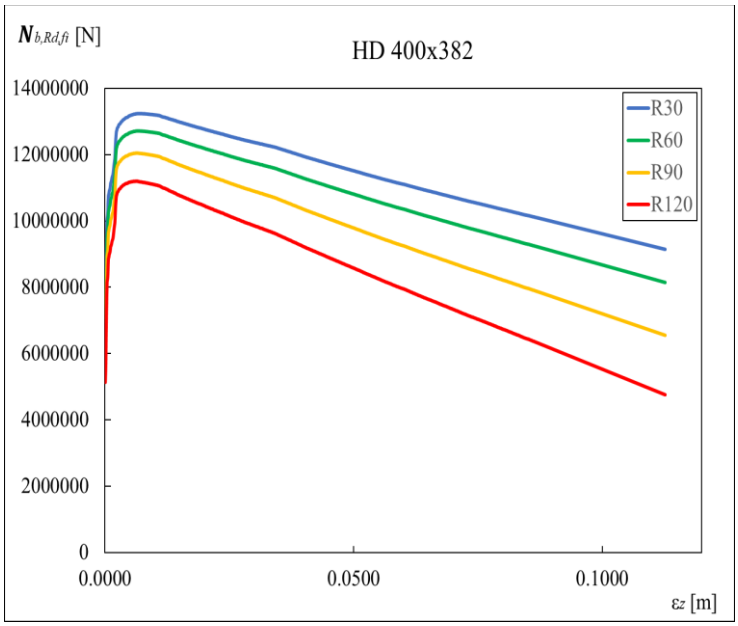

Figure AC73: Axial buckling load of HD320x382 profile under fire

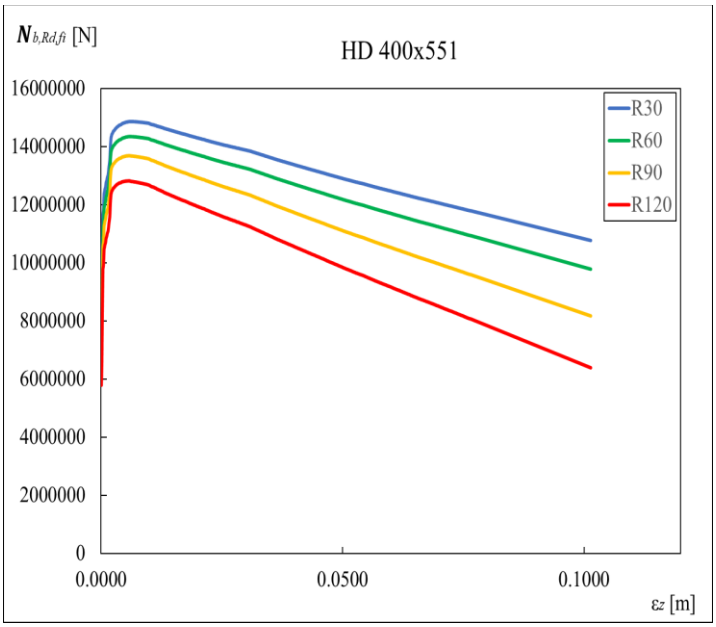

Figure AC79: Axial buckling load of HD400x551 profile under fire

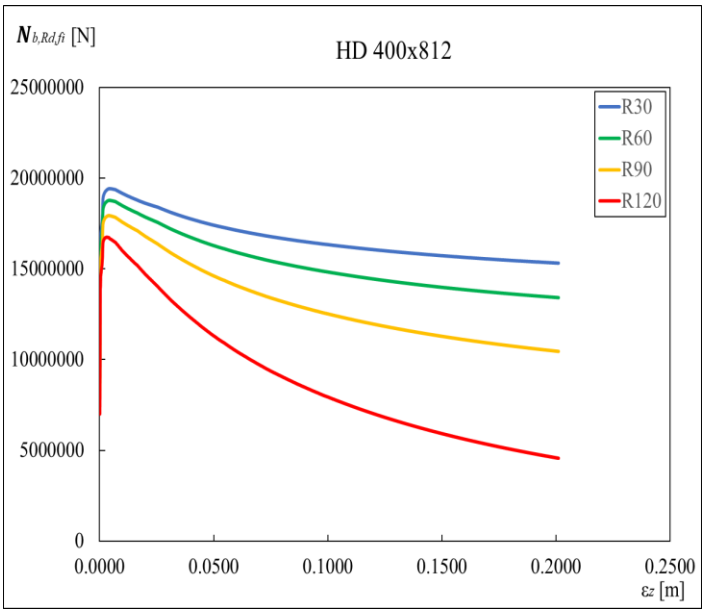

Figure AC82: Axial buckling load of HD400x812 profile under fire

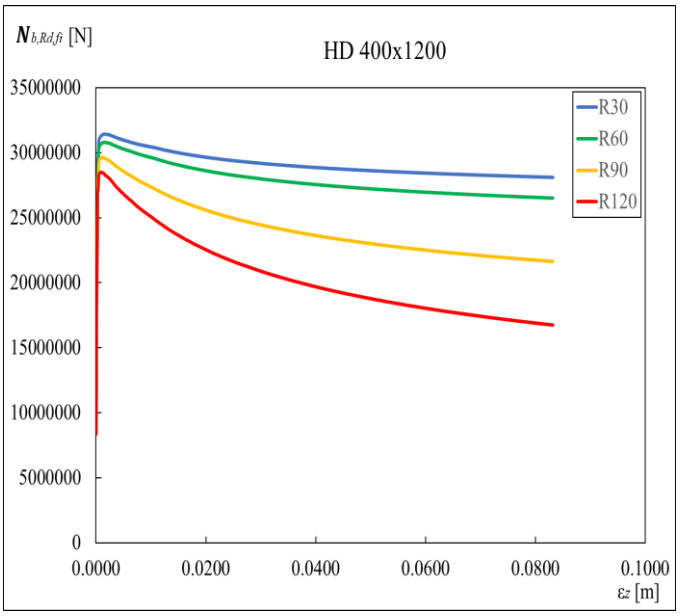

Figure AC85: Axial buckling load of HD400x1200 profile under fire

Example of Axial buckling resistance with the deformed and undeformed shape of the PEC for different fire rating (R30-60-90-120) for HEA300 Steel profile on ANSYS:

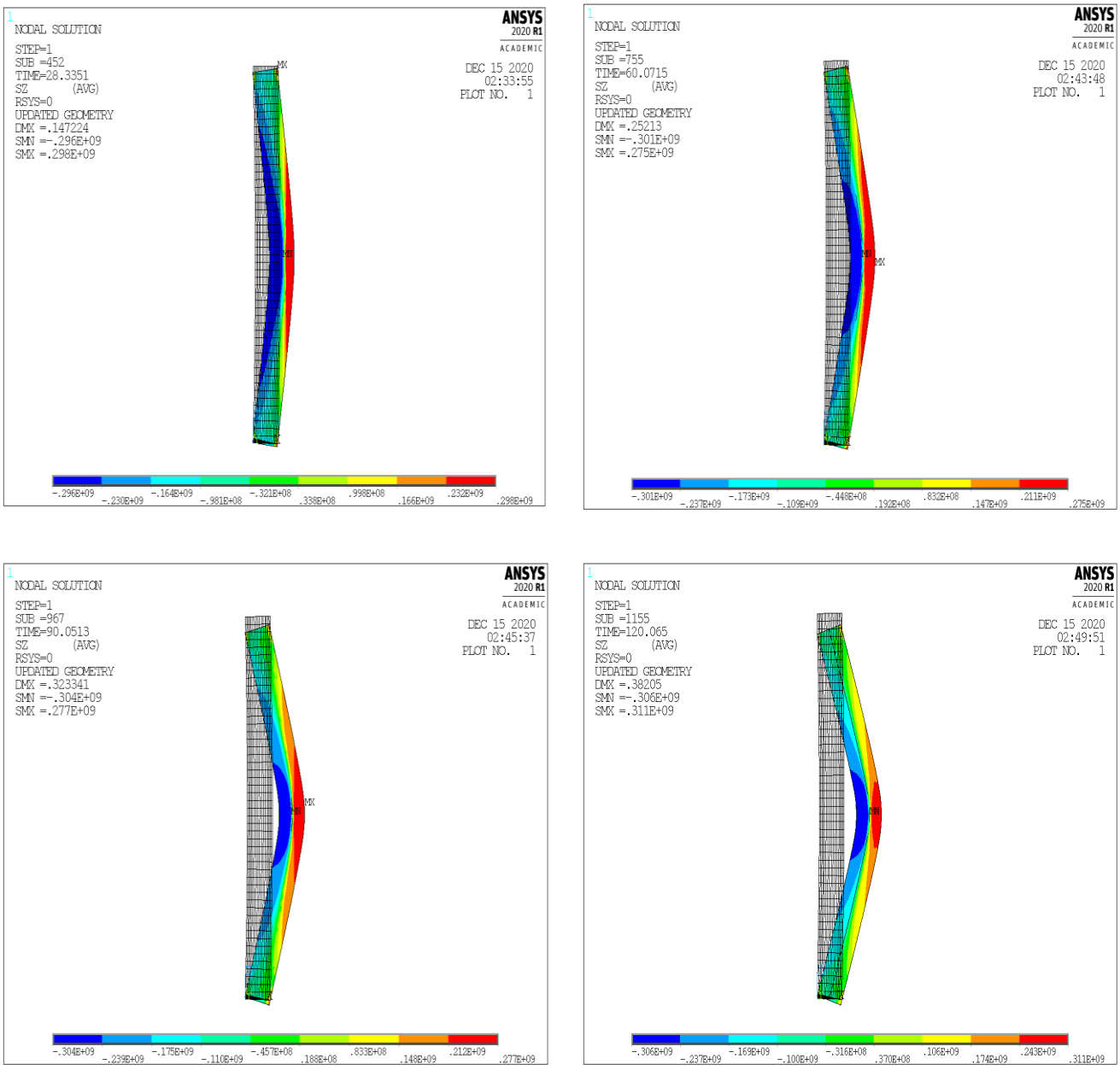

Figure AC 31: Axial buckling resistance of HEA300 Steel profile